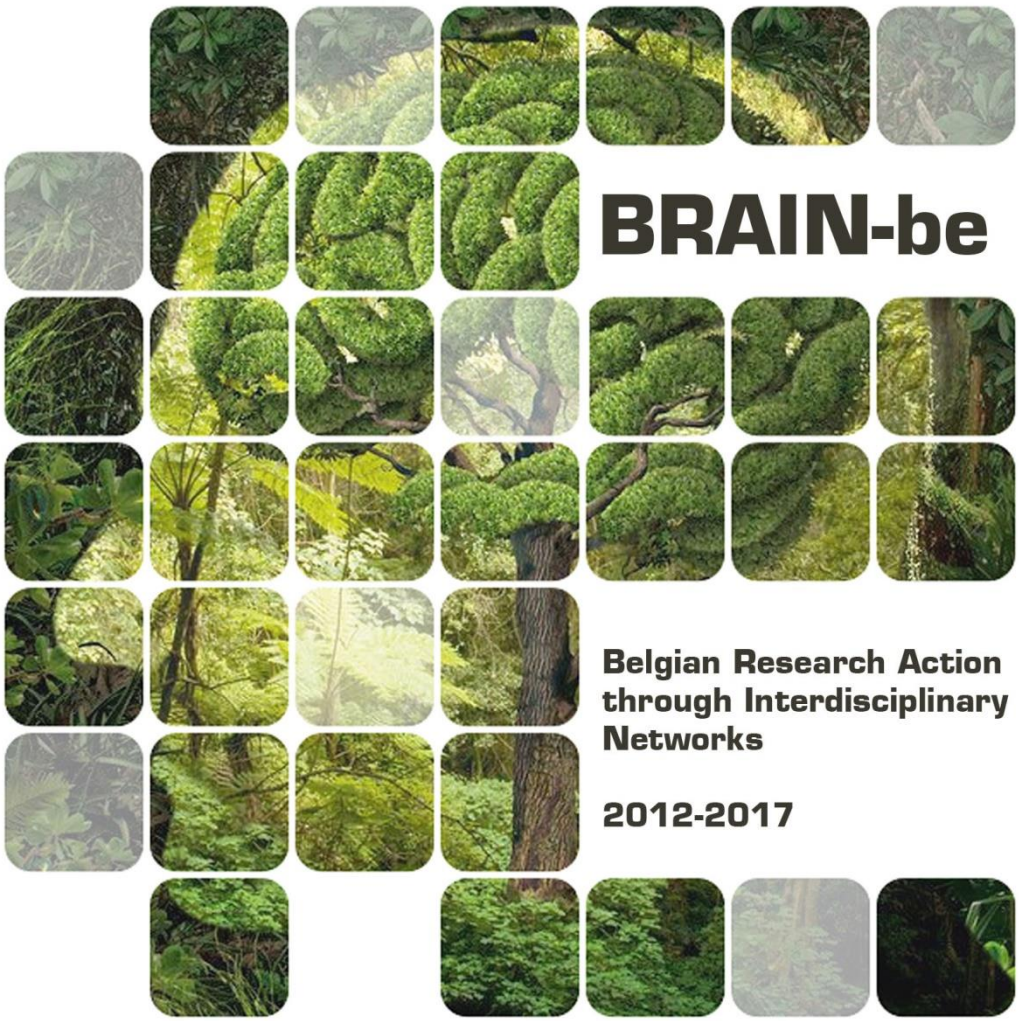

OCTAVE

Oxygenated volatile organic Compounds in the Tropical Atmosphere: Variability and Exchanges

TRISSEVGENI STAVRAKOU (Royal Belgian Institute for Space Aeronomy, BIRA-IASB) – BERT VERREYKEN (BIRA-IASB and LACy-Laboratoire de l'Atmosphère et des Cyclones) – BRUNO FRANCO (Université Libre de Bruxelles, ULB) – JEAN-FRANCOIS MÜLLER (BIRA-IASB) – CORINNE VIGOUROUX (BIRA-IASB) – JEROME BRIOUDE (CNRS, LACy) – CRIST AMELYNCK (BIRA-IASB) – LIEVEN CLARISSE (ULB) – NIELS SCHOON (BIRA-IASB) – PIERRE-FRANCOIS COHEUR (ULB)

Axis 2: Geosystems, universe and climate

belspo .be

NETWORK PROJECT

OCTAVE

Oxygenated volatile organic Compounds in the Tropical Atmosphere: Variability and Exchanges

Contract - BR/175/A2/OCTAVE
FINAL REPORT

PROMOTORS: TRISSEVGENI STAVRAKOU (BIRA-IASB)
PIERRE-FRANCOIS COHEUR (ULB)
JEROME BRIOUDE (CNRS-LACy)

AUTHORS: TRISSEVGENI STAVRAKOU (BIRA-IASB)
BERT VERREYKEN (BIRA-IASB and CNRS-LACy)
BRUNO FRANCO (ULB)
JEAN-FRANCOIS MÜLLER (BIRA-IASB)
CORINNE VIGOUROUX (BIRA-IASB)
JEROME BRIOUDE (CNRS-LACy)
CRIST AMELYNCK (BIRA-IASB)
LIEVEN CLARISSE (ULB)
NIELS SCHOON (BIRA-IASB)
PIERRE-FRANCOIS COHEUR (ULB)

Published in 2022 by the Belgian Science Policy Office
WTCIII
Simon Bolivarlaan 30 Boulevard Simon Bolivar
B-1000 Brussels
Belgium
Tel: +32 (0)2 238 34 11
http://www.belspo.be
http://www.belspo.be/brain-be

Contact person: Aline van der Werf
Tel : +32 (0)2 238 36 71

Trissevgeni STAVRAKOU, Bert VERREYKEN, Bruno FRANCO, Jean-François MÜLLER, Corinne VIGOUROUX, Jérôme BRIOUDE, Crist AMELYNCK, Lieven CLARISSE, Niels SCHOON, Pierre-François COHEUR. **Oxygenated volatile organic compounds in the Tropical Atmosphere: Variability and Exchanges (OCTAVE)**. Final Report. Brussels: Belgian Science Policy Office 2022 – 88 p. (BRAIN-be - Belgian Research Action through Interdisciplinary Networks), https://dx.doi.org/10.18758/71021078

TABLE OF CONTENTS

1. INTRODUCTION

Oxygenated Volatile Organic Compounds (OVOCs) have multiple direct sources (the ocean, the biosphere, etc.) and are also formed from the oxidation of all hydrocarbons emitted to the atmosphere. They have a significant impact on the atmospheric oxidative capacity, in particular over oceans where they were recently estimated to suppress the levels of the hydroxyl radical (OH) by ~40% (Read et al., 2012). Despite their great relevance for the global atmospheric system, and for climate in particular, even the budget of some of the most abundant OVOCs (methanol, acetaldehyde, acetone and formic acid) is currently poorly understood, due to incomplete representation of photochemical OVOC production and uncertainties in terrestrial emissions and ocean/atmosphere exchanges of OVOCs and their precursors. OCTAVE focuses on improving our knowledge of the key OVOCs and their role in tropical regions, relying on an integrated approach combining in situ measurements, satellite retrievals and modelling.

2. STATE OF THE ART AND OBJECTIVES

The scarcity of OVOC observations in tropical regions strongly contributes to the large uncertainties in terrestrial emissions and ocean/atmosphere exchanges of OVOCs and their precursors. Methanol and formic acid are exceptions, thanks to spaceborne observations by infrared sensors (IASI, Razavi et al., 2011, and TES, Cady-Pereira et al., 2012) which have led (among others) to much narrowed down estimations of biogenic methanol emissions over continents (e.g., Stavrakou et al., 2011; Wells et al., 2014). Since then, however, a new photochemical methanol source has been identified in a modelling study backed by advanced theoretical calculations: the $CH_3O_2 + OH$ reaction, of magnitude comparable to the combined terrestrial emissions (Müller et al., 2016). Although it might provide a long-needed explanation for persistent model underestimations over remote Tropical oceans, its precise magnitude and its implications for global budget assessments remain unclear, although they are clearly substantial.

Even more important for the oxidizing capacity of the atmosphere is the very large, yet unexplained model underestimation of observed acetaldehyde concentrations in remote tropical regions at surface level (e.g., Read et al., 2012) and in the free troposphere (Millet al., 2010). A major difficulty lies in the very uncertain ocean/atmosphere exchanges of OVOCs and their precursors, due to lack of measurements. Especially worrisome is the fact that the observed acetaldehyde levels appear incompatible with the observed abundances of peroxyacetyl nitrate PAN (Millet et al., 2010), a key reservoir of nitrogen oxides affecting ozone formation over remote areas. Acetone and acetaldehyde are estimated to account for $\sim$50% of PAN formation globally (Fischer et al., 2014). A better understanding of OVOC sources and sinks is clearly needed to better quantify their impact on atmospheric oxidants, on the lifetime of methane and consequently on climate.

OCTAVE aims at improving our appraisal of the budget of key OVOCs and of their role in tropical regions, by using novel in situ measurements and satellite observations, and modelling tools. More specifically, the objectives of OCTAVE are:

- To generate a 2-year dataset of **atmospheric measurements of OVOCs** (methanol, acetaldehyde and acetone) and related compounds by mass spectrometry (PTR-MS) and remote sensing infrared spectroscopy (FTIR) at the high-altitude site of Maïdo (2155 m a.s.l.) on Reunion Island, in the Indian Ocean. PTR-MS provides long-term high temporal resolution concentration measurements at ground level, and FTIR measurements provide total columns of many compounds, among which several OVOCs and related species (e.g., CH_3OH, CO, C_2H_2, HCOOH, HCHO). The detection of more challenging compounds (PAN, C_2H_4 and acetone) is also explored. These measurements are performed by BIRA-IASB.
- To **identify and quantify OVOC sources** contributing to the measurements at Reunion Island, with the help of multivariate statistical analysis, back trajectory calculations and 3-dimensional modelling. To this purpose, the FLEXPART Lagrangian model coupled with

the ECMWF global forecasts at 15 km resolution is used, and mesoscale chemistry models. This work is performed by CNRS-LACy and BIRA-IASB.

Figure 1. The Reunion Island and the Maïdo Observatory are central in the OCTAVE project.

- To apply an innovative methodology, relying on hyperspectral indices and neural networks, to generate improved and better characterized global distributions of the column abundances of methanol and other VOCs using **multi-annual (2008-2021) satellite data from the IASI sensor** on the MetOp platforms. The retrieved distributions are analyzed to give insight on the source regions and types, role of transport, seasonality and inter-annual variability. Altogether, this suite of observations from a single sounder provides a rather unique view of the sources and transport patterns in the tropical regions. This work is carried out by the ULB.
- To perform an **updated model evaluation of the budget of OVOCs**, based on spaceborne data (for CH_3OH), and a wide collection of aircraft, ship-based and ground-based measurements, including those obtained at Reunion Island. The in-situ data is used to evaluate OVOC sources and sinks in the area, with the help of high-resolution chemistry-transport models. The modelling activities are crucial to integrate the different observational datasets and interpret the observations in terms of the processes at play. This work is carried out by BIRA-IASB.

To achieve the project objectives and to **enhance collaboration among the teams**, a joint Ph.D. thesis has been set up, promoted by Crist Amelynck at BIRA-IASB and by Jérôme Brioude at CNRS-LACy, for an overall duration of 4 years. The hired Ph.D. candidate, Bert Verreken, spent the first 2 years of the project at CNRS-LACy at Réunion Island where he became well acquainted with the methods for backtrajectory calculations, Lagrangian inversion and the Meso-NH mesoscale model for simulating transport and chemistry at Reunion Island, under the supervision of Jérôme Brioude. Subsequently he spent the remaining 2 years at BIRA-IASB to apply those methods for the analysis of the local measurements This close collaboration between CNRS and BIRA-IASB on data exploitation worked flawlessly until the end of the project.

The OCTAVE project is at the core of an **intensive field campaign** (OCTAVE-IOP), coordinated by CNRS-LACy, which took place between March and May 2018 at Reunion Island. During that campaign, CNRS-LaMP (Aurelie Colomb's team) performed complementary (O)VOC measurements and HCHO measurements at the Maïdo observatory and deployed a second PTR-

MS instrument in the area between the shore and the observatory. Several international groups participated to the OCTAVE-IOP (Univ. Helsinki, Univ. Colorado, Univ. Hokkaido, Univ. Grenoble-Alpes, Geosciences Environnement Toulouse, see annexes) and allowed a wide dissemination of the project results. More details are provided in Section 5.

3. METHODOLOGY

3.1 Local (O)VOC measurements at Reunion Island (WP1)

3.1.1 In situ PTR-MS (O)VOC measurements at the Maïdo Observatory

Online *in situ* (O)VOC concentration measurements at high temporal resolution were performed at the Maïdo Observatory with a high-sensitivity PTR-Quad-MS instrument (hs-PTR-MS, Ionicon Analytik GmbH, Innsbruck, Austria) between 16 October 2017 and 26 November 2019.

The measurement set-up is shown in Figure 2. Air was sampled at 2.9 m above the roof of the observatory (8.2 m above ground level) and pumped at a flow rate of about 8 L min^{-1} towards the instrument through a 10.35 m long, heated (5-10 degrees above ambient temperature) and thermally insulated 3/8″ outer diameter PFA sampling line. A PTFE membrane particle filter (2 μm pore size) was installed 2.5 m downstream the sampling point. The outside part of the sampling line and the filter box were fixed to a strong support structure in order to withstand high wind speeds associated with the passage of cyclones or heavy tropical storms. Moreover, the inside and outside part of the sampling line could be disconnected and the interface plate removed prior to bad weather conditions.

Part of the sampled air was subsampled by the hs-PTR-MS instrument, which was operated at a drift tube temperature and pressure of 333 K and 2.1 hPa, respectively. The ratio of the electric field E to the air number density N in the drift tube, E/N, was 135 Td. The instrument was mainly operated in Multiple Ion Detection (MID) mode in which it continuously cycled through a list of pre-set m/z values. The total cycle time, which determines the time resolution of single compound measurements, was 2.7 minutes. During a single cycle 3 ion species were followed which are related to precursor ions and impurities ($H_3{}^{18}O^+$ (m/z 21, 2 s dwell time), O_2^+ (m/z 32, 100 ms), $H_3O^+.H_2O$ (m/z 37, 100 ms)) and 16 ion species (dwell time of 10 s each) which are related to specific (O)VOCs. The m/z ratios of the latter and the corresponding tentative compound identification are listed in Table 1. Ions at m/z 47, tentatively attributed to formic acid, were only monitored after 27 June 2018 after high ion signal intensities at this m/z ratio had been observed in African biomass burning plumes reaching Réunion Island. The ion signal at m/z 31 (protonated formaldehyde) has not been considered for further analysis because of the large discrepancies between the formaldehyde (HCHO) concentrations obtained with the hs-PTR-MS instrument and with an Aerolaser HCHO analyser (operated by the Laboratoire de Météorologie Physique, LaMP, Clermont-Ferrand, France), despite regular calibrations of the hs-PTR-MS versus relative humidity. This discrepancy is probably due to interferences from other compounds at m/z 31 (e.g. methyl hydroperoxide), which could not be quantified during the hs-PTR-MS deployment at Maïdo. As background ion signals at m/z 93 frequently exceeded ambient ion signals, we were not able to quantify toluene as well.

Background measurements were performed every 4 hours by sampling zero air, obtained by scrubbing VOCs from ambient air by a catalytic converter. Background ion signals at some m/z ratios (e.g. m/z 45, acetaldehyde) were found to vary significantly with the ion signal at m/z 37,

which was considered as a proxy for air humidity. This humidity dependence of the background ion signals was taken into account when quantifying (O)VOC concentrations.

Figure 2. Top left: air sampling from the roof of the observatory; Top right: support structure to guide the sampling line; Bottom: (O)VOC measurement set-up in the laboratory (hs-PTR-MS and associated set-up for zero and calibration measurements and remote instrument control).

The hs-PTR-MS instrument was calibrated for the compounds that were present in a gravimetrically prepared VOC/N_2 calibration gas mixture (Apel-Riemer Environmental, Miami, FL, USA, stated accuracy of 5%) by dynamically diluting controlled flows of the calibration gas mixture in zero air. These calibrations were performed every 3-4 days. Formic and acetic acid calibration coefficients and their humidity dependencies were obtained from literature data (Baasandorj et al. 2015) and first principles.

Average calibration coefficients and their ranges over the entire campaign are shown in Table 1 as well. Only the calibration coefficients of formaldehyde, isoprene, isoprene oxidation products and methyl ethyl ketone showed a non-negligible humidity dependence, which was determined almost every 2 months by humidifying the zero air by means of a dewpoint generator (LI-610, LI-COR, NE, USA) during calibrations. (O)VOC ion signals were normalized in order to account for potential drifts in source ion production and (O)VOC mixing ratios were obtained by dividing the background subtracted normalized ion signals by the species-specific calibration factors.

The set-up was fully operated by remote control, except for the 3-weekly filter changes and the humidity-dependent calibration measurements. The biannual maintenance of the instrument (replacement of ion source and detector) was performed on-site by BIRA-IASB personnel.

Table I. m/z values of monitored (O)VOC ion species, tentatively attributed (O)VOC compounds, mixing ratios in the calibration gas bottles and average calibration coefficients and ranges.

m/z	compound	Chemical formula	Concentration in calibration bottle (ppbv)	Calibration coeff. and range (ncps/ppbv)
31	formaldehyde	HCHO	1024	1.4 [0.9-2.8]
33	methanol	CH_3OH	1009	10.2 [8.9-11.7]
42	acetonitrile	CH_3CN	538	15.1 [13.4-18.2]
45	acetaldehyde	CH_3CHO	925	12.7 [11.2-15.3]
47	formic acid	HCOOH	N.A.	6.1 [4.6-8.4]
59	acetone	CH_3COCH_3	967	14.9 [12.5-18.9]
61	acetic acid	CH_3COOH	N.A.	6.8 [5.1-9.6]
63	dimethyl sulfide	CH_3SCH_3	983	8.1 [6.7-10.5]
69	isoprene	C_5H_8	485	3.8 [2.9-5.4]
71	MVK/MACR*	C_4H_6O	1012	9.7 [7.8-12.9]
73	methyl ethyl ketone	C_4H_8O	513	12.4 [10.0-16.6]
79	benzene	C_6H_6	543	7.1 [5.7-9.8]
81	sum of monoterpenes**	$C_{10}H_{16}$	994	5.1 [4.0-7.1]
93	toluene	C_7H_8	471	7.1 [5.6-10.2]
107	xylenes	C_8H_{10}	473	6.3 [4.6-9.2]
137	sum of monoterpenes**	$C_{10}H_{16}$	994	1.5 [1.1-2.1]

*506 ppbv MVK and 506 ppbv MACR, contributions from isoprene hydroxyhydroperoxide (ISOPOOH) cannot be excluded; **limonene was present in the calibration bottle.

3.1.2 PTR-MS (O)VOC measurements at other locations at Réunion Island

A second hs-PTR-MS instrument has been deployed by the Laboratoire des Sciences du Climat et de l'Environnement (LSCE, Paris, France) in collaboration with LaMP in the framework of the Intensive Octave Campaign in April-May 2018. Measurements with this instrument were performed at a coastal (Le Port) and a forested (Bélouve) site. Prior to that campaign, both hs-PTR-MS instruments were calibrated against the home-made calibration unit of BISA and the commercial calibration gas unit (CGU, Ionicon, Austria) of LSCE in order to allow comparison of hs-PTR-MS VOC measurements at the different locations. A good agreement was found between calibration coefficients obtained for the common gases provided by the different gas calibration units for each hs-PTR-MS instrument (see Table II). This quality check was repeated in 2019 at the start of the BIOMAÏDO campaign in which a third PTR-MS instrument, a PTR-TOF-1000 Ultra from the Laboratoire d'Aérologie (LA, Toulouse, France), was involved. This instrument mainly focused on micrometeorological BVOC flux measurements at a forested site on the island. During the BIOMAÏDO campaign, the LSCE hs-PTR-MS instrument performed measurements at Petite France, halfway on the slope between the west coast of the Island and the Maïdo summit.

Table II. Comparison of calibration results of the BIRA-IASB PTR-MS with the two calibration gas units prior to the Intensive OTAVE Field Campaign (April-May 2018). Common compounds provided by the two calibration units are indicated in green.

	Ionicon mixture + French GC unit 05/04/2018		Apel-Riemer mixture + calibration unit BISA 05/04/2018		
m/z	compound	calib coeff (ncps/ppbv)	compound	calib coeff (ncps/ppbv)	diff (%)
33	methanol	8.841	methanol	9.683	9.5
42	acetonitrile	14.688	acetonitrile	14.260	-2.9
45	acetaldehyde	12.838	acetaldehyde	11.936	-7.0
59	acetone	13.961	acetone	13.791	-1.2
63			DMS	7.444	
69	isoprene	3.918	isoprene	3.675	-6.2
71	crotonaldehyde	13.063	MVK+MACR	9.238	-29.3
73	2-butanone	11.901	2-butanone	11.601	-2.5
79	benzene	6.834	benzene	6.399	-6.4
81	alfa-pinene	3.498	limonene	4.584	31.0
83			cis-3-hexenol	2.774	
93	toluene	6.961	toluene	6.735	-3.2
107	xylene	6.124	xylene	5.965	-2.6
137	alfa-pinene	1.636	limonene	1.371	-16.2
47	ethanol	0.373			
57	acrolein	12.174			
113	chlorobenzene	4.469			
115	chlorobenzene	1.393			
147	dichlorobenzene	2.284			
149	dichlorobenzene	1.442			

3.1.3 FTIR measurements

BIRA-IASB is monitoring FTIR solar absorption spectra at Maïdo since March 2013, in the frame of NDACC (Network for the Detection of Atmospheric Composition Change). The measurements are performed with a Bruker 125HR spectrometer in the mid-infrared region (600-4500 cm-1). The measurements are automated and remotely controlled at BIRA-IASB thanks to the implementation of BARCOS (Bruker Automation and Remote Control System) (Neefs et al. 2007). However, the monitoring requires some human intervention. We benefit from the help of the local staff at the University of Reunion Island for small technical issues, e.g. for the filling of liquid nitrogen which is required to cool the detectors. The quality of the spectra is checked at BIRA-IASB. The degradation of the quality is usually due to either the degradation of the mirrors (leading to a reduction of the Signal to Noise Ratio), or to little change of the alignment of the instrument. This required a visit at the site of the BIRA-IASB expert (C. Hermans), in spring 2018 and in September 2019.

Unfortunately, after the 1st January 2020, we encountered experimental issues with the sun-tracker which required replacement of its spare parts. By the time the spare parts were ordered, it was not possible to visit Reunion Island due to the Covid-19 crisis. The mission to fix this instrumental problem could only take place very recently, on October 2021. Since then, the measurements started again.

As part of the NDACC Infra-Red Working Group (IRWG), BIRA-IASB provides long-term measurements of IRWG target gases (O_3, CO, N_2O, CH_4, C_2H_6, HF, HCl, HNO_3, HCN) to the NDACC database (https://www2.acom.ucar.edu/irwg/reunion). The FTIR retrieval strategies of CO, C_2H_2, CH_3OH, HCOOH, and HCHO have been determined in the past for Maïdo (Vigouroux et al. 2009, 2012, 2018). Within OCTAVE, the time-series of these gases have been updated up to 1st January 2020 (due to instrumental failure and the pandemic crisis), and started up again on October 2021.

The retrievals of PAN, C_2H_4 and acetone are challenging due to their very weak absorption signature in the infrared, close to the noise level of the spectra and that can also be masked by other stronger absorbing gases in the same spectral region (in particular water vapour).

In this task, we worked on the optimization of the retrieval strategies for these species (selection of spectral windows, interfering gases, spectroscopic data, a priori profiles, regularization strength, …). It was successful for the PAN time-series: the background, seasonal cycle, as well as stronger events can be detected. For C_2H_4, we found that this species is at the detection limit, leading to highly noisy retrievals, especially during 2013-2014. However, the retrievals were promising when considering only 2019 data, probably because 2019 was a year with particularly intense fires. This species can therefore be studied with our FTIR measurements during biomass burning events in the future, but its retrieval during the background season at the Maïdo site mostly lies below detection limit. The spectral signature for acetone proves to be too weak and covered by saturated water vapour lines, which makes its detection impossible at Maïdo. We tried to retrieve acetic acid instead, since this is a relevant OCTAVE species (measured by both PTR-

MS and IASI instruments). This species is more promising, with the enhancements due to the biomass burning events well observed in 2019.

3.2 Analysis of local measurements (WP2)

The analysis of in-situ (O)VOC concentration measurements is complex. Their temporal variability depends on (i) air mass transport towards the observatory, (ii) strength of emission sources which may vary in time and may depend on local meteorological conditions, (iii) physico-chemical interactions during transport, and (iv) meteorological conditions at the observatory. Mesoscale chemistry models, (e.g., the Non-Hydrostatic Mesoscale atmospheric model, Meso-NH; Lac et al. 2018) are used to consider these effects as much as possible. However, they are computationally expensive and complex to set up. Moreover, high-resolution local emission inventories (biogenic and anthropogenic) are required for Reunion Island to accurately describe atmospheric composition at the Maïdo observatory. Currently, no high-resolution anthropogenic emission inventory is available for Reunion Island. As such, other methods were used to analyse the data generated during the OCTAVE project.

Atmospheric composition is highly affected by air transport towards a measurement site. Accurate information on atmospheric transport towards the Maïdo observatory is critical for analysis of in-situ data. Atmospheric transport models are capable to simulate air-mass transport, either from a source (forward in time), or towards a measurement site (backwards in time). One of these models is the FLEXible PARTicle dispersion model, FLEXPART (Stohl et al. 1998; Pisso et al. 2019). It is a Lagrangian Particle Dispersion Model (LPDM) which ingests meteorological data from numerical weather prediction models (NWPs) to simulate transport of a large number of air parcels, which represent a single air mass, in a turbulent atmosphere. At the start of the OCTAVE project, FLEXPART was run using data generated by either operational global NWPs or from the Weather Research and Forecasting (WRF) research model (FLEXPART-WRF, Brioude et al. 2013). While current global models cannot resolve the complex profile of Reunion Island, WRF can be set up to perform realistic transport features towards Maïdo. However, as WRF is a research model, this takes time to set up and run. Therefore, it is not suitable to analyse the 2-year dataset generated for OCTAVE. In 2015, a regional model of FLEXPART was developed in the framework of STRAP (Synergie Transdisciplinaire pour Répondre aux Aléas liés aux Panaches volcaniques) to trace the dispersion of volcanic plumes over Reunion Island during an intensive field campaign (Tulet et al. 2017; Rose et al., 2021). This regional version of FLEXPART, FLEXPART-AROME, ingests data from the AROME (Applications of Research to Operations at Mesoscale) model. AROME is the operational model used by Météo France. It is run four times a day with a 2.5 x 2.5 km^2 horizontal resolution over the southwestern Indian Ocean. It was found that the model sufficiently reproduces mesoscale transport features around Reunion Island. For FLEXPART-AROME to be used for OCTAVE, it was key to improve on the representation of turbulence in the model. As the Maïdo observatory is located near the top of the planetary boundary layer (PBL), consistency in PBL parameterisation between the NWP and the LPDM is critical.

Traditionally, FLEXPART versions use a PBL parameterisation independent from the NWP model. In order to address this issue, Brioude et al. (2013) implemented turbulent transport driven directly by turbulent kinetic energy (TKE) retrieved from the NWP model in FLEXPART-WRF. However, their implementation resulted in the violation of the conservation of the well-mixedness criterion, as described by Thomson (1987), and therefore these TKE-driven modes were not suitable for use. Due to its importance for Maïdo, the effort to drive turbulence by TKE was revisited in FLEXPART-AROME. In order to constrain transport between regions with different TKE, the Thomson reflection—transmission formalism (Thomson et al. 1997) was applied. This method had already been successfully implemented in the Stochastic Time-Inverted Lagrangian Transport (STILT) model (Lin et al. 2003). However, although the implantation of the Thomson formalism in FLEXPART-AROME strongly reduced accumulation in the model, it resulted in accumulation of air-parcels near the surface. To resolve this, the implementation of a novel adaptive time step to handle discrete changes in TKE proved essential (Verreyken et al. 2019).

Once the FLEXPART-AROME model was developed, it was employed to trace air masses arriving at the Maïdo observatory 24-hours backwards in time (i.e., generate back-trajectories) covering the 2-year campaign. By identifying primary emission regions (anthropogenic near the coast, biogenic at high altitude and marine over sea), we qualified the effect of transport on the (O)VOC composition at Maïdo. Transport modes and sources affecting the atmospheric composition at Maïdo have been identified in a study combining a Positive Matrix Factorisation (PMF) analysis and back-trajectories (Verreyken et al. 2021). PMF is a technique used to isolate the signature of sources on atmospheric composition (e.g., Rocco et al. 2020; Pernov et al. 2021). The PMF decomposes a measurement matrix (x_{ij}) in a combination of factor profiles (f_{kj}), factor contributions (g_{ik}), and a residual (e_{ij}):

$$x_{ij} = \sum_{k=1}^{p} g_{ik} \times f_{kj} + e_{ij}, \quad (1)$$

where i, j, and k represent measurement time, measured compound, and the selected factor, respectively. The total number of factors (p) represents the expected number of sources affecting the dataset and is chosen by the analyser. Equation 1 is solved iteratively by initialising g_{ik} and f_{kj} as a set of random numbers and minimising the residual objective function $Q = \sum_i \sum_j e_{ij}/u_{ij}$, where u_{ij} is the uncertainty for measurement x_{ij}. The major constraint in solving this equation, however, is that neither the source factors, nor the source contribution matrices may contain negative values. A drawback of the algorithm is that it does not take into account chemical loss rates for specific species but rather represents the chemical ageing of air-masses as a linear combination between a primary emission source factor and a secondary source factor. In doing so, the PMF cannot differentiate between distinct chemical lifetimes of species emitted by a source. The PMF analysis was performed using software developed by the United States Environmental Protection Agency (EPA), EPA PMF 5.0 (Norris et al. 2014). Verreyken et al. (2021) for the first time applied a mesoscale LPDM to identify the sources most affecting air quality at the observatory. An earlier study by Lesouëf et al. (2011) made use of the Meso-NH model to qualify the potential impact of emission sources located on the island in meteorological situations representative of different seasons for Reunion Island. The added advantage of the approach from

Verreyken et al. (2021) was the use of 2-year real meteorological forecast data and the use of a PMF analysis to identify the times when specific source contributions were highest.

A separate study focussing on observations of biomass burning (BB) plumes has been carried out (Verreyken et al. 2020). The chemical ageing of pyrogenic emissions may provide valuable clues of atmospheric interactions of specific VOCs (e.g., Jost el al. 2013; de Gouw et al. 2006; Chaliyakunnel et al. 2016). The study: (i) analysed the chemical composition of the BB plumes upon arrival at Maïdo, (ii) compared in-situ and remote measurements of specific air pollutants with the Copernicus Atmospheric Monitoring Service Near-Real-Time (CAMS-NRT) atmospheric composition model which is part of the Integrated Forecast System (IFS) at the European Centre for Medium-Range Weather Forecasts (ECMWF), (iii) employed forward simulations of CO emissions from pyrogenic events, as estimated by the Global Fire Assimilation System (GFAS) v1.2 inventory, from FLEXPART, driven with data generated by the global meteorological model from the IFS at ECMWF, (iv) estimated the impact of BB events in Africa and Madagascar on the local atmospheric composition of the remote marine boundary layer over the southwestern Indian Ocean. To evaluate the chemical composition of the BB plumes, the abundance of (O)VOCs related to pyrogenic emissions were first isolated from the mesoscale source contributions by means of subtracting a median diel profile of the associated season from the discrete intrusions of BB plumes occurring at the Maïdo observatory. These excesses of VOCs (ΔVOC) were divided by the excess CO (ΔCO) giving rise to the enhancement ratio ($\mathrm{EnR_{VOC}} = \frac{\Delta VOC}{\Delta \mathrm{CO}}$). By comparing $\mathrm{EnR_{VOC}}$ to the emission ratio ($\mathrm{ER_{VOC}}$, defined as the the EnR at the source), we infer information on production or loss of the VOC in the BB plume during transport. The emission ratios were calculated using the emission factors (EFs, defined as mass of VOC emitted per kg of dry fuel burned) from literature. For this, a recent publication by Andreae (2019) who compiled results from both laboratory studies and field campaigns, reporting EFs for different types of fuels, was used. The EnR for several VOCs have been determined in 2012 at Reunion Island using data from the FTIR by Vigouroux et al. (2012). The difference between their work and the study by Verreyken et al. (2020), done in the framework of OCTAVE, is not only that they were able to use in-situ data, but critically, that they could focus efforts on relatively young BB plumes due to an abundance of data sampled in these conditions. By using the FLEXPART, transport of ΔCO from pyrogenic sources located in Africa and Madagascar was simulated. These simulates served to (i) support the calculation of NO_2 concentrations from a Multi-AXis Differential Optical Absorption Spectroscopy (MAX-DOAS) instrument operated by the University of Colorado, (ii) calculate the average age of plumes intruding at the Maïdo observatory, and (iii) estimate the effect of BB in southern Africa and Madagascar on the pristine marine boundary layer over the South-West Indian Ocean. The latter was done by multiplying the ΔCO tracer from FLEXPART with the EnRs from data taken at Maïdo.

Lastly, analyses performed in the framework of the OCTAVE intensive field have also contributed to the OCTAVE project. Rocco et al. (2020) have performed a source apportionment study of HCHO at Reunion Island using hs-PTR-MS data at Maïdo, supplemented by HCHO data from an Aerolaser GmbH (AL 4021 model; Garmisch-Partenkirchen, Germany) instrument and additional hs-PTR-MS (similar instrument deployed by the Laboratoire des Sciences du Climat et de

l'Environnement, LSCE) measurements deployed at other location on the island. The source apportionment was done by both a Chemical-Kinetics-Based (CKB) calculation and a PMF analysis. CKB methods have been used in the past to determine the photochemical age of air masses (Yuan et al. 2012) or determine the concentrations of NMVOCs (Parrish et al. 2007). The CKB method has previously been applied by Fried et al. (1997) to estimate the source of HCHO in the US. It relies on information of sources, transport towards -, and other observations at, the measurement site to estimate how much each expected source contributed to the HCHO measurements.

3.3 IASI retrievals of (O)VOCs (WP3)

The objective is to set up a robust suite of algorithms for retrieving the (O)VOCs detected in the IASI satellite measurements, all based on the same general approach. The priority is given to methanol, at the heart of the scientific questions of OCTAVE, and the methodological developments are then extended to other species. In OCTAVE, we developed and applied the version 3 of the ANNI (Artificial Neural Network for IASI) general retrieval framework (Franco et al. 2018). This is an innovative method of fast retrievals, based on (1) the calculation of a Hyperspectral Range Index (HRI) and (2) the implementation of an artificial neural network (NN) to convert the HRI into vertical abundance of the target compound. A schematic is presented in Figure 3. This approach builds on the recent IASI retrievals of ammonia and dust (Whitburn et al. 2016; Van Damme et al. 2017; Clarisse et al. 2019).

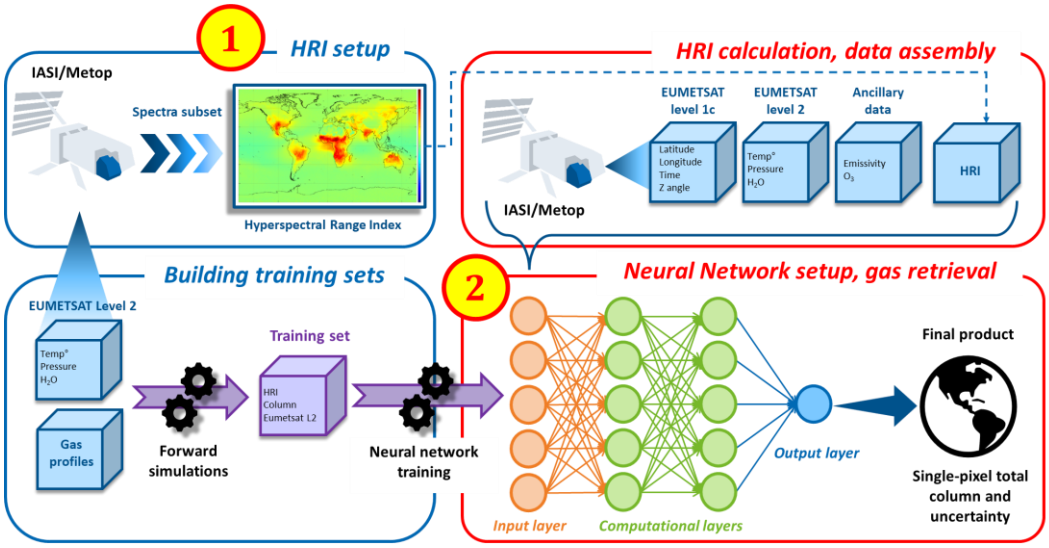

Figure 3. Schematic of the ANNI v3 general retrieval framework.

The first key step is the setup and calculation, for each target species and for each IASI observation, of the HRI. It is a dimensionless metric of the magnitude of the signature of a target absorber in an IASI spectrum, relative to the spectral variability of a "background" atmosphere in the absence of the target gas, i.e., a variability resulting from all other parameters contributing to the spectral radiance, such as other atmospheric gases (Walker et al. 2011). As the HRI is linearly correlated

to the column abundance of the target species, it can be converted – along with other variables – in gas total column. The strength of the HRI is its ability to encompass a large spectral range (hundreds of cm^{-1}), hence to take full advantage of every spectral channel in which the target gas absorbs. Thanks to its sensitivity, the HRI is highly suitable for the detection of weak, broadband infrared absorbers such as the VOCs. For a suite of VOCs detectable in IASI spectra, we have built the covariance matrices, the Jacobians (the gas spectral signature), and selected the most appropriate spectral ranges needed to calculate the HRI. An important point is the calculation of the covariance matrices. As such matrix is a statistical characterization of the correlation between the different spectral channels in the absence of the target gas, it has been built from IASI spectra that do not contain observable amount of the target gas. These spectra were selected from the 2013 IASI observations through an iterative filtering process (Clarisse et al. 2019), ensuring that the selected spectra are representative for various atmospheric conditions and environments.

Previous VOC retrievals used constant multiplicative factors or look-up tables to convert the HRI in total column, which is restrictive because they do not account for, e.g., the state of the atmosphere and Earth's surface. Here, we use a supervised NN for this operation, which can mimic in a comprehensive way the complex connections between the HRI, the state of the atmosphere and surface, and the gas abundance. The NN strength lies in its ability to cope with many input parameters, while not requiring too expensive, sometimes repetitive calculations. Setting up a NN requires a training phase in which the NN learns from the presentation of an extensive dataset including all the necessary input and output variables representative for real IASI observations. In the ANNI v3 framework, the NN inputs are the HRI, a spectral baseline temperature, the H_2O columns, the temperature profile, the surface pressure and emissivity, and the IASI viewing angle (and the column of the main interfering compounds, if relevant), whereas the output is the gas column. For each target species, we built a training set from over 1,000,000 synthetic IASI spectra simulated by a line-by-line radiative transfer model. The advantage of such a synthetic training set is that it is free of the noise and/or scarcity of real measurements, and that the spectra can be generated in large amounts in order to make the training set – and hence the NN – representative of all possible conditions. Two separate synthetic datasets are assembled per target species, one being representative of conditions close to emission sources and the other of mixing/transport conditions (see Whitburn et al. 2016; Franco et al. 2018, for the rationale). Each training set leads to a specific NN that is used to retrieve globally the target species in emission and transport regimes, successively. The training performances are carefully evaluated, and the number of computational nodes and layers deployed by the NN is adapted to ensure optimal performance while keeping the NN as small as possible to prevent overfitting.

In addition to the total column, the NN returns an associated error that is calculated via a perturbation method of the input variables (Whitburn et al. 2016; Franco et al. 2018). A pre-filter prevents the retrieval on cloudy scenes or for observations with missing ancillary data. A post-filter specific to each target species, based on the gas column-to-HRI ratio, is also set up to discard the individual retrievals affected by too large uncertainties or by poor measurement sensitivity to the target gas. This post-filter is not (directly) driven by the gas abundance but rather by the thermal contrast (Franco et al. 2020). Finally, the constant climatological background of target gas

abundance that is not accounted for by the HRI is estimated by (1) comparison with conventional retrievals performed on a subset of IASI spectra, (2) comparison with ground-based FTIR column measurements, and (3) model simulations (e.g., Franco et al. 2018, 2020). The determined offset is thus added to the individual retrieved columns. Once set up, the NN is fed for each individual IASI observation with the appropriate input data.

For each target species, two different products are retrieved. The first one is a near real time product, which is retrieved using the IASI Level 2 information to describe the state of the atmosphere and surface in the NN. The second is a reanalysed product, making use of the ERA-5 reanalysis (Hersbach et al. 2020) for the meteorological input data. This latter has the advantage to provide more consistency throughout the IASI observational time series. The ANNI v3 retrievals have been applied to all the individual observations of IASI/Metop-A (since October 2007), -B (since March 2013), and -C (since September 2019), offering a unique long record of global spaceborne VOCs measurements. For OCTAVE, the ANNI framework has been applied to the retrieval of methanol (CH_3OH), formic acid (HCOOH), acetic acid (CH_3COOH), peroxyacetyl nitrate (PAN), acetone (CH_3COCH_3), acetylene (C_2H_2), hydrogen cyanide (HCN), and ethylene (C_2H_4).

3.4 Global modelling evaluation of OVOC budget and impacts (WP4)

3.4.1 Evaluation of PTR-MS data at Maïdo using the WRF-Chem model

We selected the regional model WRF-Chem (Weather Research and Forecasting Model with Chemistry) for simulating the OVOC distribution at Reunion Island and evaluating the PTR-MS data obtained at Maïdo. WRF-Chem is more appropriate for this task than the MAGRITTEv1.1 regional model due to its finer resolution and better ability to represent transport processes above and around Reunion Island. We tested two different nested grid configurations, either with an outer 60 km grid spacing domain, and inner grids of 15 and 5 km, or with an outer 12.5 km grid and inner grids of 2.5 km and 500 m (Figure 4). The initial and lateral boundary conditions for the large domain are from NCEP reanalyses (for meteorology) and from the MOZART model output (for the chemical compounds).

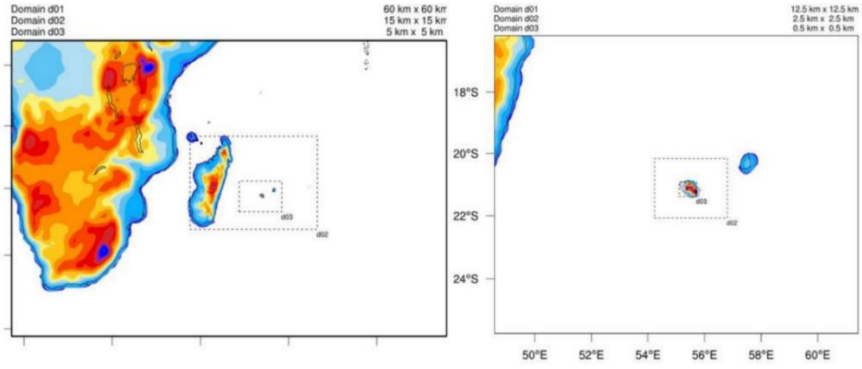

Figure 4. The two triple-nesting configurations used with the WRF-Chem model.

The model uses the MOZART gas-phase chemistry with the GOCART aerosol module. Anthropogenic emissions are from the global EDGAR/HTAPv2 inventory at 0.1°×0.1°, and biomass burning emissions are obtained from the FINN inventory. Biogenic emissions of isoprene are calculated on-line using meteorological fields calculated by WRF. The distribution of plant functional types, isoprene basal emission rates and leaf area index were provided by CNRS-LACy at 100 m resolution and re-gridded onto the WRF-Chem grid. The isoprene emissions were further reduced by 30%. The simulations span from October to December 2017. The meteorological fields are re-initialized every two days using NCEP data to ensure the realism of WRF-calculated dynamical fields. The chemical initial conditions of each two-day run are obtained from the previous simulation.

3.4.2 Global model evaluation of OVOC budgets

The model used for global evaluation of the budget and distribution of OVOCs is the Model of Atmospheric composition at Global and Regional scales using Inversion Techniques for Trace gas Emissions (MAGRITTE v1.1). A new chemical mechanism for NMVOC oxidation has been developed and implemented in MAGRITTEv1.1 (Müller et al., 2019). With 99 organic species and >240 gas-phase reactions and 67 photolytic reactions, this mechanism treats the chemical degradation of isoprene and the chemical formation pathways of acetaldehyde, acetone and methanol, the target species of OCTAVE. It accounts for an extensive evaluation of recent findings related to isoprene degradation, as well as for recent assessments of the methanol source due to the $CH_3O_2 + OH$ reaction (Müller et al. 2016; Caravan et al. 2018; Bates et al. 2021). This reaction is the single largest source of methanol above oceans and produces about 31 Tg/yr globally, in close agreement with the recent study of Bates et al. (2021). The terrestrial biogenic source of acetaldehyde and ethanol are taken from MEGANv2.1 (Millet al. 2010). The biogenic emissions of isoprene and methanol are calculated with the MEGAN-MOHYCAN model (Guenther et al. 2012; Stavrakou et al. 2011). Anthropogenic VOC sources are from EDGAR4.3.2 (Huang et al. 2017). Anthropogenic emissions of all other species are from HTAPv2 (Janssens-Maenhout et al. 2015). Biomass burning emissions are based on GFEDv4 (Giglio et al. 2013) with emission factors from Andreae (2019). The dry deposition scheme for organic compounds has been revised, and the deposition velocities of the main OVOCs were extensively evaluated against field observations (Müller et al. 2018). The model also includes oceanic emissions of methanol (24 Tg/yr), acetone (63 Tg/yr), and acetaldehyde (55 Tg/yr) (Müller et al. 2018), consistent with previous model estimations (Millet et al. 2010; Bates et al. 2021).

3.4.3 Revisiting the global methanol budget

An inversion system based on MAGRITTEv1.1 and constrained by IASI data has been developed. In a first step, the potential discrepancies between IASI and other methanol measurements were examined. Comparisons between FTIR ground-based methanol columns and IASI co-located data are presented in the Results section (WP3). Initial direct comparisons of the model with IASI columns and airborne in situ data indicated the existence of significant discrepancies between the measurement datasets. The model has been used in order to provide a quantitative assessment

of those discrepancies. Since the aircraft instruments measure in situ concentrations, not total columns, assimilation (through inverse modelling) of those concentrations into a modelling system is useful in order to generate 4-d CH_3OH distributions constrained by the aircraft campaigns. To that effect, we conduct an inversion of methanol emissions for years 2012-2013 constrained by the campaign-averaged (density-weighted) measured methanol mixing ratios at the model resolution (2°×2.5°) for three campaigns (see Figure 5). Only below-tropopause PTR-MS data are used. Pixels with scarce data (less than 10 measurements) are discarded. The IASI biases relative to the aircraft are determined by comparing the optimized model columns to the co-located IASI columns.

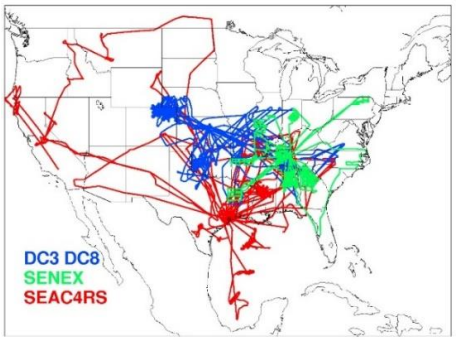

Figure 5. Flight tracks of the 3 campaigns used to derive aircraft-constrained methanol columns for comparison with IASI.

Next, for each year, 3 global inversions are conducted (OPT1, OPT2, and OPT3). In OPT1, uncorrected monthly IASI methanol columns are used as constraints; in the other inversions, the IASI data are bias-corrected based on comparisons with either FTIR data (OPT2) or aircraft data (OPT3).

4. SCIENTIFIC RESULTS AND RECOMMENDATIONS

4.1 Local (O)VOC measurements at Reunion Island (WP1)

4.1.1 Importance of the PTR-MS (O)VOC dataset and recommendation of its use to better understanding sources and sinks of oxygenated organic compounds

Volatile organic compounds play a major role in tropospheric chemistry by being precursors of major air pollutants and short-term climate forcers, such as tropospheric ozone and secondary organic aerosol (SOA), which affect human and ecosystem health and climate. Estimation of the impact of VOCs on air composition and prediction of its evolution requires a good knowledge of their sources and sinks. The budgets of many VOCs and especially oxygenated VOCs (OVOCs) are still highly uncertain due to a lack of knowledge of their formation and loss processes, but also to a shortage of measurements, especially in the southern hemisphere and at remote, tropical marine locations. The Maïdo Observatory at Réunion Island, a small volcanic Island in the remote southwestern Indian Ocean, turned out to be a very interesting location to perform local *in situ* (O)VOC measurements for several reasons:

- Besides some short-term ship-borne measurements (e.g. Colomb et al. 2009) and some exploratory measurements on the Island (Duflot et al. 2019), no *in situ* (O)VOC measurements have been performed in the pristine atmosphere of this part of the Indian Ocean.
- Many other atmospheric constituents are continuously measured at the Maïdo Observatory (which is part of the GAW and ACTRIS networks), which facilitates (O)VOC data interpretation.
- The high-altitude observatory is mostly located in the free troposphere during nighttime and in the planetary boundary layer during daytime. This is an extra complication for data analysis/interpretation, but allows for measurements in the undersampled free troposphere.
- The combination of lush vegetation and daily cloud formation along the slope between the coast and the Maïdo observatory makes Réunion Island an ideal location to study the impact of biogenic (O)VOC emissions on cloud formation and in-cloud (O)VOC processing.

The high temporal resolution 2-year hs-PTR-MS (O)VOC dataset acquired in the framework of the OCTAVE project can therefore be considered as unique and very valuable for evaluation of regional or global chemistry and transport models, but also for evaluation of high spatiotemporal resolution mesoscale models given the high temporal resolution of the dataset (2.7 minutes). Furthermore, the data may contribute to a better understanding of (O)VOC sources and sinks at this location and as potential inputs to physicochemical models for SOA and cloud formation and processing.

4.1.2 Timeline of the dataset

The measurements were performed between 16 October 2017 and 26 November 2019. The timeline in Figure 6 shows that gaps in the dataset were limited and mainly due to shutdown of the instrument prior to the passage near the Island of the intense tropical cyclones Berguitta (9-20/01/2018) and Dumazile (1-6/03/2018), some technical problems (power shut-down at the observatory) and maintenance activities. Also shown on the timeline are the OCTAVE intensive field campaign and the BIO-MAÏDO field campaign which took place on Réunion Island and for which the hs-PTR-MS data at the Maïdo Observatory were of high interest.

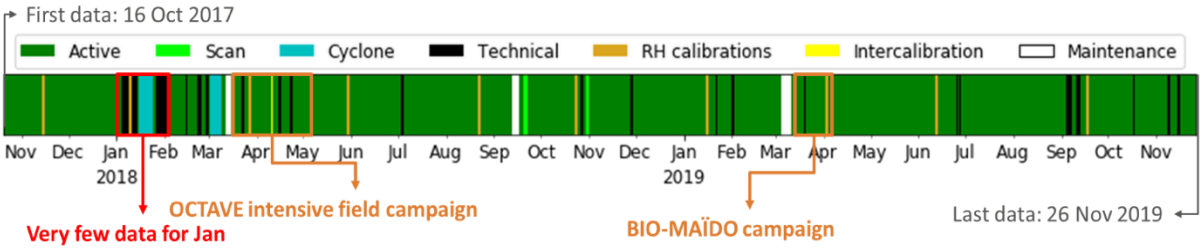

Figure 6. Timeline of the hs-PTR-MS (O)VOC measurements in the framework of the OCTAVE project.

Several special events occurred during the 2-year measurement period, which may have had an impact on the (O)VOC concentrations, such as the severe tropical storm Eliakim and the tropical cyclone Fakir. Moreover, the period was characterized by several local volcanic eruptions, but those did not seem to have affected (O)VOC concentrations at the Maïdo observatory.

4.1.3 Quality and availability of the dataset

The mixing ratios of thirteen (O)VOCs have been derived from the monitored ion signals during the OCTAVE campaign. Some of those compounds are expected to be predominantly emitted by distinct sources (e.g. acetonitrile from biomass burning, dimethyl sulfide from oceans, isoprene from vegetation, benzene and xylene from anthropogenic activities), whereas others are known to have multiple sources. Their average daytime and nighttime mixing ratios, roughly corresponding to planetary boundary layer and free tropospheric conditions, respectively, are shown in Table III. The median and interquartile ranges of the detection limits, the relative precision and accuracy of the mixing ratios for measurements at the highest time resolution (i.e. a cycle time of 2.7 min and a dwell time of 10 s for each (O)VOC) are shown in Table IV. Also shown in this tables are the completeness of the dataset for individual compounds and the fraction of data above the detection limit. The completeness for the different compounds varies between 68 and 74 percent, except for formic acid for which the first measurements only started on June 27th 2018. Besides the data gaps indicated in the timeline, the completeness of the dataset is strongly determined by the regular zero air measurements (every 4 hours) and calibration measurements (every 3-4 days).

The high-resolution hs-PTR-MS dataset is available online (Amelynck C., Schoon, N. and Verreyken, B.: Long-Term in situ (O)VOC measurements at the Maïdo Observatory (Reunion

Island). Royal Belgian Institute for Space Aeronomy (BIRA-IASB) [data set], https://doi.org/10.18758/71021061, 2021).

Table III. Interquartile range of 30-minute average (O)VOC mixing ratios at the high altitude Maïdo Observatory during nighttime (22:00-05:00 LT, free troposphere) and daytime (10:00-17:00 LT, planetary boundary layer). The last column indicates the median 30 minutes average mixing ratio during nighttime with the standard deviation between parenthesis. If the measurement is below the limit of detection (LoD), we write < LoD. Table adapted from Verreyken et al. (2021).

Compound	Daytime MR (pptv)	Nighttime MR (pptv)	Nighttime median MR (σ) (pptv)
methanol	990-1531	525-887	724 (228)
acetaldehyde	179-311	61-101	78 (41)
acetonitrile	84-109	79-110	94 (39)
acetone	355-526	259-379	304 (152)
acetic acid	248-511	64-164	99 (226)
Dimethyl sulfide	11-20	7-16	11 (7)
isoprene	80-223	< 9	< 9
MVK/MACR/ ISOPOOH	48-136	< 3-8	4 (11)
MEK	35-69	11-21	15 (10)
benzene	12-25	4-11	6 (9)
xylenes	< 10-21	< 10	< 10
sum of monoterpenes	< 16-24	< 16	< 16
formic acid	557-1045	172-335	225 (474)

Table IV. Completeness of the high-resolution dataset, percentage of data above the detection limit and statistical parameters for the quantified compounds monitored during the OCTAVE campaign.

Compound	m/z	Complete-ness (%)	> DL (%)	Detection limit (pptv)	Relative precision (%) (1σ)	Relative accuracy (%) (2σ)
				Median [25th percentile – 75th percentile]		
methanol	33	71	100	157 [147-169]	8 [6-11]	18 [14-23]
acetaldehyde	45	71	80	67 [59-79]	21 [13-30]	42 [28-61]
acetonitrile	42	74	100	7 [6-8]	8 [7-9]	17 [15-19]
acetone	59	71	100	15 [13-19]	4 [4-5]	11 [10-12]
acetic acid	61	71	97	34 [29-41]	11 [7-18]	55 [52-62]
dimethyl sulfide	63	74	17	25 [23-27]	41 [35-45]	81 [71-90]
isoprene	69	74	56	24 [20-29]	19 [12-31]	38 [26-61]

MVK/MACR/ ISOPOOH	71	71	60	10 [9-12]	15 [10-26]	31 [20-53]
MEK	73	68	74	14 [13-16]	25 [17-35]	50 [34-71]
benzene	79	71	51	10 [9-14]	35 [26-44]	70 [52-89]
xylenes	107	71	8	30 [27-34]	40 [32-45]	80 [64-91]
sum of monoterpenes	137	74	8	41 [34-54]	43 [33-51]	86 [66-102]
formic acid	47	49	82	135 [119-151]	19 [12-29]	63 [56-77]

4.1.4 Concentration variability of some selected (O)VOCs at the Maïdo observatory

All compounds except acetonitrile showed a pronounced diurnal variability, as shown in Figure 7 for a subset of compounds. This variability is determined by many factors such as surface emissions and their potential dependence on environmental conditions, long-range and mesoscale transport towards the measurement location, efficiency of secondary (O)VOC production and boundary layer dynamics. The application of mesoscale transport models such as FLEXPART-AROME is required for correct interpretation of this variability, as will be explained in more detail in the results of WP2.

The variability in local environmental conditions between summer 2018 and 2019 is clearly reflected in the diurnal profiles of isoprene, the emission of which is known to be strongly light and temperature dependent. Furthermore, the seasonal variability of isoprene and its oxidation products is well correlated with the seasonal local light and temperature variation. Most compounds, however, do not follow this clear seasonal pattern, but show enhanced concentrations between August and November, a period which covers the biomass burning season. This is illustrated for CH_3CN, a typical long-lived biomass burning product, in Figure 8. The strong increases in CH_3CN mixing ratios correlate with the occasional arrival of biomass burning plumes from Africa or Madagascar at the observatory. Methanol, acetone, benzene and formic and acetic acid mixing ratios in those plumes are also strongly enhanced with respect to background concentrations. Further analysis of those pollution events will be discussed in the results section of WP2 as well.

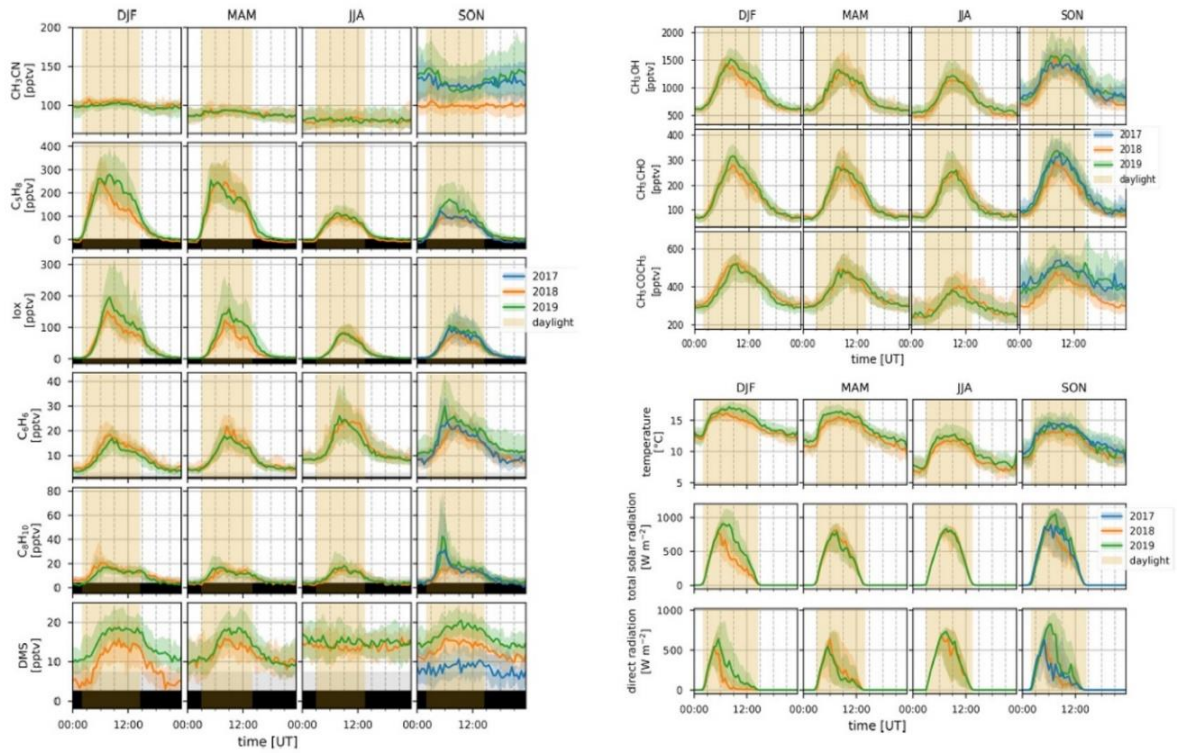

Figure 7. Median dial profiles (lines) and the interquartile distance (shaded area) for DJF (December-January-February), MAM (March-April-May), JJA (June-July-August) and SON (September-October-November) in 2017, 2018 and 2019, for some selected (O)VOCs and environmental conditions. The yellow shaded area means daylight measurements. Adapted from Verreyken et al. (2021).

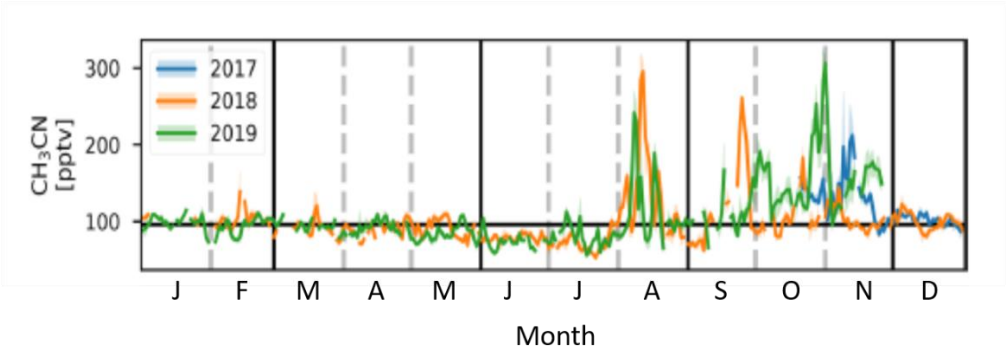

Figure 8. Seasonal variability of daily averaged CH_3CN concentrations in 2017, 2018 and 2019.

4.1.5 FTIR retrievals

Following the retrieval strategies defined in Vigouroux et al. (2012, 2018), we have updated the time-series of the target gases at Maïdo: CO, C_2H_2, CH_3OH, HCOOH, and HCHO (Figure 9). These data have been used in WP2, where they have been compared to local PTR-MS measurements. The HCOOH FTIR data have been used for the validation of IASI data (WP3), and contributed to Franco et al. (2019, 2021). The CH_3OH FTIR data have been used by the modelling partners (WP4). The CO and HCHO FTIR data have also been exploited for the validation of TROPOMI data (Sha et al, 2021; Vigouroux et al. 2020), within the Prodex/BELSPO TROVA-2 project.

We worked on optimizing the retrieval of PAN from our ground-based spectra, and obtained a product with a reasonable precision (about 5%), considering the very weak PAN spectral signature which makes its detection challenging. Indeed, the biomass burning events which took place on 9-11 November 2017 were observed in the PAN data series as in the other well-detected species of the OCTAVE dataset (Figure 9). In 2019, the strong biomass burning events observed in the PAN time series (e.g., 1 October, 31 October –1 November) were attributed to plumes from Southern Africa and Madagascar, by using CO and HCHO daily observations from the TROPOMI satellite sounder. The calculated correlation between PAN and CO during the biomass burning season (August-November) is equal to 0.75 in 2019, and to 0.58 for the whole 2013-2019 time series. The higher correlation in 2019 is likely due to the fact that 2019 was a year with particularly intense fires, allowing for an easier detection of PAN enhancements. However, systematic uncertainties linked to this weak signature might complicate the PAN long-term time-series analysis. In addition, instrumental interventions (2015, 2018) might have caused problems in the long-term consistency of the data that have to be further investigated. Comparisons with satellites and models could help to distinguish between real variability or systematic error, and to consolidate our systematic error budget.

As mentioned before, the detection of acetone at Maïdo was not successful (the spectral signature being too weak and covered by saturated water vapour lines), so we optimized the retrieval strategy of acetic acid instead. We obtain a precision of about 10% on individual total columns. The biomass burning events are well seen in the time-series during the fire season (Figure 9). The correlation with CO is 0.54 and 0.61 for the whole period and in 2019, respectively.

Despite the optimization of C_2H_4 retrievals, this species is at the detection limit, and this leads to a large scatter in the columns, and a precision estimated to about 45%, when we use a stricter limit on the noise of the spectra (RMS < 0.14 for C_2H_4; in blue in Figure 9), which results in fewer remaining data than for the other species.

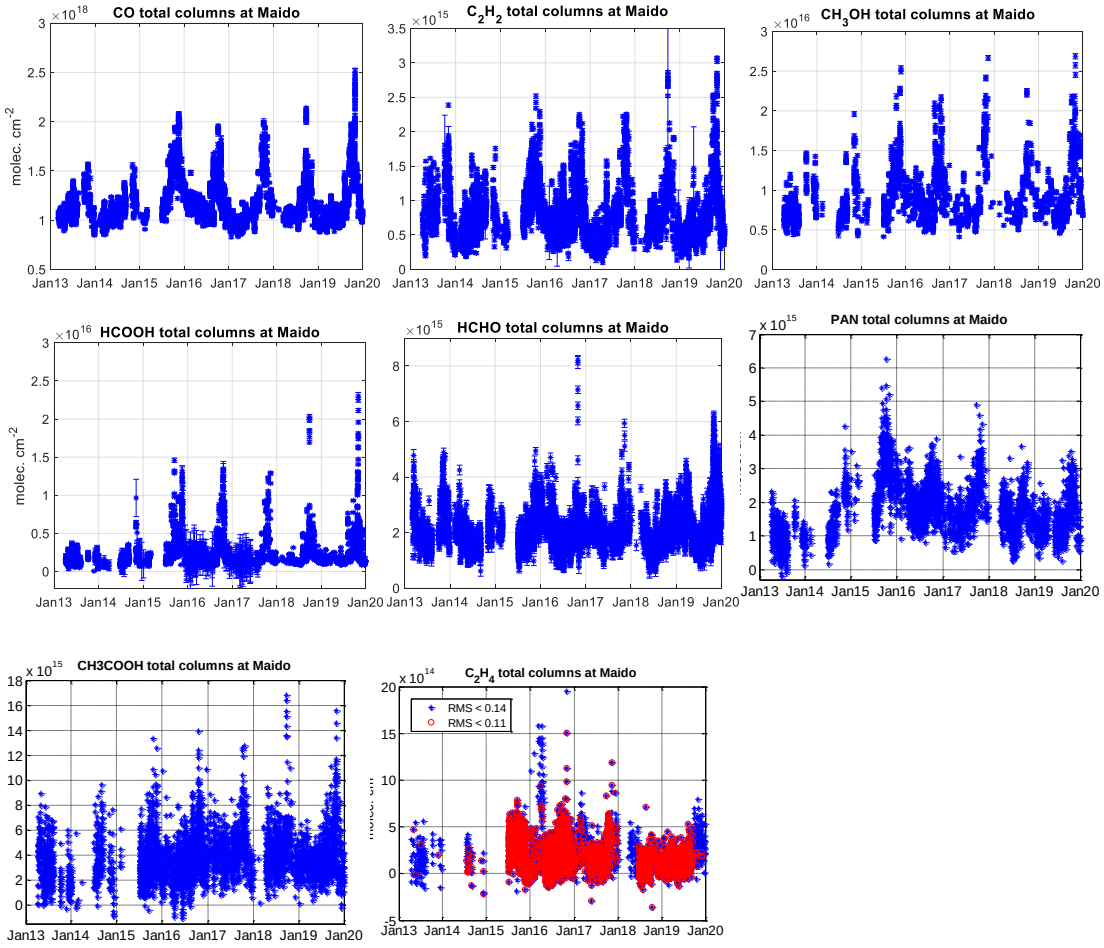

Figure 9. CO, C_2H_2, CH_3OH, HCOOH, HCHO, PAN, CH_3COOH, and C_2H_4 total FTIR columns at Maïdo during 2013-2019.

If we use an even stricter criterion on the noise of the spectra (RMS < 0.11; in red in Figure 9), the precision improves to 36%, and some high columns in spring 2016 (not observed in other species) are then filtered out, while the high columns observed during the fire season remain (as for the other species). However, few spectra remain after this filtering in some of the measurement periods (2013, end of 2019), when the signal-to-noise ratio (SNR) of the spectra was not optimum. It is therefore very important for the detection of C_2H_4 that the SNR of the spectra is as high as possible. This is usually obtained when the alignment of the instrument is perfect, the mirrors are not altered, etc., meaning that this species needs more human interventions and a higher experimental cost for an optimal detection.

The ground-based column measurements of these challenging species (PAN, C_2H_4, acetic acid) are unique or very sparse in the world. Therefore, these time-series provided within OCTAVE are of great interest. We will apply the retrieval settings optimized in this study to the spectra recorded at the Porto Velho site (Brazil), the biogenic VOCs being much more abundant than at Maïdo, as already observed for e.g., HCHO (Vigouroux et al. 2018), the measurements at this new site will be facilitated. Both sites can then be used for the IASI and model comparisons.

4.2 Analysis of local measurements (WP2)

4.2.1 Developing FLEXPART-AROME: a new mesoscale transport model to simulate atmospheric transport at Reunion Island

The analysis of *in situ* data acquired in the framework of the OCTAVE campaign prompted the development of FLEXPART-AROME, a new mesoscale Lagrangian particle dispersion model (LPDM) based on the Weather Research and Forecast limited area version of the FLEXible PARTicle dispersion mode, FLEXPART-WRF. In order to use the offline LPDM in a complex domain, the turbulence in the LPDM needs to be driven by turbulent kinetic energy (TKE) obtained from the numerical weather prediction model (NWP). The initial implantation of TKE-driven turbulence in FLEXPART-WRF resulted in accumulation of particles in low-turbulent regions (Brioude et al., 2013) which was in violation of the conservation of the well-mixedness criterion to validate this type of models (Thomson 1987). However, the Stochastic Time-Inverted Lagrangian Transport (STILT) model (Lin et al. 2003) was able to include TKE-driven turbulence in their framework by implementing the Thomson transmission-reflection formalism at discrete TKE interfaces (Thomson et al. 1997). Implementing this formalism in the TKE-driven modes of FLEXPART-AROME resulted in residual accumulation in high-TKE regions of the model (Verreyken et al. 2019). In order to resolve this issue, an adaptive turbulent time step was implemented.

Conservation of well-mixedness of relevant turbulent modes in FLEXPART-AROME is shown in Figure 10. Additional tests describing the dispersion of a particle release at the surface to evaluate vertical mixing, and the dispersion of a marine tracer further validated the new TKE-driven turbulent options in FLEXPART-AROME. However, due to the configuration of the FLEXPART-AROME model and its TKE modes compared to the traditional setup of FLEXPART(-WRF), the computational time to perform model simulations was increased. For the well-mixedness tests this constituted an increase of computation time up to a factor of 5.21 compared to the traditional turbulence parameterisation used in FLEXPART. The reason for this large increase is the high fraction of particles situated above the planetary boundary layer (PBL) in the model. Traditionally, they do not undergo turbulence and the computational loop to resolve these (vertical) turbulent motions, is not executed. In contrast, the novel TKE driven setup does not discriminate between particles in, or above the PBL. Instead, in regions with low turbulence, the number of steps in this loop to resolve (vertical) turbulent displacements is minimized in a natural way. However, if a large fraction of particles is above the PBL, this results in a significant slowing down of the model. The tests with the marine boundary layer tracer and the surface releases showed that the model slowed down by 6-37%. As the simulations that require this TKE-driven turbulence are generally necessary for describing the PBL consistent with the NWP and include mostly particles in this region of the model, it was estimated that this computational cost is acceptable for our purposes.

The development of FLEXPART-AROME and the novel TKE modes in the model was presented by Verreyken et al. (2019). Since its development, FLEXPART-AROME has been used in other studies analysing in-situ measurements (Verreyken et al. 2020; 2021; Mascaut et al. 2021),

generate back-trajectory forecasts in support of the BIO-MAÏDO campaign (Leriche et al., in prep), and compare results from a high-resolution trajectory model developed in the framework of BIO-MAÏDO to link VOC measurements between two sites at Reunion Island (Rocco et al., submitted). Currently it is also being adapted for use by Météo France in emergency preparedness exercises and for use in combination with AROME forecasts generated in the arctic region. Moreover, an adapted version of the new TKE mode, which was validated in Verreyken et al. (2019), was implemented in a version of FLEXPART-WRF by Cornwell et al. (2021) to simulate dust transport in a convective boundary layer. From testing different TKE modes in their setup, the adapted version of Verreyken et al. (2019) was selected as most suited for their purposes.

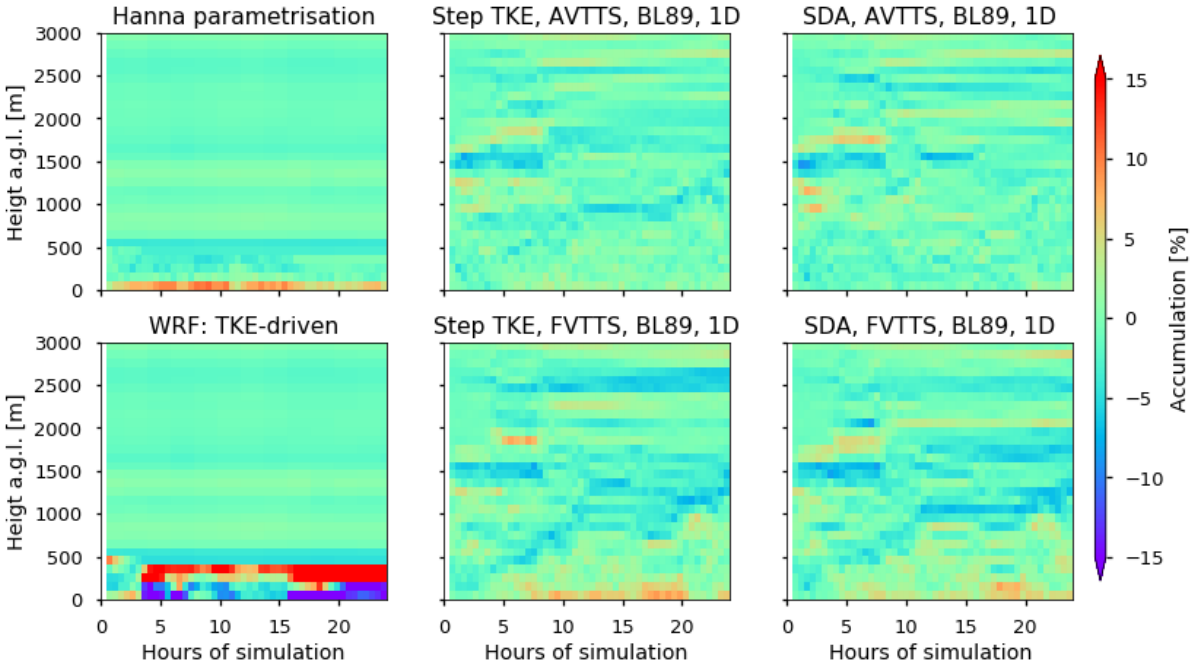

Figure 10. Results of testing the conservation of well-mixedness in the FLEXPART-AROME model. The color indicates the accumulation (or dilution) [%] in the output grid (height above ground level [m], 100 m vertical resolution, y-axis) over a simulation of 24 hours (half hour resolution, x-axis). The top left panel show the performance of the traditional turbulent parameterisation used in FLEXPART which is currently the standard in FLEXPART-WRF also. The bottom left panel shows strong accumulation/dilution at the top of the boundary layer/surface in the configuration using TKE-driven turbulence as implemented by Brioude et al. (2013). The remaining 4 panels show a selection of turbulent modes implemented by Verreyken et al. (2019) in FLEXPART-AROME. The traditional fixed vertical turbulent time step (FVTTS) configurations are shown in the lower 2 plots on the right. The novel adaptive vertical turbulent time step (AVTTS) configuration are the upper 2 plots on the right. The conceptual difference between the middle column and the right column is the distribution of TKE. The middle column distributes TKE homogeneously in a grid cell of the meteorological mode and considers the Thomson transmission—reflection formalism only at the edges between grid cells (Step TKE). The rightmost column localises TKE by interpolating between the two adjacent TKE values and considers the Thomson transmission—reflection formalism at each displacement in a small discontinuity approximation (SDA). Turbulence is considered only in the vertical (1D) and the turbulent mixing length was calculated using the Bougeault-Lacarrère parameterisation (BL89; Bougeault and Lacarrère, 1989). It is clear that the AVTTS configuration conserves well-mixedness better than any other turbulent mode currently available in FLEXPART-AROME. Figure adapted from Verreyken et al. (2019).

4.2.2 Source apportionment of HCHO at Maïdo based on PTR-MS (O)VOC and Aerolaser HCHO measurements

The first study using the OCTAVE in-situ (O)VOC dataset was by Rocco et al. (2020) who used it to support a source apportionment study of HCHO during the OCTAVE intensive observation period (OCTAVE IOP). This was done by using two source apportionment techniques. The first was a Chemical-Kinetics-Based (CKB) calculation method. The CKB method uses information of other VOC observations, both at the measurement site and at emission sources, to estimate the expected amount of HCHO. By comparing this estimated HCHO concentration with measurements, the effect of missing sources can be quantified. The second method uses a positive matrix factorisation (PMF) approach. PMF is a data-driven method that characterizes a number of source factors which affect the dataset with different contributions over time. Application of the CKB method resulted in an estimation of the HCHO contributions from primary anthropogenic emissions, primary biogenic emissions, and from aged (i.e., secondary formation linked to) biogenic emissions. A large fraction of HCHO was unaccounted for by this method and attributed to 'unknown' sources. The PMF method allowed to identify contributions of primary biogenic emissions, secondary formation linked to biogenic emissions, primary anthropogenic sources linked to evaporative or combustion emissions (separately), and a background factor which was characterised as 'unknown'.

Figure 11 illustrates the apportionment of HCHO to the different sources according to both methods. CKB leaves 89 % of HCHO unaccounted for, much higher compared to the result from PMF (32 %). The fraction of known contributions, however, is similarly partitioned by both methods, the secondary biogenic source being the strongest contributor (67% for CKB, 59 % for PMF), followed by the primary anthropogenic source (25% for CKB, 22% for PMF), and the primary biogenic source contributes the least among the known sources (8% for CKB, 19% for PMF). Rocco et al. (2020) was the first study contributing to the identification of HCHO sources in the remote marine atmosphere.

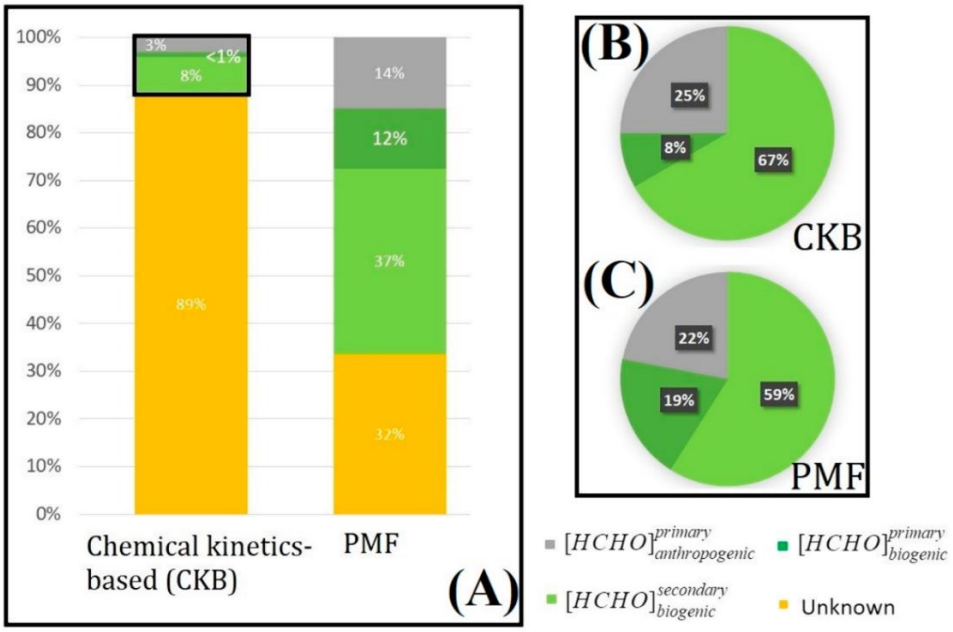

Figure 11. (A) Estimation of formaldehyde sources at the Maïdo site with CKB and PMF analysis. Percentages in pie chart format for the known part for (B) CKB and (C) PMF. Figure from Rocco et al. (2020).

4.2.3 Characterisation of African biomass burning plumes and impact on the atmospheric composition over the southwest Indian Ocean

A second case study using the OCTAVE dataset was presented in Verreyken et al. (2020). It focused on biomass burning (BB) intrusions recorded with the hs-PTR-MS instrument at the Maïdo observatory recorded at the beginning of August in 2018 and 2019. By combining the *in situ* (O)VOC data with the long-term operational observation of CO performed at the observatory, enhancement ratios (EnRs, with respect to CO) were calculated (Table V). Comparison of these EnRs with the expected emission factors of the (O)VOCs at the sources may result in important clues about atmospheric chemistry as pyrogenic emissions provide a unique opportunity to quantify changes in the chemical composition of the plumes and extrapolate information on atmospheric chemistry. Verreyken et al. (2020) identified the formation of both acetone and formic acid in the BB plume during transport from the source to the observatory. The production of acetone was accounted for by the emission ratios of known acetone precursors from pyrogenic sources. The production of formic acid however could not be accounted for by known precursors at the source. As such, a missing source of formic acid in biomass burning plumes is suggested from the analysis. The result of Verreyken et al. (2020) was consistent with Chaliyakunnel et al. (2016) who used satellite observations over Africa for their analysis.

Additionally, comparison of in-situ ozone measurements at the time of the BB plume intrusions at the observatory with the Copernicus atmospheric monitoring service's near-real-time atmospheric composition model (CAMS-NRT) for 2019 showed that the CAMS-NRT model underestimated ozone formation in the BB plumes (Figure 12). Comparison of NO_2 from CAMS-NRT with NO_2 from a Multi-Axis Differential Optical Absorption Spectroscopy instrument for the

University of Colorado (CU MAX-DOAS), deployed at the observatory, revealed that the discrepancies in ozone were correlated with discrepancies in NO_2 concentrations. As the in-situ CO observations were consistent with the model, the ozone and NO_2 discrepancy could not be due to bad resolution of transport from the source towards the measurement site. Indeed, it is more likely that misrepresentation of either VOC and NO_x emissions at the source, or of NO_x recycling during transport are the sources of discrepancies observed between the in-situ and CAMS-NRT modelled ozone concentrations at the location of Maïdo. Lastly, efforts were made to simulate transport of pyrogenic emissions with FLEXPART and qualify the impact of mesoscale emissions on measurements during the BB plume intrusions with FLEXPART-AROME. From the FLEXPART-AROME simulations, it was clear that the BB plumes were mostly recorded at times where the observatory was less sensitive to mesoscale emissions.

Table V. Calculated enhancements ratios (EnRs; pttv $ppbv^{-1}$) - relative to CO – for the identified biomass burning intrusion in Verreyken et al. (2020). Between parentheses are the standard deviations of the EnRs (pttv $ppbv^{-1}$) obtained from the linear regressions.

	3-5 Aug 2018	8-14 Aug 2018	17-19 Aug 2018	6-8 Aug 2019	10-11 Aug 2019	15-18 Aug 2019
Acetonitrile	1.61 (0.02)	1.71 (0.01)	1.69 (0.04)	1.79 (0.01)	1.69 (0.04)	2.06 (0.03)
Formic acid	29.3 (0.5)	23.5 (0.3)	17.5 (0.5)	33.8 (0.5)	24.6 (0.9)	31.2 (0.6)
Acetone	8.85 (0.22)	7.76 (0.13)	6.48 (0.14)	7.85 (0.08)	7.06 (0.26)	10.0 (0.3)
Acetic acid	18.0 (0.3)	12.9 (0.2)	9.8 (0.3)	16.3 (0.2)	13.2 (0.5)	13.7 (0.2)
Ozone	640 (19)	438 (9)	635 (27)	461 (9)	410 (20)	422 (16)
Benzene	0.83 (0.04)	0.46 (0.01)	0.27 (0.01)	0.50 (0.01)	0.50 (0.02)	0.46 (0.02)
Methanol	18.8 (0.6)	13.5 (0.4)	8.7 (0.5)	15.9 (0.3)	14.2 (0.8)	16.8 (0.7)

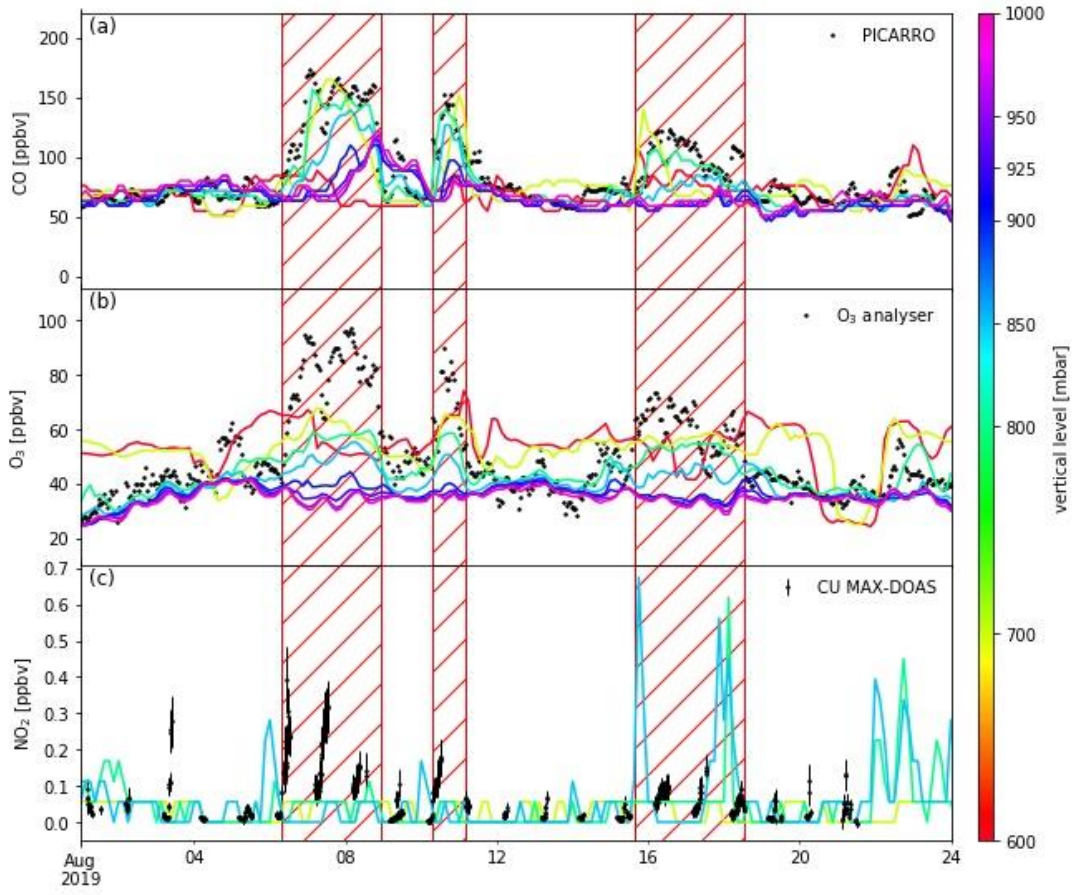

Figure 12. Comparison between the chemical composition at the location of Maïdo as computed by the CAMS-NRT model and instrumentation deployed at the Maïdo observatory. (a) CO mixing ratios [ppbv] computed by CAMS-NRT on different vertical levels (coloured lines), and measured by the PICARRO. (b) Mixing ratios for ozone [ppbv] as simulated by CAMS-NRT (coloured lines), and measured with the O_3 analyser located at Maïdo. (c) shows the NO_2 mixing ratios [ppbv] as measured with the MAX-DOAS instrument of Colorado University (CU) and as computed by CAMS-NRT. Note that the CU MAX-DOAS instrument is a remote sensing instrument of which data is collected in the limb-viewing configuration which is representative of the boundary layer near the measurement site and should correlate well with the horizontal resolution of CAMS-NRT. The other measurements are from in-situ analysers. It is found that at the location of Maïdo (792.8 mbar), there is a low bias between the CO measurements and the simulated mixing ratios. However, there is a large underestimation of both O_3 and NO_2 during periods where biomass burning plumes were observed (red hatched regions). Large discrepancies between the model and O_3 were correlated with discrepancies between the model and NO_2. Figure from Verreyken et al. (2020).

The simulations allowed quantification of the mean plume age during each intrusion and estimation of the effect of pyrogenic emissions on the marine boundary layer over the southwestern Indian Ocean. Plume ages were estimated to be between 7 and 14 days at the time of the measurement. This study was valuable as it confirms a currently missing source of formic acid as identified by Chaliyakunnel et al. (2016). Moreover, it evaluated the CAMS-NRT atmospheric chemistry model which is used to forecast air quality on a global scale. Incorrect reproduction of ozone levels in BB plumes may carry important consequences for regions downwind of pyrogenic emission sources. Lastly, the effect of pyrogenic emissions on one of the last pristine regions on Earth may be important for future studies evaluating the atmospheric composition over the southwestern Indian Ocean. The method used may also be of interest for

future intercomparisons between the chemical composition of biomass burning plumes recorded at Maïdo and in the marine boundary layer to characterise differences in chemical ageing between plumes in the free troposphere versus plumes in the marine boundary layer.

4.2.4 (O)VOC source apportionment at the Maïdo observatory by positive matrix factorization, supported by source-receptor relationships from FLEXPART-AROME

Verreyken et al. (2021) presented the variabilities in the complete 2-year (O)VOC dataset generated in the framework of the OCTAVE project by selecting tracers linked to specific sources. This work was accompanied with a source apportionment using the 2-year long dataset using the PMF technique and 24-hour back-trajectories generated for duration of the deployment of the hs-PTR-MS instrument at the Maïdo observatory. Four PMF source factors were identified from hourly averaged data recorded at Maïdo. The attribution of each species included in PMF to each factor (background, anthropogenic, primary biogenic, and secondary biogenic source factors) is shown in Figure 13. This is one factor less than what was identified by Rocco et al. (2020) using OCTAVE IOP data. While Rocco et al. were able to identify 2 source factors associated with anthropogenic emissions, Verreyken et al. were only able to identify one factor linked to anthropogenic activity. Moreover, the background factor from Verreyken et al. (2021) includes contributions from pyrogenic emissions occurring in southern Africa and Madagascar, as was evident from the enhanced contributions of the background factor during the biomass burning season at Reunion Island (September to November) with occasional increases linked to BB plume intrusions.

The discrepancies between PMF source factors identified by Rocco et al. (2020) and Verreyken et al. (2021) most likely stem from (i) the lack of representation of BB plumes during the OCTAVE IOP, (ii) a different selection of (O)VOCs included in the PMF analysis (e.g., HCHO from the additional instrument deployed in the framework of the OCTAVE IOP), and (iii) a difference in averaging strategies for the PMF input data. While Verreyken et al. (2021) preferred to average the (O)VOC concentrations over 1 hour to increase the measurement precision and match the time-resolution of CO measurement (also included in their PMF), Rocco et al. (2020) interpolated the hs-PTR-MS to 1 min intervals to match the time-resolution of the Aerolaser instrument used to measure HCHO. This averaging strategy may also contribute to why Verreyken et al. (2021) were not able to discern between evaporative and combustion sources as both sources are located further away from the observatory and are in close proximity of each other. As such, differences in arrival time at the observatory, driven by mesoscale transport features, may be resolved in a sub-hourly time-scale but not at the hourly scale. Lastly, Verreyken et al. (2021) presented diel profiles of the impact of surface emissions located in mountainous regions (mostly biogenic emissions), coastal regions (dominated by anthropogenic emissions), and over sea (marine emissions). If was found that the diel sensitivity to the different types of emissions corresponded well with the diel variation of both the PMF source factors and those of the specific VOC tracers linked to the specific sources.

Another feature that was present in all three diel profiles (from the tracers, PMF source contributions, and source-receptor relationships from FLEXPART-AROME) was the discrepancy

between profiles related to the wind direction recorded at the observatory. This was most notably so for anthropogenic tracers which were strongly enhanced in westerlies compared to easterlies. This behaviour was also noted from the FLEXPART-AROME back-trajectories which suggested enhanced sensitivities to emissions occurring in coastal regions when winds were coming from the West. However, the discrepancy between contributions in the secondary biogenic source factor when winds were coming from the East/West were not found from the source sensitivities calculated with FLEXPART-AROME back-trajectories. This indicates that there was a stronger source linked to this factor located East of the Maïdo observatory. As we are discussing stronger contributions from a source factor linked to secondary formation, this may be due to either (i) a stronger source of primary biogenic emissions located East of the observatory, or (ii) a stronger sink of the primary source before air masses reach the observatory. By looking at the horizontal distribution in a surface layer of 500 m above ground level for the 5% strongest contributions of the different source factors identified by the PMF analysis, Verreyken et al. (2021) identified the sources that affect the VOC loading at Maïdo strongest. These footprints are shown in Figure 13. The background source factor was the least sensitive to emissions from the island, indicating that its origins lie in the free troposphere. The anthropogenic source shows stronger sensitivities to emissions occurring west of the observatory, while the biogenic source factors (both primary and secondary) were found to be most sensitive to emissions occurring to the east of the observatory (Figure 14).

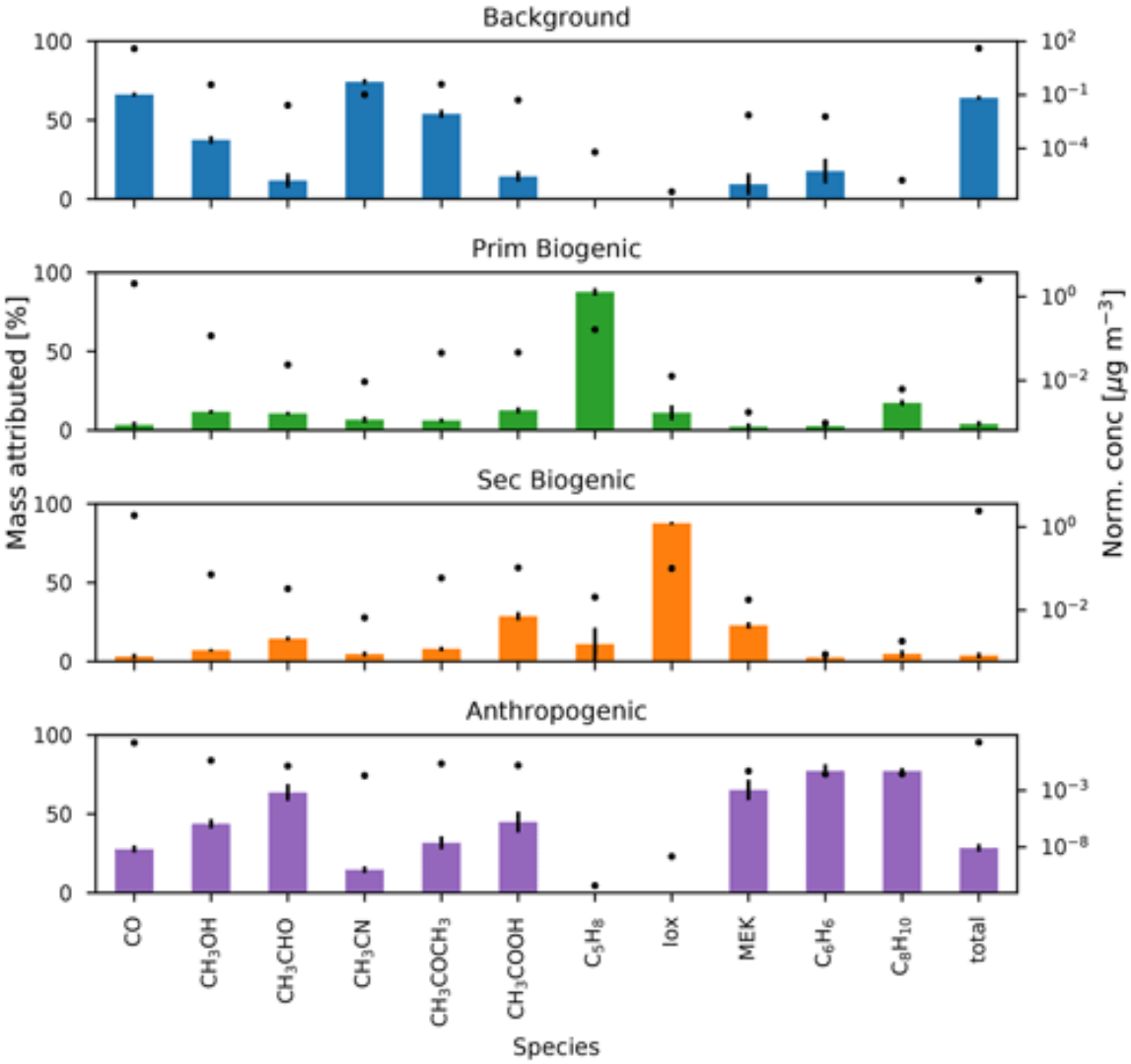

Figure 13. The median fraction of mass attributed (%) to the background, primary biogenic, secondary biogenic, and anthropogenic factors calculated by the bootstrapping algorithm (bars, interquartile distance shown by error bars) and the median normalized concentration ($\mu g\ m^{-3}$) of the factor profiles (markers). Figure from Verreyken et al. (2021).

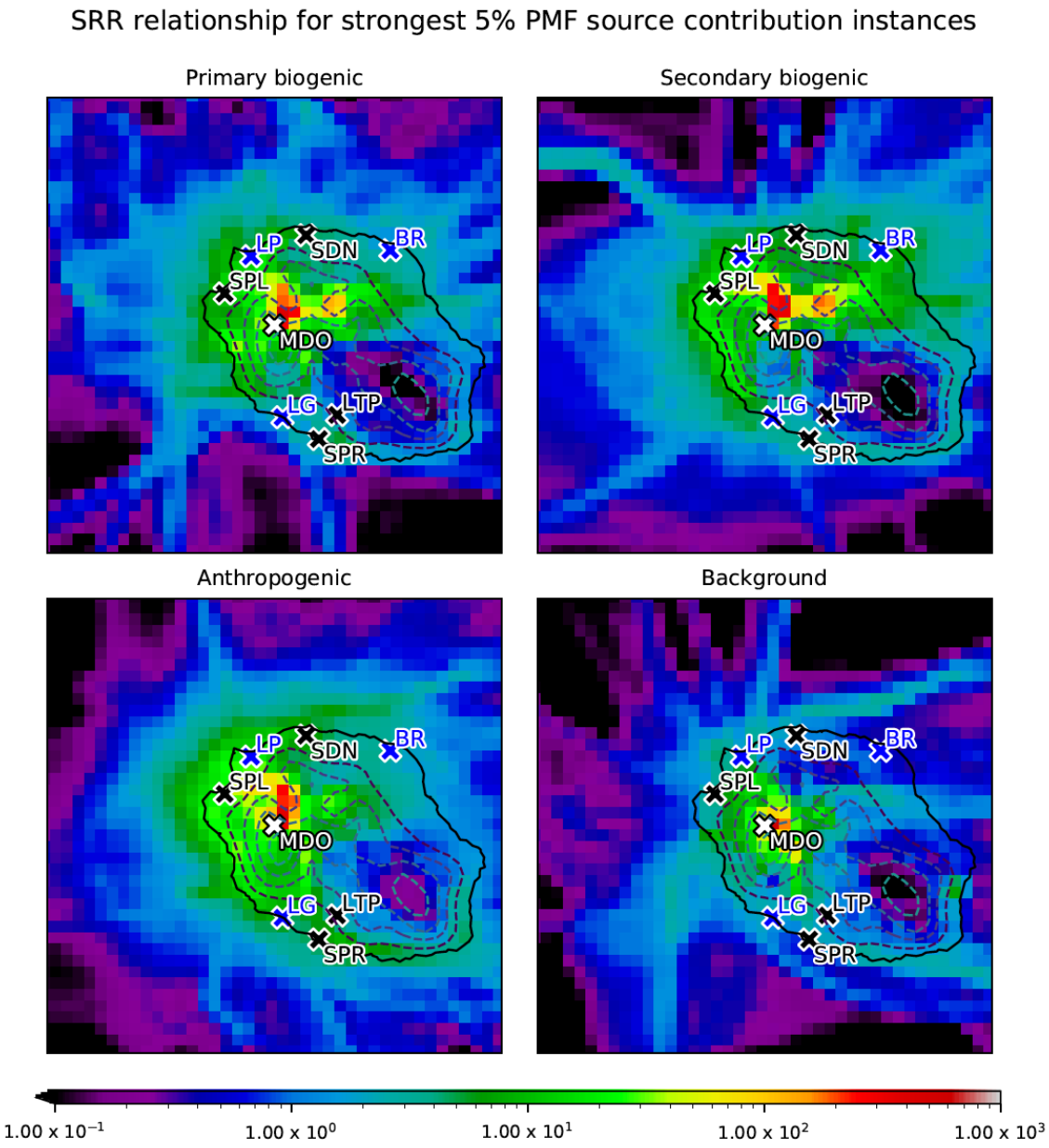

Figure 14. Source-Receptor Relationships (SRRs) showing the sensitivity of in-situ measurements at Maïdo (MDO) to emissions occurring at Reunion Island for the times within the 5% strongest contributions for the 4 different PMF source factors from Verreyken et al. (2021). The observatory is represented by a white marker (MDO) while the largest anthropogenic emission sources are located at the other markers. Blue markers indicate the location of large industrial centres located around power plants (BR, Bois Rouge; LP, Le Port; LG, Le Gol), while the black markers indicate the largest cities located on Reunion Island (SDN, Saint-Denis; SPL, Saint-Paul; LTP, Le Tampon; SPR, Saint-Pierre). The SRRs are calculated using back-trajectories located 500 m above ground level. The background source factor is least sensitive to emissions located on the Island which was expected as this factor is dominant during the night when the observatory is generally under the influence of the free troposphere. Moreover, from both the biogenic and the anthropogenic source factor, we find an influence from the valley of Rivière des Galets, between Mafate (The cirque located directly East from MDO) and Le Port. Additionally, we find that both the primary and secondary biogenic source factors have significant contributions further East from MDO, at the location of Salazie, one of the three cirques on Reunion Island. Finally, the anthropogenic source factor seems to be most affected by anthropogenic centres located West of MDO, namely LP, SPL, and LG, compared to the other major locations of human activity. Figure from Verreyken et al. (2021).

4.2.5 Application of the (O)VOC dataset in the framework of the BIOMAÏDO campaign

The latest study using (O)VOC data from the hs-PTR-MS deployed at Maïdo in the framework of OCTAVE is currently under review (Rocco et al., submitted). It was performed for the BIO-MAÏDO campaign that took place at Reunion Island in March-April 2019. During that campaign, different proton-transfer-reaction mass-spectrometry instruments were deployed at several sites of Reunion Island. A high-resolution trajectory model, MESO-CAT, driven by meteorological data provided by the mesoscale model Meso-NH (Lac et al. 2018), was used to identify dynamical connections between measurements at a site located at Petit-France (a small municipality located along the Maïdo mountain slope) and the Maïdo observatory. By making use of the high-resolution trajectory calculations combined with the CORINE land cover database, the sources affecting atmospheric composition at Maïdo have been identified by analyzing the fraction of time that was spent over specific sources in the PBL during the last 12 hours before measurements. Major categories affecting the measurements were biogenic in nature (i.e., mixed forest, 3-47%; sugar cane plantations, 1-17%). It was also found that trajectories are often located over the ocean during the day (up to 50% of the time over the last 12 hours before arriving at Maïdo). Anthropogenic sources were potentially underestimated by this approach due to their extremely local nature in the CORINE maps.

4.2.6 Recommendations for future use of the PTR-MS (O)VOC dataset

To further exploit the data generated in the framework of the OCTAVE project, use of mesoscale chemistry models is advisable. To respond to the lack of a good anthropogenic emission inventory on the scale of Reunion Island, FLEXPART-AROME back-trajectories can be further exploited to drive an inversion of e.g., benzene, the atmospheric lifetime of which is of the order of a few days. As a result, loss of benzene during transport from sources located on the Island towards the Maïdo observatory can be neglected, allowing to use the 24h back-trajectories generated for the analysis of Verreyken et al. (2021). An additional advantage is that the impact of remote sources on benzene concentrations during the day is estimated to be negligible outside of the biomass burning season. However, the FLEXPART-AROME simulations are limited in their capacity to reproduce local-scale transport and may not provide sufficient horizontal resolution to construct an anthropogenic emission inventory to realistically reproduce the atmospheric composition at Maïdo using a mesoscale chemistry model, e.g., Meso-NH or WRF-Chem. Instead, one can opt to drive FLEXPART-AROME with meteorological data obtained from Meso-NH which was used to study meteorology during the BIO-MAÏDO campaign during March—April 2019. The limiting factor in this approach is potential underrepresentation of specific sources on the data-set due to their location. Using a mesoscale chemistry model would allow a detailed source apportionment of VOCs recorded at Maïdo and potentially identify the role of the ocean for the air mass composition at Maïdo. Moreover, using Meso-NH or WRF-Chem would allow the comparison between in-situ measurements from the hs-PTR-MS instrument and remote sensing measurements from the FTIR. Preliminary studies comparing both measurements have identified the PBL dynamics at La Réunion to be a strongly limiting factor in making these comparisons. The FTIR

data is most sensitive to the presence of compounds in the FT. While hs-PTR-MS measurements can be used to characterise the lower FT, these data are registered during the night when no data is available from the FTIR. During the day, when the FTIR is active, the hs-PTR-MS instrument is located in the PBL and records the composition of air masses mostly affected by emissions originating at Reunion Island.

4.2.7 Contribution of the measurement activities at Maïdo to international collaborations and to the training of young scientists

The presence of the hs-PTR-MS instrument of BIRA-IASB at Reunion Island in the framework of OCTAVE allowed the intensification of interactions between researchers at BIRA-IASB and at Reunion Island (LACy). Moreover, due to the large interest of the French atmospheric chemistry research community in the atmospheric composition at Reunion Island, the OCTAVE campaign allowed us to build relations with several atmospheric laboratories based in France (e.g., LaMP, LSCE, Université Grenoble Alpes) which was validated in co-authored publications, the OCTAVE workshops, OCTAVE meetings, and the intensive observation period (OCTAVE IOP) that took place during spring 2018. The OCTAVE IOP additionally included an international network, with collaborators from Japan, the US, and Finland.

Additionally, the OCTAVE project allowed B. Verreyken to prepare a joint Ph.D. thesis (between Ghent University and the University of La Réunion), which he successfully defended on June 17th 2021. The OCTAVE project allowed him to build competences in atmospheric transport modelling through the further development of FLEXPART-AROME during a two-year stay at the LACy laboratory under supervision of Dr. J. Brioude. He spent the remaining two years of the project at BIRA-IASB where he used this expertise in combination with source apportionment techniques to analyse the two-year (O)VOC dataset acquired at the Maïdo observatory. Due to his involvement in OCTAVE and the contributions to other projects, he was able to build a valuable international network of researchers.

The skills Bert developed within the OCTAVE project allowed him to obtain an NRC RAP fellowship at NOAA ESRL (Boulder, Colorado, USA) where he will adapt the FLEXPART-WRF model and apply it to support campaigns in complex regions taking place in the US and to evaluate emissions from volatile chemical products (VCP) occurring in US megacities.

4.3 IASI retrievals of (O)VOCs (WP3)

4.3.1 The ANNI v3 framework for (O)VOC retrievals

The ANNI v3 framework allows the retrieval of VOCs from the daily IASI satellite overpasses, and therefore allows the production of daily regional and global distributions of these compounds. This allows the production of "quick-look" maps useful for investigating source regions, local events, and the day-to-day transport pattern of these species. Examples of daily regional maps of HCOOH are given in Figure 15, where each colored dot corresponds to an individual IASI measurement. The empty spaces are due to the gap between successive satellite orbits (within the Tropics), cloudy scenes (pre-filtering) and column data discarded after the retrieval process (post-filtering). Large HCOOH enhancements are observable in isoprene-dominated environments, such over the Southeast U.S. in June (left frame) and northern Australia in September (central frame). Other enhancements are found in biomass burning regions, as in southern Africa during the fire season (right frame). Figure 15 illustrates well, with large plumes of HCOOH originating from these hotspots, the potential of IASI observations to monitor the transport of HCOOH and indirectly of its long-lived precursors. Similar analyses can be carried out over other regions and for other species throughout the over-13-year of IASI measurements.

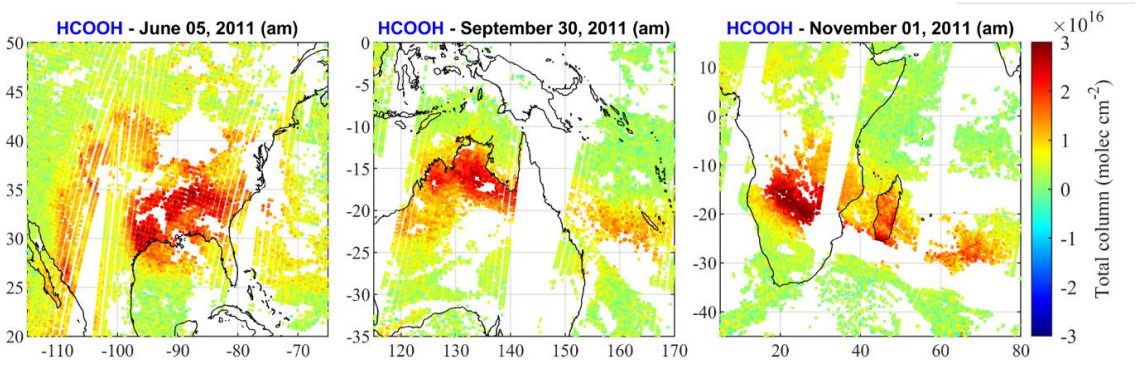

Figure 15. HCOOH total column distributions retrieved over areas of interest with the ANNI framework from single days of IASI/Metop-A observations (a.m. overpasses).

When possible, the gas total columns produced by the ANNI framework have been compared over selected regions with alternative retrievals obtained using a traditional physical inversion, that is the optimal estimation method (OEM). Examples for CH_3OH and HCOOH are given in Figure 16. The comparison of both column data sets shows an overall excellent agreement: differences occur mainly when the sensitivity to the target gas is low and are consistent with the conceptual differences between the two approaches. This not only demonstrates the robustness of the ANNI products, but also helps to illustrate the strengths and weaknesses of both retrieval approaches. More details can be found in Franco et al. (2018).

Total column abundances throughout the IASI time series have been retrieved first for CH_3OH, HCOOH and PAN. However, an important inconsistency has been detected in the CH_3OH column time series of IASI/Metop-A, before and after mid-May 2010. It is due to changes applied to the IASI instrument at this period. As the CH_3OH HRI was set up on a large subset of IASI

spectra from 2013, the methanol columns posterior to the May-2010 changes remain correct. Several first-order corrections of the pre-changes time series revealed to be unsuccessful. Therefore, we set up a new CH_3OH HRI for the pre-May 2010 time period, based on IASI spectra from 2009, consistently with the ANNI procedure. Specific NNs were trained and dedicated to the retrieval of CH_3OH columns before May 2010. After checking the consistency with the post-May 2010 time series, we merged the two periods and re-built the entire time series of methanol from 2007 to nowadays.

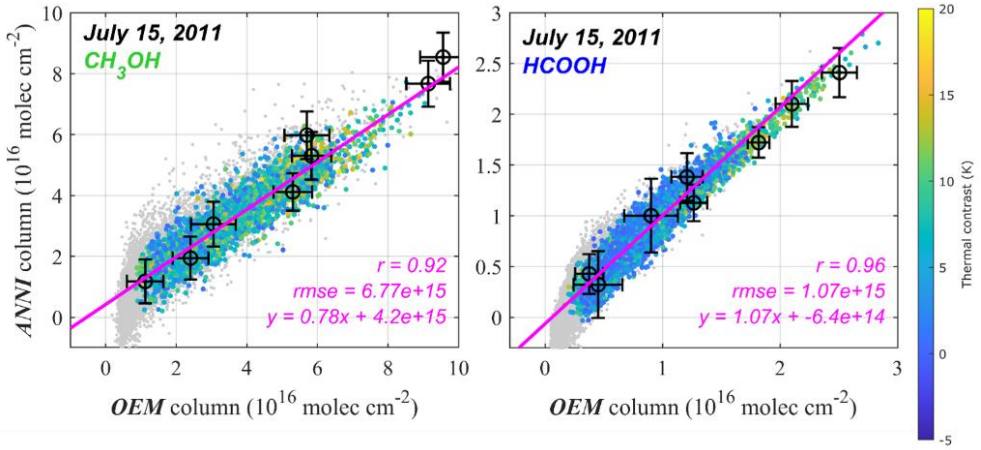

Figure 16. Comparison between CH_3OH and HCOOH total columns from the ANNI processing (y axis) and retrieved with an OEM (x axis). Pixels are colored by thermal contrast. The measurements filtered out of the comparison are depicted as gray dots. The linear regression, root-mean-square error (rmse) and coefficient of correlation (r) between the two data sets are given in magenta. The ANNI and OEM uncertainties for random measurements are indicated in black.

Whenever possible, we have compared the ANNI VOC columns with total columns from ground-based FTIR measurements. In particular, CH_3OH and HCOOH are routinely retrieved at NDACC stations located at different latitudes and in various environments (from remote to urban locations). Regarding HCOOH, a comparison of IASI-derived columns at 10 NDACC stations gives encouraging results as the IASI columns do not exhibit systematic biases to the FTIR data (Franco et al. 2020). In remote conditions, the correlation coefficients between the IASI and FTIR columns are higher than 0.6 and the slopes range from 0.80 to 1.29. However, IASI cannot capture important strong local enhancements observed at Toronto and Wollongong (it underestimates the high columns measured at these sites by up to a factor of 2). The same exercise has been conducted with the IASI-derived CH_3OH product at 7 NDACC sites (Figure 17); similar conclusions as to the HCOOH comparison can be drawn. Such underestimation of elevated VOCs columns as to FTIR measurements has also been observed in an extensive comparison of the TROPOMI formaldehyde product with observations from over 20 NDACC stations (Vigouroux et al. 2020). Recently, a first PAN column time series has been obtained from the ground-based FTIR measurements made at the high-altitude station of Jungfraujoch (Swiss Alps). The comparison with the IASI-derived PAN columns requires to account first for the > 2,000 m altitude difference between the FTIR and IASI measurements, but indicates an excellent agreement between the two datasets which share the same seasonality and exhibit no systematic PAN column biases (Mahieu et al. 2021).

Methanol being at the core of the OCTAVE project, we investigated further the reasons for IASI to underestimate the high CH_3OH columns. It appeared that the CH_3OH vertical distribution assumed in the training set was not representative enough of the source regions. Therefore, we have built a new training set, assuming a vertical distribution based on a suite of CH_3OH profiles derived from aircraft measurements, and then trained new NNs to perform new retrievals of methanol. This eventually led to the development of a new IASI CH_3OH product, which shows a much better agreement with the FTIR measurements (Figure 17). The bias in the high columns has indeed been reduced significantly, although some very high columns measured at Porto Velho are still underestimated. Most of these columns were measured during the August-September 2019 biomass burning events in Amazonia and were not entirely captured by IASI. This new IASI CH_3OH product is the one that was exploited in the other work packages of OCTAVE.

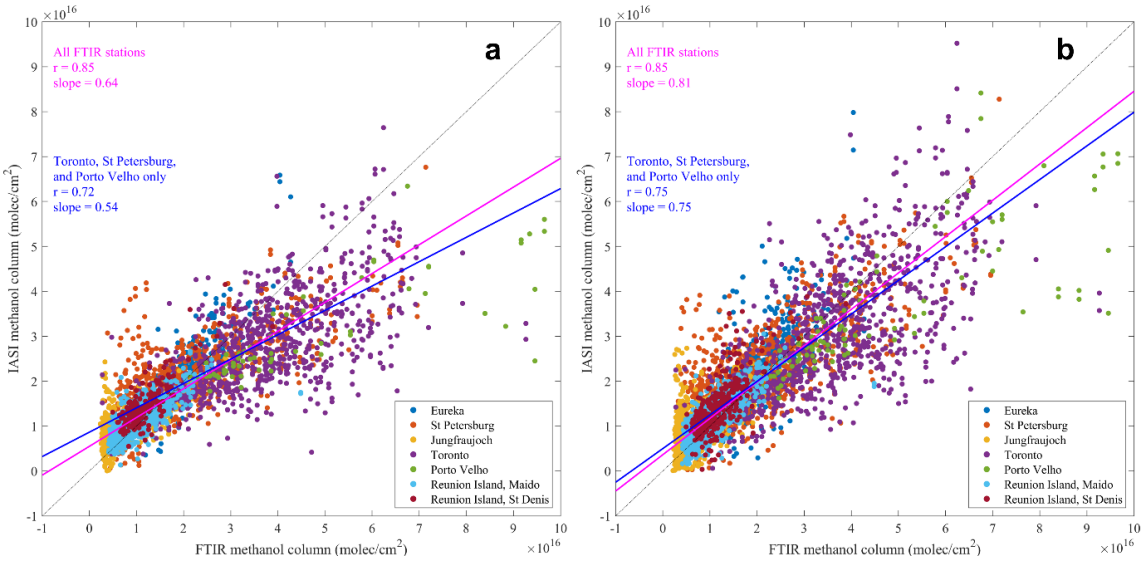

Figure 17. Comparison between IASI/Metop-A and -B, and FTIR CH_3OH total columns at 7 NDACC sites, for **(a)** the old IASI product and **(b)** the new IASI product. The linear regression, coefficient of correlation (r) and slope between the two data sets are given in magenta for the comparison involving all the stations, and in blue for the comparison at North Hemisphere mid-latitude sites only.

Total column abundances over the entire IASI/Metop-A, -B and -C time series have been retrieved first for CH_3OH, HCOOH and PAN. Figure 18 shows the monthly mean total columns of these species over January, April, July, and October, obtained from the a.m. (morning overpasses) IASI/Metop-A observations over the 2007-2019 time period. Whereas global distributions were already produced for CH_3OH and HCOOH in previous works with simplified schemes (Razavi et al. 2011; Pommier et al. 2016), the PAN product is to the best of our knowledge the first to allow daily global distribution of PAN vertical abundance so far. The global distributions of CH_3OH, HCOOH, and PAN is consistent with our knowledge of these species and of atmospheric chemistry in general, that is, CH_3OH is directly emitted into the atmosphere from plant growth mainly, whereas HCOOH and PAN are secondary products from a suite of biogenic, anthropogenic, and pyrogenic precursors whose degradation is enhanced by temperature and sunlight. The distributions highlight the important contribution of biogenic emissions from the tropical forests (Amazonia, central Africa, and north Australia) to the gas abundance. The IASI

data reveals large enhancements of CH_3OH, HCOOH, and PAN columns throughout the year over tropical regions and during summer at middle and high latitudes, which can be attributed to large primary emissions of CH_3OH and of biogenic precursors of HCOOH and PAN. The VOC tropical emissions appear to be largest in October, which corresponds to the peak of the biomass burning season in South America and Africa. Clear transport patterns are observed over the oceans in tropical regions, which is consistent with the relatively long tropospheric lifetime of these species (typically several days). In the Northern Hemisphere, CH_3OH, HCOOH and PAN exhibit a pronounced seasonal cycle: the total columns are low during the boreal winter, increase in spring and eventually peak during the boreal summer. This seasonal cycle is mainly driven by meteorology and its impact on vegetation growth, with important source contributions from the boreal forests as well as from the Southeast U.S. Emissions from India, Southeast Asia, and China also contribute with anthropogenic emissions of PAN precursors throughout the year. The VOC transport patterns observed over the oceans can be traced back to the continental emissions.

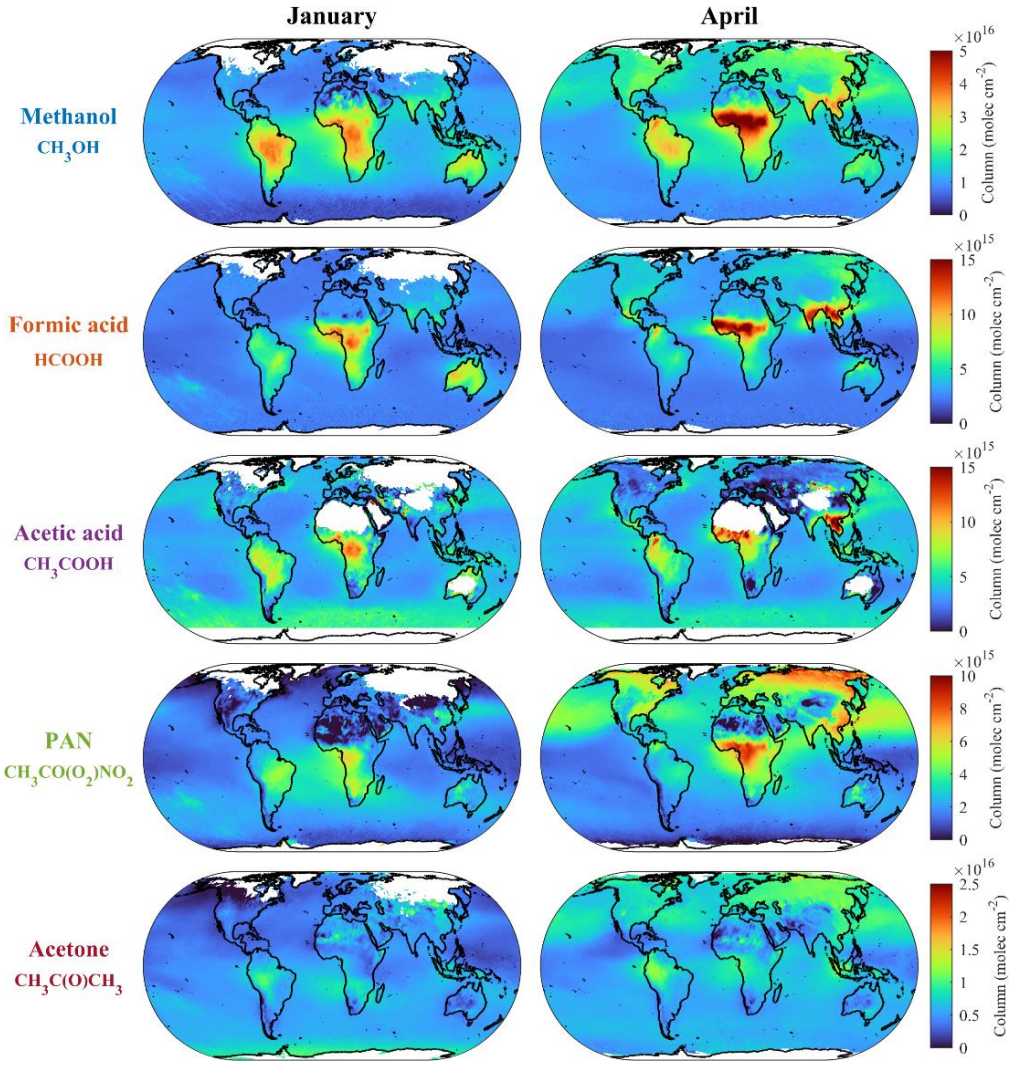

Figure 18. Monthly mean climatologies of methanol, formic and acetic acids, PAN, and acetone total columns from the 2007-2019 IASI/Metop-A observations. The blanks at high latitudes are regions where no measurements passed the filters. CH_3COOH data over deserts are discarded due to surface emissivity issues.

The distributions of CH_3OH, HCOOH, and PAN derived from the p.m. (evening overpasses) observations are similar to the a.m. distributions. The IASI measurements from the evening satellite overpasses are characterized by overall weaker thermal contrast (TC) than those from the morning overpasses. This weaker TC translates to a weaker sensitivity of the IASI measurement to the lower tropospheric layers, which leads to generally smaller HRI values for constant trace gas abundances. In contrast to CH_3OH and HCOOH, the PAN column distributions obtained with the p.m. observations match almost perfectly those of the morning overpasses. This is likely because PAN retrieval is less affected by variations in the TC as its concentrations in the lower troposphere are proportionally lower than those of the other species. The same is observed with the acetone retrieval (see section 4.3.3).

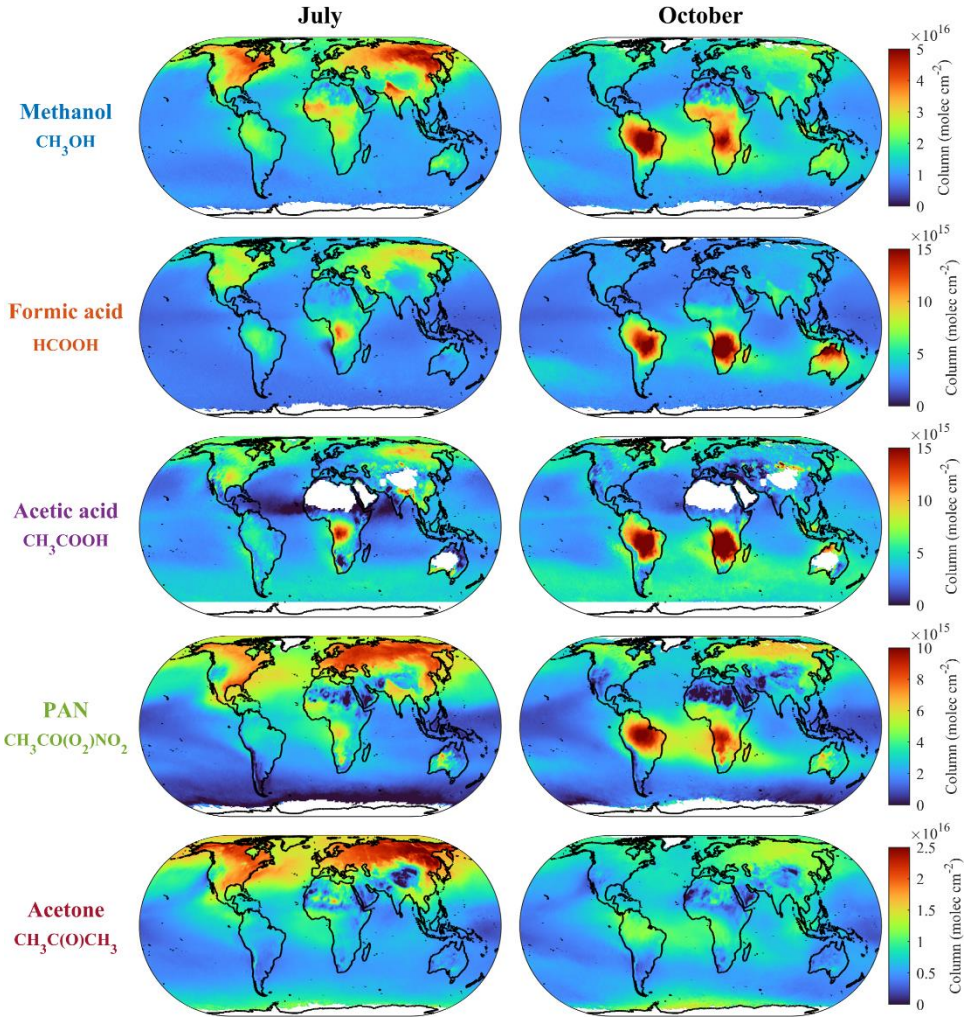

Figure 19. As Figure 18 for July and October.

4.3.2 Acetic acid columns from IASI observations

We have then applied the ANNI framework to the retrieval of acetic acid (CH_3COOH) from IASI spectra. Although detected so far in concentrated biomass burning plumes only (e.g., Clarisse et al. 2011), the high sensitivity of the HRI as a detection method, and the robustness of the NN-based retrievals, allowed us to produce the first space-based global distributions of acetic acid

(Figure 18, 19). Efforts were made to analyze and exploit conjointly the ANNI products of formic and acetic acids, the two most abundant carboxylic acids in the atmosphere and significant contributors to the acidity of clouds and rainwater. Current knowledge is unable to explain their elevated concentration levels measured in the atmosphere since their sources remain poorly known and quantified. A joint analysis of the HCOOH and CH_3COOH global maps derived from the 2007-2018 IASI/Metop-A measurements has revealed that these species exhibit similar abundance, distributions, and seasonality, as illustrated in Figure 18 and 19. This points to major sources that are common to both organic acids. We have also investigated their column time series over source regions, along with the bottom-up biogenic emissions of the main hydrocarbon precursors (i.e., isoprene and monoterpenes) from MEGAN-MOHYCAN (e.g., Bauwens et al. 2018) and the cumulated MODIS fire radiative power, a good indicator of the integrated biomass combustion. Examples are shown in Figure 20. The good correspondence in the time series suggest that the atmospheric abundance of HCOOH and CH_3COOH is indeed closely linked to the hydrocarbon emissions from the terrestrial vegetation as well as to the presence of wildfires, especially in the tropics. Over Africa, evidence has been provided that residual smoldering combustion related to wildfires might be a major driver of the organic acids' seasonality. In some regions, significant differences between the time series of the two compounds are nevertheless observed, which suggests that sources and atmospheric production pathways specific to each species also exist. Further measurements are however required to corroborate this finding. These results have been reported in Franco et al. (2020).

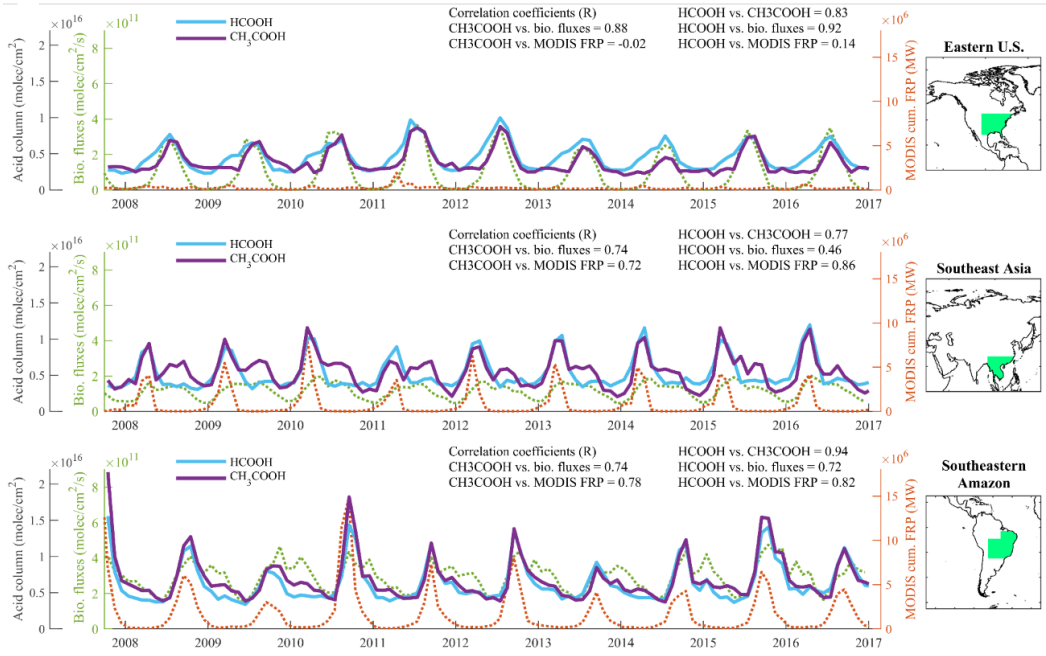

Figure 20. Time series of monthly mean HCOOH and CH_3COOH total column (blue and purple solid lines, respectively), MEGAN–MOHYCAN isoprene and monoterpenes emission fluxes (green dotted line), and cumulative MODIS fire radiative power (orange dotted line) over regions of interest.

4.3.3 Acetone columns from IASI observations

The fifth major OVOCs we have retrieved from IASI with the ANNI framework was acetone (CH_3COCH_3). Conversely to other species which were at least already identified in fire plumes, acetone was not detected in IASI spectra before. To unambiguously demonstrate that its spectral signature is present, we performed fits using the iterative optimal estimation method (OEM) as implemented in a line-by-line radiative transfer model. The example in Figure 21 shows that the overall baseline is reconstructed satisfactorily in the 1,171–1,242 cm^{-1} range where acetone absorbs. Its contribution to the radiance spectrum can be visualized with the help of a second simulation, obtained by excluding acetone from the result of the first fit. The residuals between the simulated spectra without acetone and the observed spectrum (blue line) or the simulated spectrum with acetone (green line) both visualize the broad absorption band of this compound. The above analysis has been carried out on several spectra in different parts of the world, with similar conclusions, providing convincing evidence for the detection of acetone. These findings, along with the first global distribution of atmospheric acetone obtained from a spaceborne nadir-viewing sounder (see here below), have been reported in Franco et al. (2019).

From the analysis of the acetone distribution and variability (Figure 18 and 19), we can draw conclusions similar to those for the other OVOCs discussed previously. We can indeed deduce that the dominant source of atmospheric acetone is the terrestrial vegetation at Northern Hemisphere middle and high latitudes. Human activities also contribute to the atmospheric acetone concentrations throughout the year, especially in the Northern Hemisphere. The main difference resides in the fact that, unlike the other OVOCs species, fires do not appear to be a strong source of acetone globally.

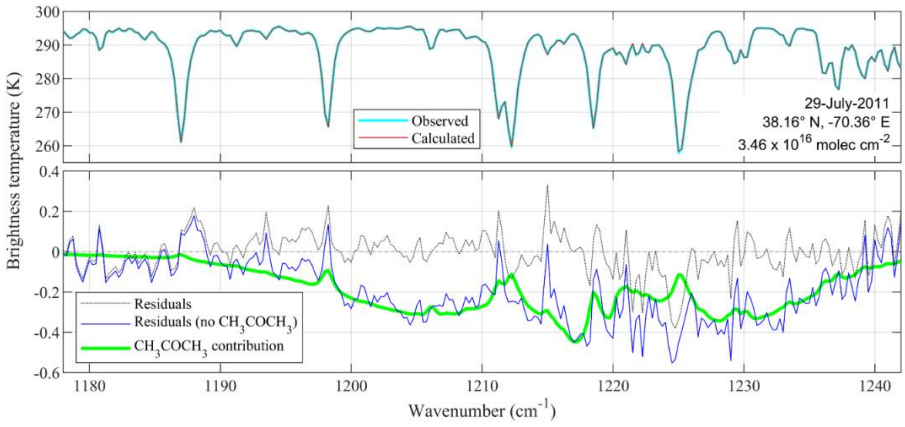

Figure 21. Evidence of acetone (CH_3COCH_3) detection in IASI spectra. The observed and calculated spectra are displayed in the upper frame in light blue and red, respectively, while the black dotted line in the lower frame is the fitting residuals between those. The difference between the fitted spectra reconstructed with and without acetone is in solid green line, while the difference between the observed spectrum and the fitted spectrum reconstructed without acetone is in blue.

Since no other total column measurements of acetone and acetic acid are currently available, we have compared the IASI data to measurements from aircraft campaigns (Franco et al. 2019, 2020). The comparison for acetone is displayed in Figure 22. Because the airborne measurements of

OVOCs usually do not span the entire troposphere – lower stratosphere, we have derived acetone and acetic acid total columns from composite aircraft-model profiles that consist of free tropospheric airborne measurements, complemented by model profiles (from IMAGES) for the missing parts in the upper troposphere – lower stratosphere (UTLS). The comparisons suggest that the satellite OVOCs measurements present a low bias relative to the composite aircraft-model data. Nonetheless, it is worth noticing that this type of comparison is relatively difficult to interpret as it convolves many assumptions and uncertainties. The aircraft measurements are indeed relatively scarce in space and time, especially for acetic acid. Moreover, many of the aircraft measurements available were performed over the oceans where the satellite sensitivity is typically lower.

4.3.4 Acetylene and hydrogen cyanide columns from IASI observations

In the past, global distributions of acetylene (C_2H_2) and hydrogen cyanide (HCN) were produced from the IASI observations, using a fast retrieval scheme based on a preliminary version of the HRI (Duflot et al. 2015). These retrievals showed some limitations outside the Tropics. Therefore, global distributions of C_2H_2 and HCN total columns retrieved with the ANNI framework have been generated to investigate the spatial and seasonal variability of these compounds. Their column climatologies over April, July and October obtained from the 2007-2019 IASI/Metop-A observations are shown in Figure 23. Compared to the previous versions, the ANNI products show a better and more consistent sensitivity outside the Tropics. In winter, C_2H_2 distributions present a strong latitudinal gradient, likely due to the more abundant anthropogenic emissions (fossil fuels and biofuels) in the Northern Hemisphere. The columns peak at mid latitudes of the Northern Hemisphere in late winter – early spring, just before the increase of OH chemistry, the main C_2H_2 sink in the atmosphere. In the boreal summer, hotspots are observed in Asia (India and Eastern China), with important outflows over the oceans due to the relatively long lifetime of acetylene (10-15 days). In fall, the contribution of the typical biomass burning regions in the tropics is noticeable, while the C_2H_2 columns are at the lowest levels in the Northern Hemisphere. The HCN distribution and seasonality appear to be mainly driven by the biomass burning regimes, with noticeable hotspots over Africa throughout the year, in Asia (especially India and Southeast Asia) during the boreal spring and summer, at mid and high latitudes of the Northern Hemisphere in July, and in the tropics in October. It is interesting to note that the important hotspot over Indonesia is mainly due to the massive 2015 Indonesian wildfires which emitted a substantial HCN amount from peatlands. Large outflows can be observed from the continental source regions. The ANNI HCN product is described in Rosanka et al. (2021).

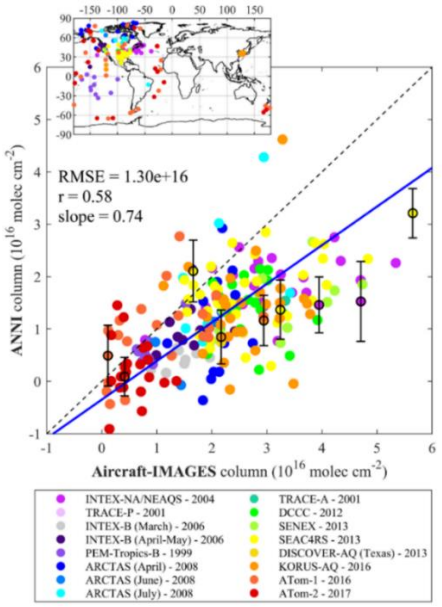

Figure 22. Comparison between acetone total columns derived from composite aircraft-model profiles (located in inset), with the closest individual IASI column obtained the same day as the composite profile. The linear regression, root mean square error (RMSE) and coefficient of correlation (r) are given. The IASI column uncertainties are displayed for random measurements (in black).

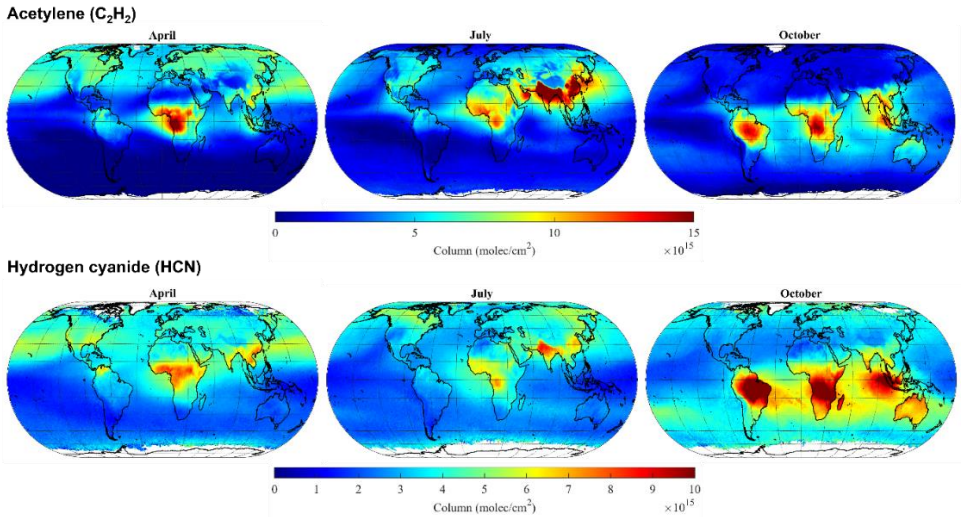

Figure 23. Monthly mean climatologies of acetylene and hydrogen cyanide total columns from the 2007-2019 IASI/Metop-A observations. The blanks at high latitudes are regions where no measurements passed the filters.

4.3.5 Ethylene columns from IASI observations

The spatially dense measurements from IASI offer a good opportunity to monitor ethylene (C_2H_4). Therefore, in addition to the VOCs already retrieved with the ANNI framework, C_2H_4 total columns have also been obtained from the entire IASI datasets. Investigation of the preliminary C_2H_4 product revealed that confident retrievals can be performed in fire plumes only, and that no global distributions can be obtained as for the other target compounds. Indeed, ethylene is a short-lived species closely related to biomass burning, hence its abundance in remote conditions is weak and its signal in the IASI spectra is often below the detection threshold. Moreover, the C_2H_4 column is challenging to retrieve owing to a strong CO_2 line that partly overlaps the main absorption feature of ethylene in the thermal infrared (the *Q*-branch of the ν7 vibrational band

near 949 cm^{-1}). Consequently, we have implemented a specific filter to isolate the confident C_2H_4 measurements in fire plumes from the relatively noisy background. It has also appeared that the C_2H_4 retrieval depends largely on the altitude of the fire plume. Such information is required prior to the retrieval process to produce representative columns of ethylene from the IASI observations. We can approximate the altitude of the fire plume from the height of the atmospheric aerosol layers detected by the CALIPSO (Cloud-Aerosol Lidar and Infrared Pathfinder Satellite Observation) satellite instrument. This operation has of course to be repeated for every case study, and the altitude of the fire plume adjusted accordingly.

To demonstrate the potential of the C_2H_4 retrievals performed using the CALIPSO information, Figure 24 shows regional daily distributions of C_2H_4 total columns over North America, which illustrate a large fire plume from massive wildfires that erupted simultaneously in British Columbia and the Northwest Territories, Canada, in August 2017. In this example, the large C_2H_4 column enhancements allow to visualize the extent of the fire plume as well as its exceptional long-range transport across the Atlantic Ocean until it reaches Europe. Ethylene column enhancements have also been captured at the NDACC FTIR stations of Eureka (Nunavut, Canada) and Jungfraujoch (Swiss Alps) when parts of the original plume passed over these sites, i.e., on 18-19 August 2017 at Eureka and on 20-21 August 2017 at Jungfraujoch.

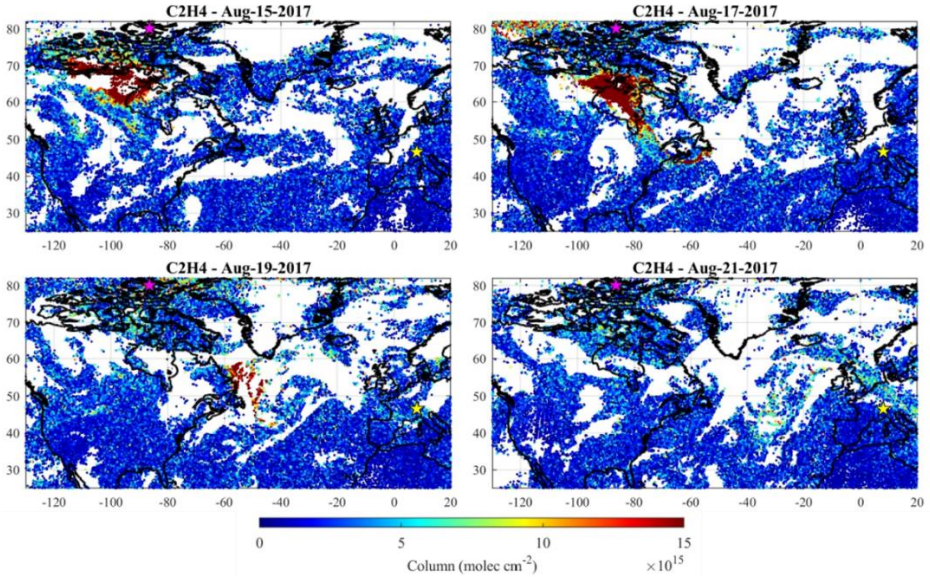

Figure 24. Daily distributions of C_2H_4 total columns from IASI/Metop-A and -B observations over North America. Each dot corresponds to a single IASI observation. The pink and yellow star symbols give the location of the Eureka (Nunavut, Canada) and Jungfraujoch (Swiss Alps) NDACC FTIR stations, respectively.

4.3.6 Recommendations for future work on IASI (O)VOC developments

The ANNI framework is operational and now ensures the retrieval of 8 (O)VOCs throughout the entire operational time series of IASI/Metop-A, -B, and -C (i.e., since 2007). It has proved to be sensitive, flexible, and robust for the retrieval of such weak infrared absorbers. The retrieval of acetic acid and acetone represents a step beyond what was envisioned in the initial OCTAVE proposal. Altogether, this suite of IASI products constitutes an extensive and unique decadal dataset of global (O)VOCs column abundance from a single satellite sounder, which is of high

value for tackling scientific questions in link with the atmospheric composition. Key tasks for future improvements and exploitation of these products are identified here below: The reanalyzed product developed for each retrieved species ensures a full consistency of the retrieved columns throughout the IASI observational time series, which will permit to obtain from space decadal trends of the tropospheric abundance of major (O)VOCs at the global scale.

- The validation of the IASI (O)VOCs products is an ongoing task. The preliminary comparisons performed between IASI and ground-based FTIR measurements are encouraging. Nonetheless, further efforts are needed to tackle local IASI underestimation of the high columns. In that perspective, a more thorough collocation in space and time of the IASI measurements might be required. Ground-based FTIR column measurements of C_2H_2 and HCN being available at several NDACC stations, the new IASI products will also be evaluated. The limited availability of PAN column measurements at NDACC sites, and the absence of such measurements for acetone and acetic acid, might hamper a complete validation of these IASI products. A comparison with column data derived from composite aircraft-model profiles has been attempted but led to mitigated conclusions considering the uncertainties inherent to the comparison methodology. More work is therefore needed to further evaluate these IASI products.
- Multi-year measurements of various (O)VOCs in the UTLS have been produced from ACE-FTS (Atmospheric Chemistry Experiment–Fourier Transform Spectrometer) solar occultations, for instance for PAN and acetone (Tereszchuk et al. 2013; Dufour et al. 2016). Although these UTLS partial columns cannot be compared directly to the IASI total columns, the ACE-FTS (O)VOCs measurements might be used to evaluate the consistency with the IASI (O)VOCs products.
- One limitation, which is present for all the satellite-derived products of minor trace gases is that, because of the limited information content in the spectrum, no accurate vertical profile can be retrieved. The production of averaging kernels by the ANNI retrieval framework is part of future developments and will allow improved comparisons with models and independent measurements.
- Retrieval of other (O)VOCs identified recently in the IASI spectra, such as glycolaldehyde ($HOCH_2CHO$; De Longueville et al. 2021), can be attempted in the future with the ANNI framework.

4.4 Global modelling evaluation of OVOC budget and impacts (WP4)

4.4.1 Modeling atmospheric composition at Reunion Island using the WRF-Chem model

Comparison of WRF-Chem results using the large domain and relatively coarse resolution (5km in inner domain) with FTIR column data collected at Maïdo exhibits fair agreement (not shown) except for systematic overestimations for longer-lived species including CO, methanol, ethane and PAN. Those discrepancies are attributed to biases in the lateral boundary conditions. The results at 5 and 15 km resolution are nearly identical, and even the 60km-resolution results are not significantly worse than the finer-resolution results. This suggests that the total columns are mostly driven by large-scale meteorological and emission patterns, and any boundary-layer enhancements due to local emissions represent only a minor contribution. In further WRF-Chem simulations, we remove the biases for the long-lived species by adjusting the lateral boundary conditions provided by MOZART on the basis of those comparisons ($CO \times 0.6$, $CH_3OH \times 0.6$, $PAN \times 0.7$, and $C_2H_6 \times 0.6$).

Horizontal resolution has a strong impact on the comparisons with PTR-MS data at Maïdo. In the following, we discuss only the high-resolution model results (500m over Reunion Island). The model succeeds in reproducing the temporal variability of observed near-surface temperature, whereas the performance for solar downward radiation is more variable (Figure 25), reflecting the difficulty to reproduce local cloudiness at the site.

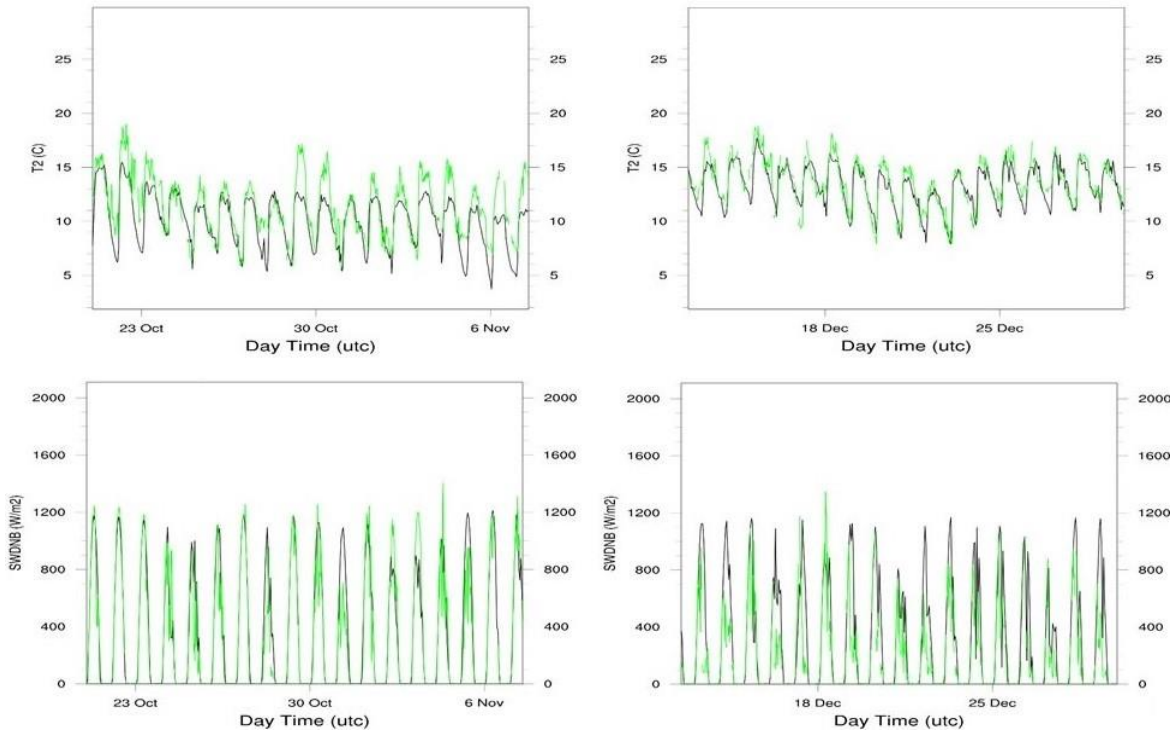

Figure 25. Upper row: observed (green) and WRF (black) 2-meter temperature at Maïdo in October (left) and December 2017 (right). Lower row: same for downward solar radiation (W m^{-2}).

Comparison of the WRF-Chem results with FTIR data at Maïdo is shown on Figure 26. The results are highly dependent on the lateral boundary conditions of the model. For formaldehyde, a strong diurnal cycle is calculated, due to local emissions and is not supported by the data. A possible overestimation of anthropogenic NMVOC emissions is suggested by the PTR-MS data comparisons (see further below).

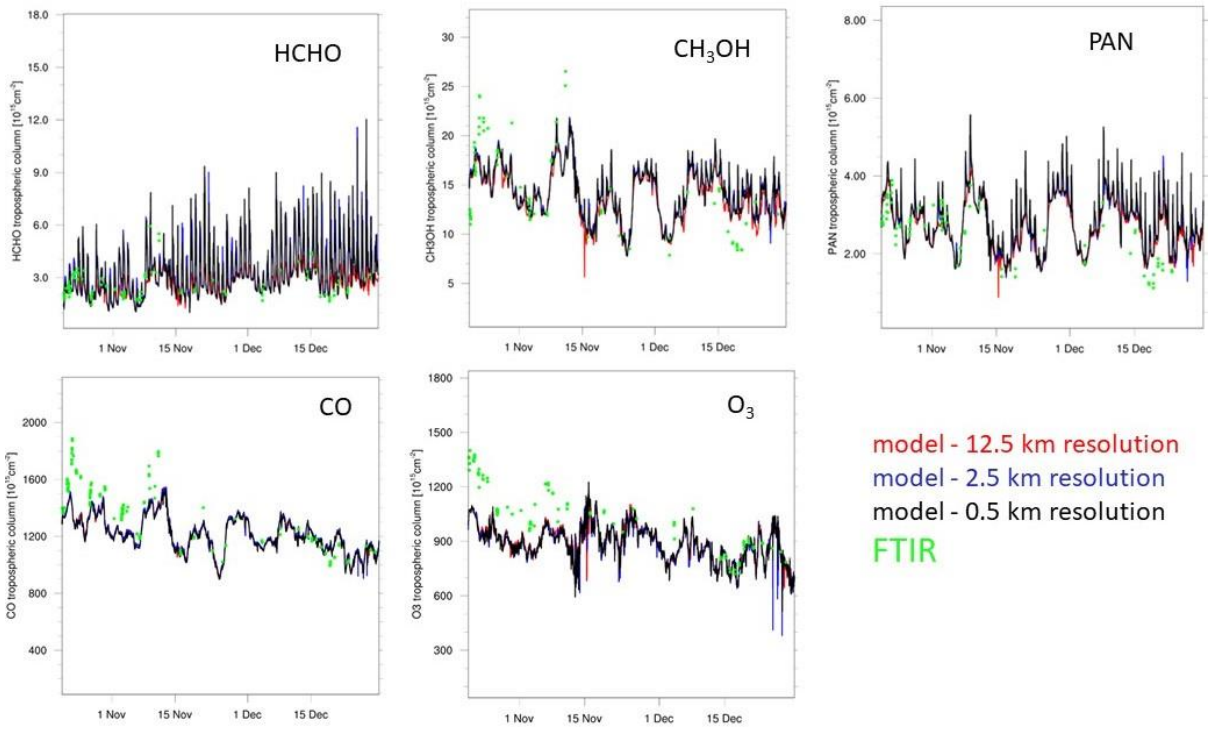

Figure 26. Green dots: FTIR total columns of OVOCs and CO, and tropospheric O_3 column at Maïdo (green dots) in Oct-Dec 2017. Curves: WRF-Chem simulation using the small domain definition.

The modelled averaged diurnal cycle of near-surface OVOC concentrations is compared with the PTR-MS data on Figure 27-28. The impact of model resolution is evident. For methanol, the broad daytime maximum is best reproduced with the finest resolution, reflecting the influence of local daytime biogenic emissions. Anthropogenic emissions of NMVOCs appear to be strongly overestimated in the model, as shown by the model overestimation for MEK (Figure 27) and toluene (not shown). Sensitivity calculations indeed show that the simulated toluene and MEK levels are largely due to local NMVOC emissions. For acetone, acetaldehyde and acetic acid, the model appears to lack a significant daytime production, presumably due to direct biogenic emission and/or photochemical formation from unknown NMVOC precursors. The large underestimation for acetic acid and acetaldehyde is in line with previous model assessments (e.g., Read et al. 2012; Khan et al. 2018). It would be even worse with the reduced anthropogenic emissions suggested by the data as discussed above.

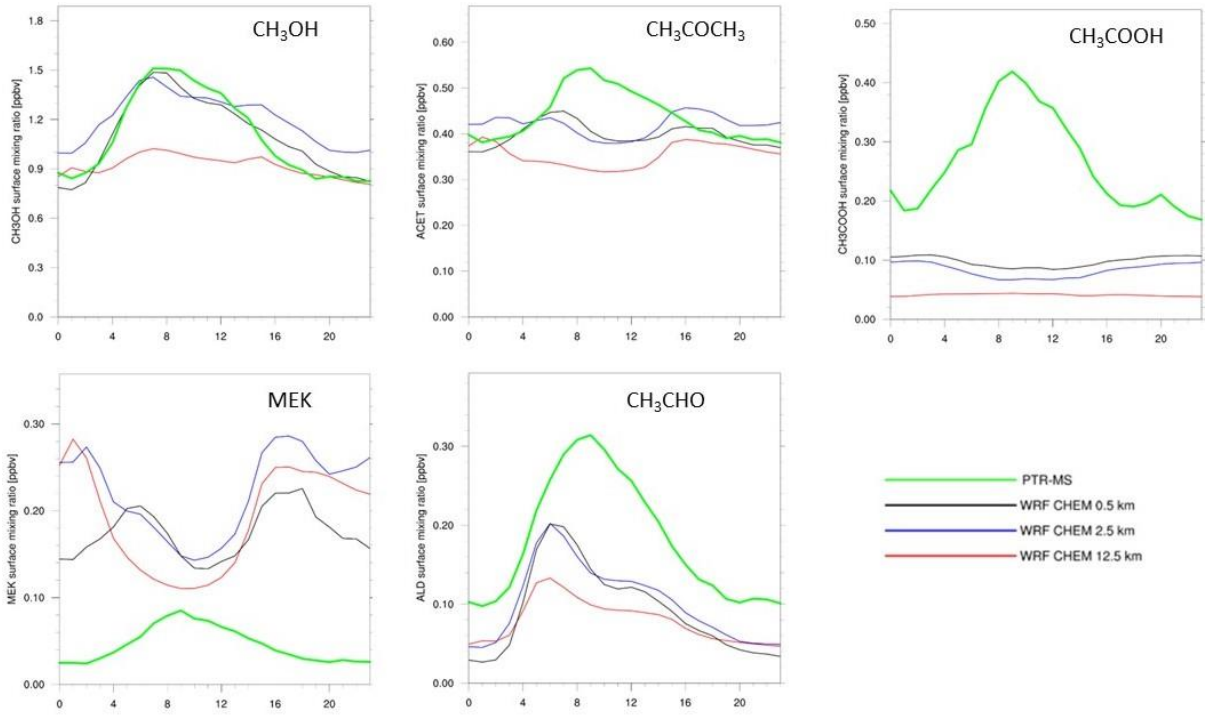

Figure 27. Observed and simulated average diurnal cycle of methanol, acetone, acetic acid, methylethyl ketone and acetaldehyde at Maïdo. The model results are shown for 3 resolutions.

A fair agreement is found for formaldehyde (Figure 28), which might be fortuitous given the overestimation of anthropogenic NMVOCs. Both isoprene and its oxidation products are overestimated, although the best agreement is found at the highest resolution. A sensitivity calculation conducted without anthropogenic emissions indicates a very strong sensitivity of isoprene concentrations to those emissions. This is due to the impact of NOx on OH, the main oxidant of isoprene. This unexpected crucial importance of NOx emissions for simulating biogenic compounds represents a serious limitation for our study, since high-resolution anthropogenic emissions are currently unavailable for Reunion Island. The coarse resolution of the inventory used in WRF-Chem (EDGAR-HTAPv2, 0.1°×0.1°) implies limited reliability of model predictions for short-lived compounds like isoprene.

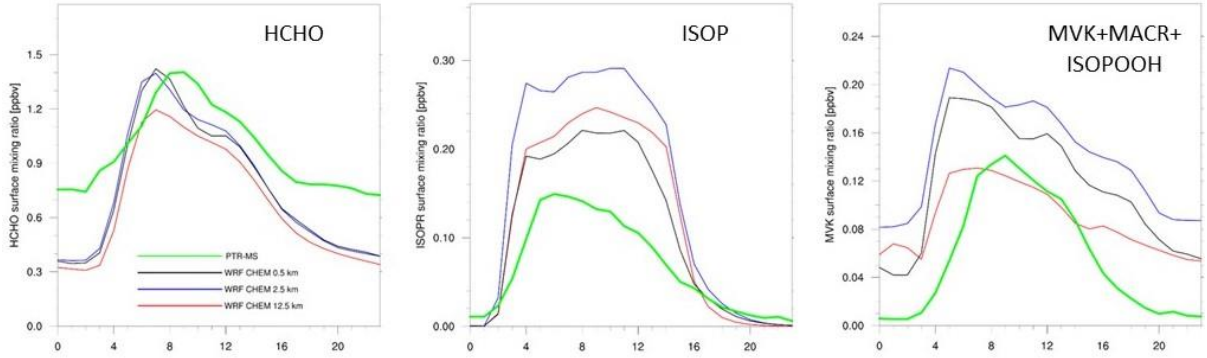

Figure 28. Observed and simulated average diurnal cycle of formaldehyde, isoprene and the sum MVK + MACR + ISOPOOH at the Maïdo observatory. The model results are shown for 3 resolutions.

4.4.2 Evaluating IASI methanol column using aircraft data over the U.S.

The source inversion constrained by aircraft campaigns succeeds very well in reducing the widespread model underestimations found when using a priori emission inventories (Figure 29). The calculated methanol vertical profiles at the 3 campaigns are also greatly improved by the optimization (Figure 30).

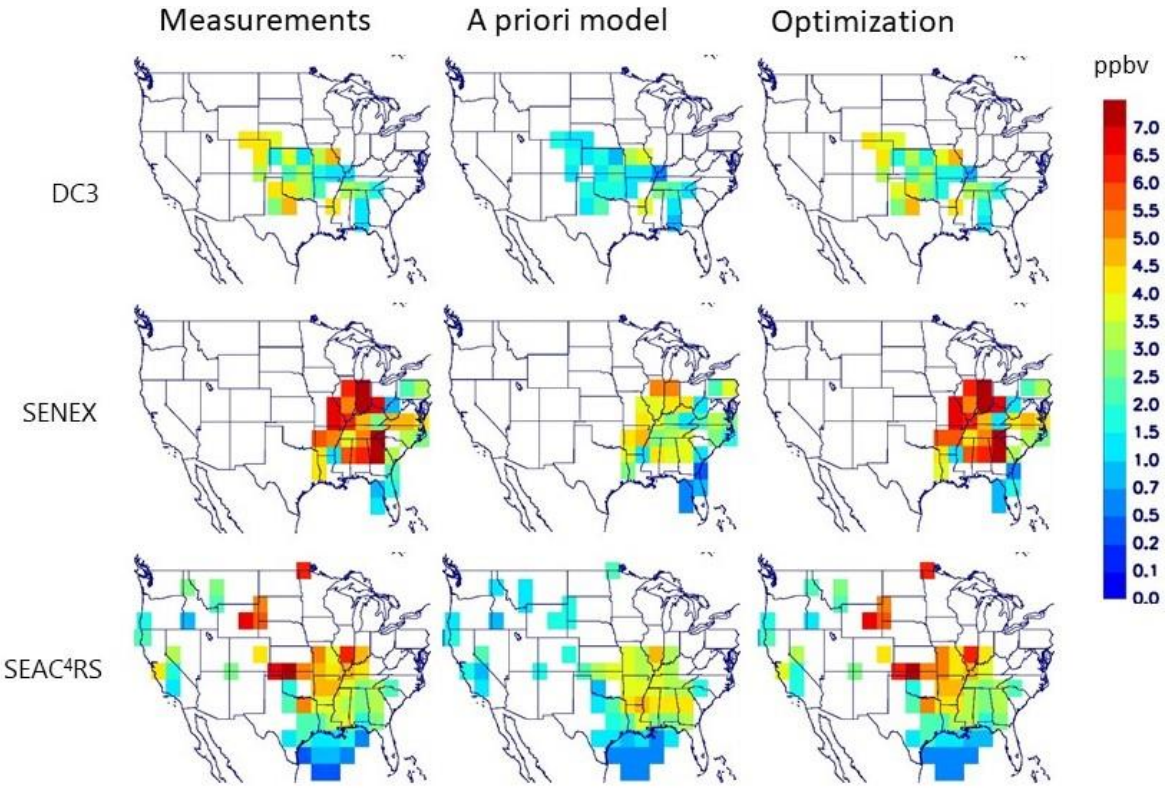

Figure 29. Average methanol mixing ratio observed in 3 aircraft campaigns (left) and simulated by the MAGRITTE model using a priori emissions (middle) and using emissions constrained by the aircraft measurements.

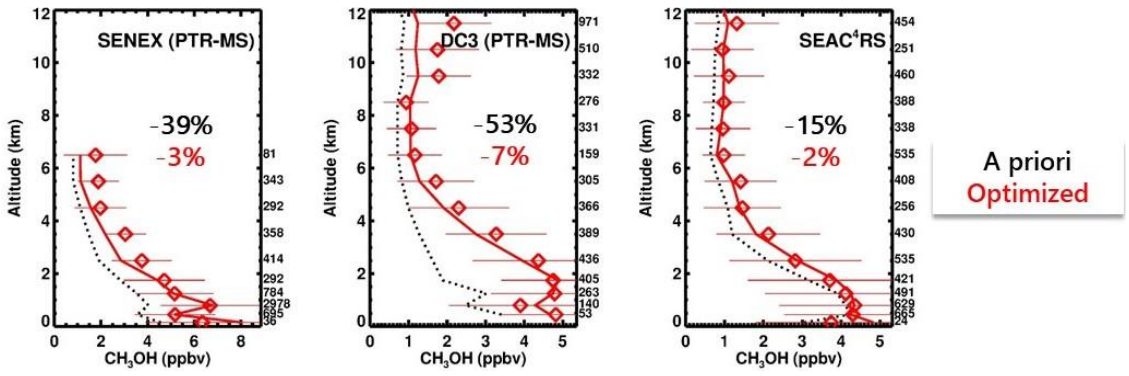

Figure 30. Vertical profiles of observed methanol mixing ratios (symbols) and simulated values using a priori (black) and optimized emissions (red curves). The average relative biases are indicated inset.

Under the assumption that the aircraft observations are unbiased, the optimized model is a fair approximation of the real methanol distribution. The IASI and optimized model columns at the

locations and times (month and year) of the aircraft data are compared in Figure 31. For all 3 campaigns, IASI underestimates the large columns. Note that the slopes derived through linear regression (0.40) or with a Theil-Sen estimator (0.39) are very close. A similar regression is also obtained when we select only IASI data on the precise same days as the aircraft measurements. In this case, a slope of 0.36 is derived, with a low correlation (0.48). As seen on Figure 31, the regression based on aircraft data deviates strongly from the 1:1 line as well as from the regression based on FTIR data.

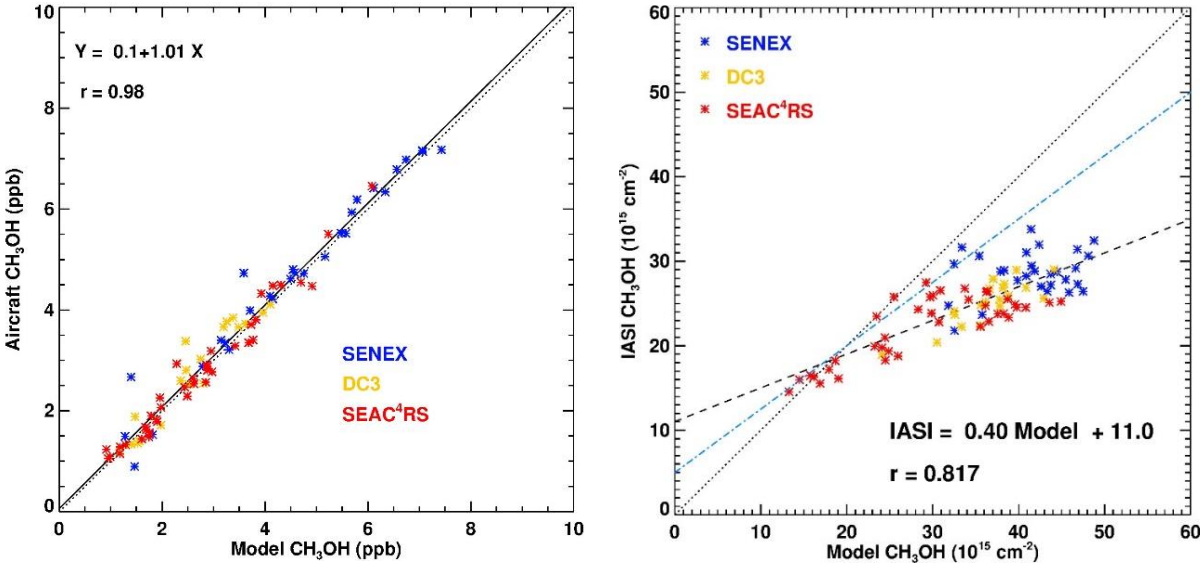

Figure 31. Left: Campaign-averaged CH_3OH mixing ratios measured in 3 aircraft campaigns vs. model values constrained by those data. Right: Campaign-averaged IASI columns vs. corresponding model values constrained by aircraft data. Only 2°×2.5° pixels with at least 30 aircraft data are used. The linear regression is the dashed line. For comparison, the regression of IASI versus FTIR columns at 3 continental sites is shown as the blue dash-dotted line.

4.4.3 Global-scale inversion of methanol columns

The adjoint inversion scheme used for deriving top-down methanol emission updates is based on the adjoint of IMAGESv2 (Stavrakou et al. 2011). The adjoint method is used to compute the derivatives of the cost function (misfit between the model and the observations) with respect to a number of control variables (emission parameters) and update the fluxes at every model grid cell once per month.

Two emission categories are optimized, the pyrogenic and biogenic emissions, while anthropogenic and ocean emissions are kept at their a priori values. The number of unknowns to be determined by the inversion is equal to ca. 25 000 (8000 for biomass burning, 17 000 for biogenic). The errors on the emission parameters are assumed to be a factor of two for biogenic emissions, and a factor of 2.5 for biomass burning. Spatial and temporal correlations are as in Stavrakou et al. (2011). The spatial correlations between errors on the emissions from two grid cells are assumed to decay exponentially with the distance d between the grid cells, $e - d/l$, with l = 500 km for both emission categories. Temporal correlations are assumed to decrease linearly between 0.25 for adjacent months and zero for a 6-month time lag. Table VI summarizes the

global inversions of emissions based on IASI data. For each setup, adjoint inversions are conducted for years 2012-2013 and 2016-2018.

Table VI. Description of the global methanol source inversions constrained by IASI observations.

Runs	Data used	Description
OPT1	IASI	No correction
OPT2	$1.33 \times IASI - 6.7 \times 10^{15}$	Correction based on FTIR data
OPT3	$2.5 \times IASI - 27.5 \times 10^{15}$	Correction based on aircraft data from 3 campaigns

As seen on Figure 32, the bias corrections lead to enhanced values over source areas. Over oceans, the columns are strongly decreased. Since the bias corrections were determined based on data over land, oceanic data are excluded from the inversions. Comparison of the data used in the inversions with the modelled columns after optimization shows very good agreement over continents. Over oceans, as expected, the model overestimates the data when bias-correction is applied. OPT1 agrees fairly well with uncorrected IASI data over ocean, except over the central Pacific, where the model is too high.

The seasonal variations of observed and optimized model columns at mid-latitudes are shown in Figure 33. The bias corrections lead to very low columns in winter, which the model cannot match. Those values are very likely unrealistic as the bias corrections are mostly constrained by high values (well above 10×10^{15} molec. cm^{-2} for OPT3, Figure 32). During summer, the strongest enhancements derived in OPT3 (about of factor 2) are found in Western Canada, Northwestern U.S. and Northern China.

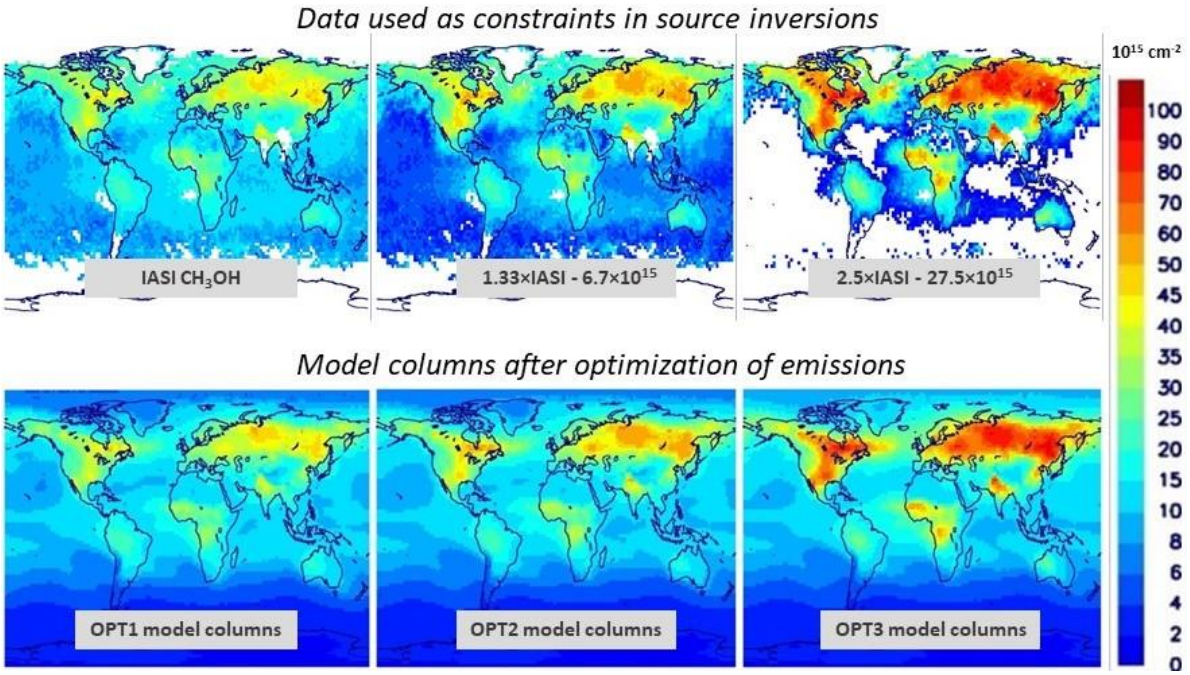

Figure 32. Data used in emission optimizations for July 2013 (top row) and modelled methanol columns after source inversion.

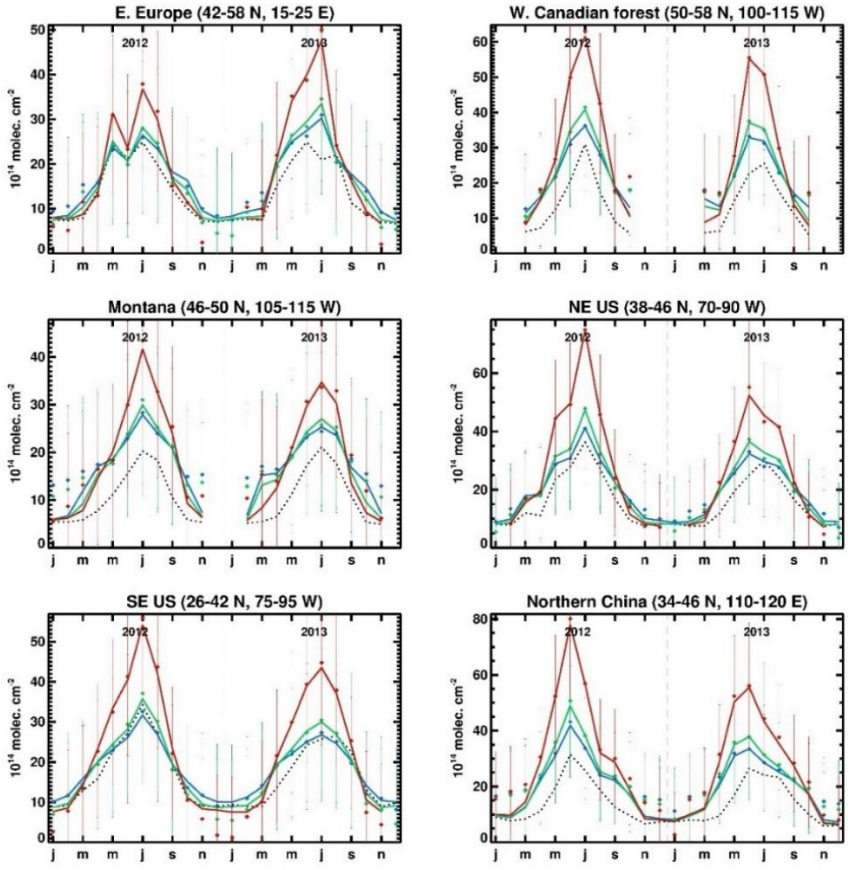

Figure 33. Monthly CH_3OH columns (2012-2013) over large regions. Symbols represent the data, curves the optimized model results (blue: OPT1, green: OPT2, red: OPT3, and black dotted line: a priori).

Table VII summarizes the global methanol budget for year 2013. Whereas the chemical lifetime and the photochemical production of methanol remain unchanged after optimization, and the biomass burning source is found to decrease by 15-30%, the biogenic source is enhanced by ~22% in OPT1 and OPT2 and by 60% in OPT3. The oceanic and anthropogenic sources were not optimized.

Table VII. Global a priori and top-down methanol budget for 2013.

	A priori	OPT1	OPT2	OPT3
		Source (Tg/year)		
Biogenic	110	134	136	176
Biomass burning	6.6	4.6	4.8	5.6
Ocean	47.4	47.4	47.4	47.4
Anthropogenic	10.6	10.6	10.6	10.6
Photochemical production	47.1	46.4	46.5	46.5
Global total	222	243	245	284
		Sink (Tg/year)		
Photochemical loss	109	117	118	139
Dry deposition (land)	47.7	57.3	59.4	77.1
Dry deposition (ocean)	58.0	61.5	59.9	61
Wet deposition	5.9	6.1	6.2	7
Lifetime (days)	4.67	4.61	4.59	4.53

In all cases, the optimizations result in enhanced emissions over semi-arid areas including the Western US, Australia, Sahel and Central Asia (Figure 34). Decreases are found over Indonesia, Southern Brazil and Paraguay. Over Amazonia and Eastern U.S., only OPT3 predicts emission increases. The largest enhancements are found over Quebec and Kazakhstan (factor ~10 in OPT3).

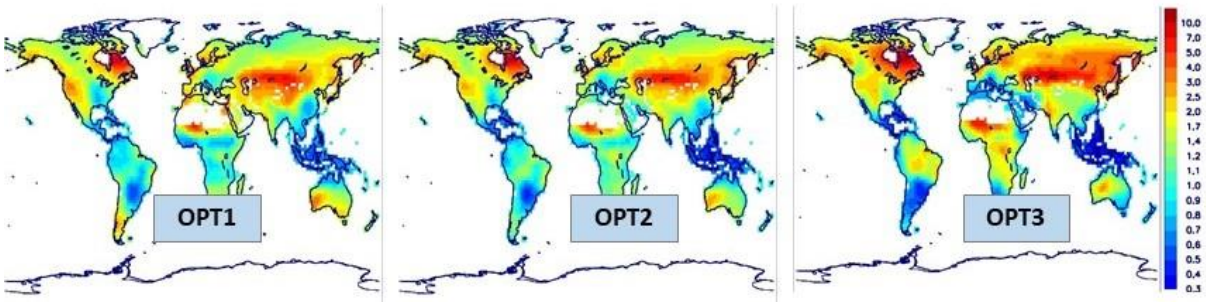

Figure 34. Ratio of optimized over a priori biogenic emissions (annual mean) for year 2013 according to optimizations OPT1, OPT2 and OPT3.

As expected, the model agrees best with ground-based FTIR observations at Toronto and St Petersburg in optimization OPT2 (Figure 35). Simulation OPT3 consistently overestimates FTIR data (by ~25% on average), except in 2013 in Toronto. The a priori simulation underestimates the data by ~30%. The performance of the OPT1 simulation is only slightly worse compared to OPT2.

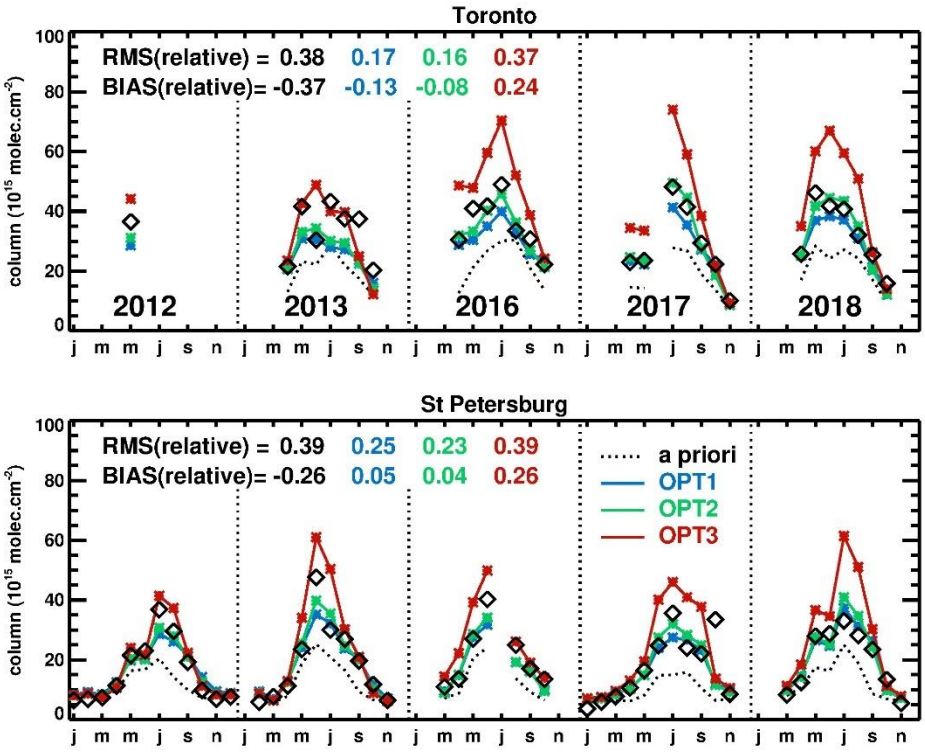

Figure 35. Monthly-averaged CH_3OH columns modelled (curves) and observed by FTIR (symbols) at Toronto and St Petersburg in 2012-2013 and 2016-2018. Dashed lines: a priori run. Blue, green and red lines: result of emission inversion constrained using IASI data. The model results are smoothed using the provided FTIR averaging kernels. See text for details.

In contrast with this result, the OPT3 optimization leads to the best model agreement with aircraft data over land, as seen from the comparison with SENEX and SEAC^{4}RS campaigns in 2013 (Figure 36), but also over oceans at mid- and high latitudes, as seen from the comparison with the merged ATom (Atmospheric Tomography Mission) dataset obtained between 2016 and 2018 over the Pacific and Atlantic oceans as well as over North America (https://espo.nasa.gov/atom/content/ATom).

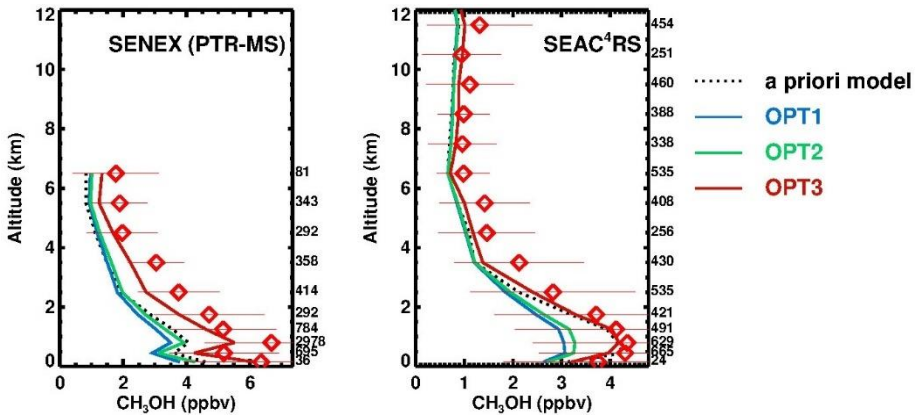

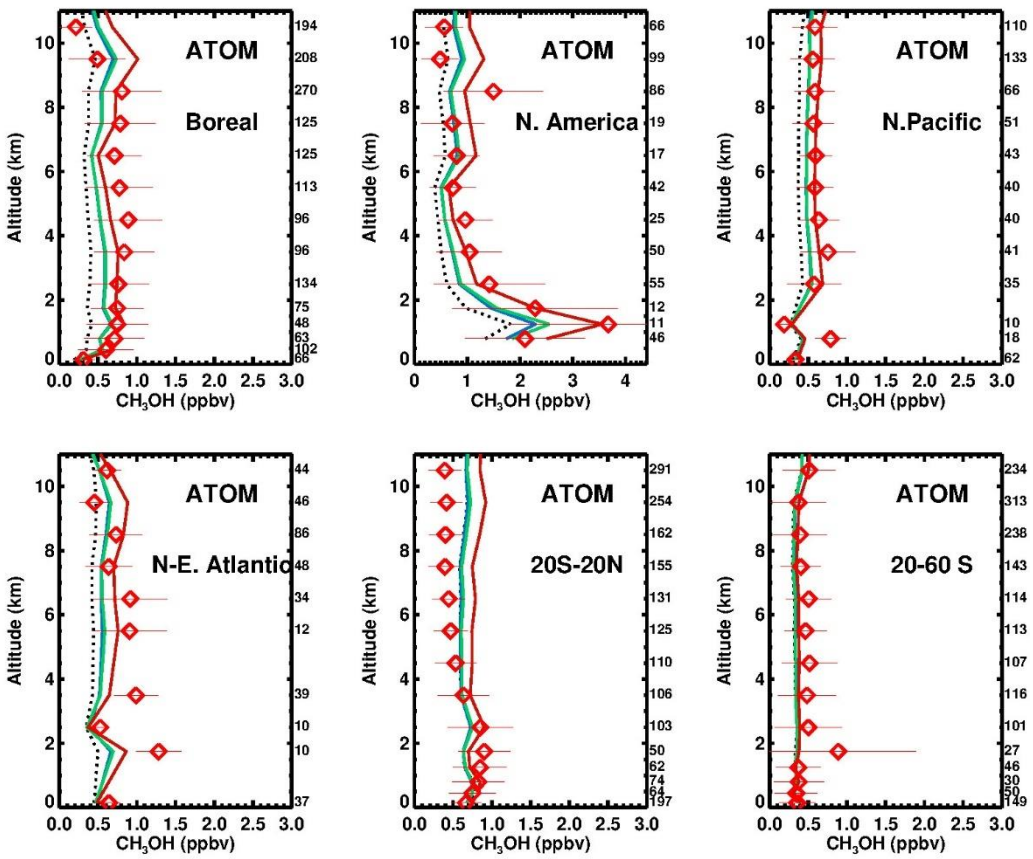

Figure 36. Vertical profiles of observed CH_3OH mixing ratios (symbols) and simulated values using a priori (dotted lines) and optimized emissions (colored curves).

OPT1 and OPT2 underestimate the data by 35-40% on average over land in 2013 (below 8 km altitude). The OPT3 model performs best over remote regions impacted by the continental source. In the Tropics, however, the source enhancement of run OPT3 aggravates the model overestimation (20 S-20 N, Figure 36).

A similar conclusion can be drawn from a comparison of model results with a compilation of surface mixing ratio measurements at 57 sites, summarized in Table VIII.

Table VIII. Comparison of model results with in situ methanol concentrations. The number of sites is indicated in parentheses.

	A priori	OPT1	OPT2	OPT3
Europe (21)	0.74	0.92	0.84	0.83
U.S. (13)	0.73	1.10	1.06	1.16
Amazonia (9)	1.17	1.34	1.41	1.79
Marine (14)	0.81	0.90	0.90	0.97
ALL (57)	0.82	1.01	1.00	1.25

Overall, the OPT1 and OPT2 optimizations lead to a best agreement with the data, but the OPT3 run does very well at mid-latitudes and over oceans.

4.4.4 Recommendations for future model exploitation of the PTR-MS and IASI data

- WRF-Chem is appropriate for simulating long-lived compounds over Reunion Island, even at low resolution (12.5 km), but it is very dependent on the quality of the lateral boundary conditions
- Anthropogenic VOC emissions from global emission databases appear largely overestimated in HTAP over Reunion Island.
- High-resolution anthropogenic emissions ($\sim 1\times1 km^2$) are required to simulate reactive species on Reunion Island and more specifically at Maïdo observatory. Such high-resolution inventory is currently unavailable. A "quick and dirty" solution (convolution of low-resolution EDGAR data with high-resolution data available for CO or CO_2) is recommended in the absence of better alternative.
- Cross-evaluation of IASI, FTIR and aircraft in situ data indicate significant biases between the different datasets, for reasons yet unclear. IASI appears to underestimate the high columns; the magnitude of the bias is moderate against FTIR data, and much more pronounced against aircraft-based columns.
- The derivation of methanol emissions by inverse modeling based on IASI data leads to enhanced emissions over semi-arid areas, similar to previous work (Stavrakou et al. 2011). The magnitude of the emission update inferred by the inversion is very dependent on the bias-correction applied to the data. No single optimization succeeds in reproducing all measurement techniques simultaneously. We highly recommend dedicated intercomparison campaigns aiming to compare FTIR columns with aircraft profiles above FTIR sites (spiral flights). This could be done e.g., within ACTRIS (Aerosol, Clouds and Trace Gases European Research Infrastructure).

5. DISSEMINATION AND VALORISATION

5.1 OCTAVE publications in peer-reviewed journals (in chronological order)

1. Franco, B., L. Clarisse, T. Stavrakou, T., J.-F. Müller, M. Van Damme, S. Whitburn, J. Hadji-Lazaro, D. Hurtmans, D. Taraborrelli, C. Clerbaux, P.-F. Coheur: A general framework for global retrievals of trace gases from IASI: application to methanol, formic acid and PAN. *Journal of Geophysical Research*, 123, 13963-13984, https://doi.org/10.1029/2018JD029633, 2018.
2. Liu, Z., Nguyen, V. S., Harvey, J., Müller, J.-F., and Peeters, J.: The photolysis of alpha-hydroperoxycarbonyls. *Physical Chemistry Chemical Physics*, 20, 6970-6979, https://doi.org/10.1039/C7CP08421H, 2018.
3. Vigouroux, C., C. A. B. Aquino, M. Bauwens, C. Becker, T. Blumenstock, M. De Mazière, O. García, M. Grutter, C. Guarin, J. Hannigan, F. Hase, N. Jones, R. Kivi, D. Koshelev, B. Langerock, E. Lutsch, M. Makarova, J.-M. Metzger, J.-F. Müller, J. Notholt, I. Ortega, M. Palm, C. Paton-Walsh, A. Poberovskii, M. Rettinger, J. Robinson, D. Smale, T. Stavrakou, W. Stremme, K. Strong, R. Sussmann, Y. Té, and G. Toon, NDACC harmonized formaldehyde time-series from 21 FTIR stations covering a wide range of column abundances. *Atmospheric Measurement Techniques*, 11, 5049-5073, https://doi.org/10.5194/amt-11-5049-2018, 2018.
4. Stavrakou, T., Müller, J.-F., Bauwens, M., I. De Smedt, M. Van Roozendael, A. Guenther: Impact of short-term climate variability on volatile organic compounds emissions assessed using OMI satellite formaldehyde observations. *Geophysical Research Letters*, 45, 1621-1629, http://doi.org/10.1029/2018GL078676, 2018.
5. Franco, B., L. Clarisse, T. Stavrakou, J.-F. Müller, A. Pozzer, J. Hadji-Lazaro, D. Hurtmans, C. Clerbaux, and P.-F. Coheur, Acetone atmospheric distribution retrieved from space. *Geophysical Research Letters*, 46, 2884-2893, https://doi.org/10.1029/2019GL082052, 2019.
6. Verreyken, B., Brioude, J., and Evan, S.: Development of turbulent scheme in the FLEXPART-AROME v1.2.1 Lagrangian particle dispersion model. *Geoscientific Model Development*, 12, 4245–4259, https://doi.org/10.5194/gmd-12-4245-2019, 2019.
7. Müller, J.-F., T. Stavrakou, and J. Peeters: Chemistry and deposition in the Model of Atmospheric composition at Global and Regional scales using Inversion Techniques for Trace Gas Emissions (MAGRITTE v1.1). Part A. Chemical mechanism. *Geoscientific Model Development*, 12, 2307-2356, https://doi.org/10.5194/gmd-12-2307-2019, 2019.
8. Worden, H. M., Bloom, A. A., Worden, J. R., Jiang, Z., Marais, E., Stavrakou, T., Gaubert, B., and Lacey, F.: New Constraints on Biogenic Emissions using Satellite-Based Estimates of Carbon Monoxide Fluxes. *Atmospheric Chemistry and Physics*, 19, 13569–13579, https://www.atmos-chem-phys.net/19/13569/2019, 2019.
9. Rocco, M., Colomb, A., Baray, J.-L., Amelynck, C., Verreyken, B., Borbon, A., Pichon, J.-M., Bouvier, L., Schoon, N., Gros, V., Sarda-Esteve, R., Tulet, P., Metzger, J.-M., Duflot, V., Guadagno, C., Peris, G. and Brioude, J.: Analysis of Volatile Organic Compounds during the

OCTAVE Campaign: Sources and Distributions of Formaldehyde on Reunion Island, *Atmosphere*, 11(2), 140, https://doi:10.3390/atmos11020140, 2020.

10. Vigouroux, C., Langerock, B., Bauer Aquino, C. A., Blumenstock, T., Cheng, Z., De Mazière, M., De Smedt, I., Grutter, M., Hannigan, J. W., Jones, N., Kivi, R., Loyola, D., Lutsch, E., Mahieu, E., Makarova, M., Metzger, J.-M., Morino, I., Murata, I., Nagahama, T., Notholt, J., Ortega, I., Palm, M., Pinardi, G., Röhling, A., Smale, D., Stremme, W., Strong, K., Sussmann, R., Té, Y., van Roozendael, M., Wang, P., and Winkler, H.: TROPOMI–Sentinel-5 Precursor formaldehyde validation using an extensive network of ground-based Fourier-transform infrared stations. *Atmospheric Measurement Techniques*, 13, 3751–3767, https://doi.org/10.5194/amt-13-3751-2020, 2020.
11. Link, M., T. Nguyen, K. Bates, J.-F. Müller, D. Farmer: Can isoprene oxidation explain high concentrations of atmospheric formic and acetic acid over forests? *ACD Earth and Space Chemistry*, https://doi.org/10.1021/acsearthspacechem.0c00010, 2020.
12. Verreyken, B., Amelynck, C., Brioude, J., Müller, J.-F., Schoon, N., Kumps, N., Colomb, A., Metzger, J.-M., Lee, C. F., Koenig, T. K., Volkamer, R., and Stavrakou, T.: Characterisation of African biomass burning plumes and impacts on the atmospheric composition over the South-West Indian Ocean. *Atmospheric Chemistry and Physics*, 20, 14821–14845, https://acp.copernicus.org/articles/20/14821/2020, 2020.
13. Yanez-Serrano, A. M., Bourtsoukidis E., Alves, E., Bauwens, M., Stavrakou, T., Llusia, J., Filella, I., Guenther, A., Williams, J., Artaxo, P., Sindelarova, K., Doubalova, J., Kesselmeier, Penuelas, J.: Amazonian BVOC emissions under global change: a review of current research and future directions. *Global Change Biology*, https://doi.org/10.1111/gcb.15185, 2020.
14. Franco, B Clarisse, L., Stavrakou, T., Müller, J.-F., Taraborrelli, D., Hadji-Lazaro, J., Hannigan, J.W., Hase, F.,Hurtmans, D., Jones, N., Lutsch, E., Mahieu, E., Ortega, I., Schneider, M., Strong, K., Vigouroux, C., Clerbaux, C., Coheur, P.-F.: Spaceborne measurements of formic and acetic acid : a global view of the regional sources. *Geophysical Research Letters*, https://doi.org/10.1029/2019GL086239, 2020.
15. Verreyken, B., C. Amelynck, N. Schoon, J.-F. Müller, J. Brioude, N. Kumps, C. Hermans, J.-M. Metzger, and T. Stavrakou: Measurement report: Source apportionment of volatile organic compounds at the remote high-altitude Maïdo observatory. *Atmospheric Chemistry and Physics*, 21, 12965–12988, https://doi.org/10.5194/acp-21-12965-2021, 2021.
16. Morfopoulos, C., J.-F. Müller, T. Stavrakou, M. Bauwens, P. Friedlingstein, I. Colin Prentice, P. Regnier: Vegetation responses to climate extremes recorded by remotely sensed atmospheric formaldehyde. *Global Change Biology*, 1-14, https://doi.org/10.1111/gcb.15880, 2021.
17. Sha, M. K., Langerock, B., Blavier, J.-F. L., Blumenstock, T., Borsdorff, T., Buschmann, M., Dehn, A., De Mazière, M., Deutscher, N. M., Feist, D. G., García, O. E., Griffith, D. W. T., Grutter, M., Hannigan, J. W., Hase, F., Heikkinen, P., Hermans, C., Iraci, L. T., Jeseck, P., Jones, N., Kivi, R., Kumps, N., Landgraf, J., Lorente, A., Mahieu, E., Makarova, M. V., Mellqvist, J., Metzger, J.-M., Morino, I., Nagahama, T., Notholt, J., Ohyama, H., Ortega, I., Palm, M., Petri, C., Pollard, D. F., Rettinger, M., Robinson, J., Roche, S., Roehl, C. M., Röhling, A. N., Rousogenous, C., Schneider, M., Shiomi, K., Smale, D., Stremme, W., Strong,

K., Sussmann, R., Té, Y., Uchino, O., Velazco, V. A., Vigouroux, C., Vrekoussis, M., Wang, P., Warneke, T., Wizenberg, T., Wunch, D., Yamanouchi, S., Yang, Y., and Zhou, M.: Validation of methane and carbon monoxide from Sentinel-5 Precursor using TCCON and NDACC-IRWG stations, Atmos. Meas. Tech., 14, 6249–6304, https://doi.org/10.5194/amt-14-6249-2021, 2021.

18. Simu, S. A., Miyazaki, Y., Tachibana, E., Finkenzeller, H., Brioude, J., Colomb, A., Magand, O., Verreyken, B., Evan, S., Volkamer, R., and Stavrakou, T.: Origin of water-soluble organic aerosols at the Maïdo high-altitude observatory, Réunion Island in the tropical Indian Ocean. *Atmospheric Chemistry and Physics*, https://doi.org/10.5194/acp-2021-277, 2021.
19. Mahieu, E., Fischer, E. V., Franco, B., Palm, M., Wizenberg, T., Smale, D., Clarisse, L., Clerbaux, C., Coheur, P.-F., Hannigan, J. W., Lutsch, E., Notholt, J., Pardo Cantos, I., Prignon, M., Servais, C., and Strong, K.: First retrievals of peroxyacetyl nitrate (PAN) from ground-based FTIR solar spectra recorded at remote sites, comparison with model and satellite data. *Elementa: Science of the Anthropocene*, 9 (1), 00027, https://doi.org/10.1525/elementa.2021.00027, 2021.
20. Rosanka, S., Franco, B., Clarisse, L., Coheur, P.-F., Pozzer, A., Wahner, A., and Taraborrelli, D.: The impact of organic pollutants from Indonesian peatland fires on the tropospheric and lower stratospheric composition. *Atmospheric Chemistry and Physics*, 21, 11257–11288, https://doi.org/10.5194/acp-21-11257-2021, 2021.
21. De Longueville, H., Clarisse, L., Whitburn, S., Franco, B., Bauduin, S., Clerbaux, C., Camy-Peyret, C., and Coheur, P.-F.: Identification of short and long-lived atmospheric trace gases from IASI space observations. *Geophysical Research Letters*, 48, e2020GL091742. https://doi.org/10.1029/2020GL091742, 2021.
22. Rose C., Rissanen, M. P., Iyer, S., Duplissy, J., Yan, C., Nowak, J. B., Colomb, A., Dupuy, R., He, X.-C., Lampilahti, J., Tham, Y. J., Wimmer, D., Metzger, J.-M., Tulet, P., Brioude, J., Planche, C., Kulmala, M., and Sellegri, K.: Investigation of several proxies to estimate sulfuric acid concentration under volcanic plume conditions. *Atmospheric Chemistry and Physics*, 21, 4541–4560, https://doi.org/10.5194/acp-21-4541-2021, 2021.

5.2 PhD thesis

Verreyken, B.: Source attribution of oxygenated volatile organic compounds in the remote tropical atmosphere: analysis of a near-continuous 2-year (O)VOC data set recorded at the Maïdo observatory, La Réunion. Joint thesis between *Ghent University, Faculty of Sciences* and *Université de La Réunion, Laboratoire de l'Atmosphère et des Cyclones*. Ghent, Belgium and Saint-Denis, France, 17 June 2021.

5.3 Conference abstracts (in chronological order)

1. Stavrakou et al. Oxygenated Compounds in the Tropical Atmosphere of the ICOS site of La Reunion Island. ICOS Belgium Science Conference**,** Gembloux, Belgium, 20 October 2017

2. Franco, B., Clarisse, L., Coheur, P.-F., Clerbaux, C., Hurtmans, D., Stavrakou, T., and Müller, J.-F. et al. Quasi-global view of methanol, formic acid and PAN distributions obtained from IASI with neural networks. EGU Conference, Vienna, 9-13 April 2018
3. Verreyken, B., et al. Coupling FLEXPART to the AROME mesoscale model. EGU Conference, Vienna, 9-13 April 2018
4. Stavrakou,T., J.F. Müller, M. Bauwens et al. Oxygenated Compounds in the Tropical Atmosphere (OCTAVE): estimation of top-down methanol and formic acid fluxes based on IASI columns. EGU Conference, Vienna, 9-13 April 2018
5. Verreyken et al. First PTR-MS measurements at La Réunion Island: influences of biomass burning and backtrajectory calculations. EGU Conference, Vienna, 9-13 April 2018
6. Vigouroux, C., et al. First formaldehyde TROPOMI validation using NDACC harmonized total columns obtained within the FTIR network. EGU Conference, Vienna, 9-13 April 2018
7. Müller et al. An updated isoprene oxidation and deposition scheme in IMAGES model. 15th IGAC Science Conference, Takamatsu, Japan, 25-29 September 2018
8. Stavrakou et al. The impact of climate variability on volatile organic compounds emissions assessed using spaceborne formaldehyde from SCIAMACHY and OMI. 15th IGAC Science Conference, Takamatsu, Japan, 25-29 September 2018
9. Franco, B., Clarisse, L., Stavrakou, J., Müller, J.-F., Hadji-Lazaro, J., Hurtmans, D., Taraborrelli, D., Van Damme, M., Whitburn, S., and Coheur, P.-F.: Global distributions of five major OVOCs retrieved from IASI measurements., EGU Conference, 7-12 April 2019
10. Stavrakou, T., J.-F. Müller, B. Franco, L. Clarisse, M. Bauwens, P.-F. Coheur, and C. Clerbaux, Improved understanding of global methanol sources and sinks using novel atmospheric constraints. EGU Conference, 7-12 April 2019
11. Franco, B., Clarisse, L., Stavrakou, J., Müller, J.-F., Hadji-Lazaro, J., Hurtmans, D., Taraborrelli, D., Clerbaux, C., and Coheur, P.-F.: Ratios of atmospheric formic acid and acetic acid seen from space, EGU Conference. 7-12 April 2019
12. Rissanen, M., et al. Iodic acid and new particle formation observed at the high-altitude station of Maïdo (Réunion). EGU Conference, 7-12 April 2019
13. Verreyken, B., C. Amelynck, D. Fonteyn, J.-F. Müller, T. Stavrakou et al. In situ OVOC measurements in the tropical marine atmosphere for the OCTAVE project. EGU Conference, 7-12 April 2019
14. Verreyken, B., Amelynck, C., Schoon, N., Brioude, J., Stavrakou, T. and Müller, J.-F. Diurnal and seasonal variabilities in ground-based in-situ (OVOC) measurements at the Maïdo observatory (South-West Indian Ocean). ICOS Belgium science conference, Antwerp, Belgium
15. Vigouroux et al. Validation of TROPOMI/S5P HCHO using UV-Vis DOAS and FTIR ground-based networks. Living Planet Symposium, 13-17 May 2019 and S5P Validation Team Workshop 11-14 November 2019
16. Stavrakou, T., J.-F. Müller, B. Franco, M. Bauwens, L. Clarisse, P. Coheur, C. Clerbaux: Improved evaluation of the global methanol budget thanks to novel multi-platform observations. AGU Fall Meeting, 9-13 December 2019

17. Müller, J.-F., J. Peeters, T. Stavrakou: Isoprene oxidation and its impact on the oxidizing capacity: effects of recent mechanistic updates. AGU Fall Meeting, 9-13 December 2019
18. Franco, B., Clarisse, L., Stavrakou, T., Müller, J.-F., Hadji-Lazaro, J., Hurtmans, D., Clerbaux, C., and Coheur, P.-F.: Over 10 years of five major oxygenated volatile organic compounds retrieved in biomass burning plumes from IASI satellite measurements. AGU Fall Meeting, 9-13 December 2019
19. Franco B., Clarisse, L., Hadji-Lazaro, J., Hurtmans, D., Lecomte, G., Turquety, S., Clerbaux, C., and Coheur, P.-F.: Large VOC enhancements in recent massive wildfires observed from space. EGU General Assembly. 4-8 May 2020.
20. Stavrakou, T., J.-F. Müller, M. Bauwens, I. De Smedt, M. Van Roozendael: Distribution and trends of biogenic emissions over South American ecocystems deduced by multiyear inversion of satellite formaldehyde data. 19th GEIA Virtual Science Conference, 23 June 2020
21. C. DiMaria, D. Jones, A. Bloom, H. Worden, K. Miyazaki, K. Bowman: Improving the temperature dependence of modeled isoprene emissions in MEGAN with remote sensing constraints. AGU Virtual Fall Meeting, 7-11 December 2020
22. Worden, H., R. Buchholz, B. Gaubert, D. Edwards, L. Emmons, A. Bloom, J. Worden, J. Stavrakou: Investigating the impact of carbon cycle processes on low anomalies in atmospheric carbon monoxide and potential feedbacks in atmospheric chemistry. AGU Fall Meeting, 13-17 December 2021
23. Morfopoulos, C., J.-F. Müller, T. Stavrakou, M. Bauwens et al. Vegetation responses to climate extremes recorded by remotely-sensed atmospheric formaldehyde. EGU General Assembly, 19-30 April 2021
24. Verreyken, B., Amelynck, C., Schoon, N., Müller, J.-F., Brioude, J., Kumps, N., … Stavrakou, T. (2021). Diurnal and seasonal variability in VOC composition at the remote tropical high-altitude Maïdo observatory (21.1°S, 54.4°E, 2160 m altitude). EGU Conference, April 2021
25. Franco, B., Clarisse, L., Clerbaux, C., and Coheur, P.-F.: Analysis of space-based observations of peroxyacetyl nitrate (PAN) and its relations to other atmospheric tracers. EGU General Assembly, 19-30 April 2021
26. Müller, J.-F., T. Stavrakou, M. Bauwens, C. Amelynck, N. Schoon, C. Vigouroux, B. Franco, L. Clarisse, P. F. Coheur, C. Clerbaux, K. Strong, and M. Makarov: Top-down global methanol budget: the view from IASI, FTIR and in situ measurements. AGU Fall Meeting, 13-17 December 2021

5.4 Organization of international workshops

- ***1st Annual OCTAVE progress meeting,*** BIRA-IASB, Brussels, 1 March 2018 (19 participants)

  This meeting includes contributions on (i) the first PTR-MS measurements at Reunion Island; (ii) the coupling between FLEXPART and AROME to model local air masses; (iii) the first quasi-global distributions of methanol, formic acid, and PAN from IASI; (iv) an improved chemical mechanism in IMAGES/MAGRITTE CTM. The OCTAVE intensive field campaign is discussed. It is an international effort conducted by Reunion, Belgium,

France, US, Finland and Japan. The campaign ails to cast light on the drivers of VOC diurnal variability, the VOC speciation and the origin of VOCs. The agenda and a short summary are available in **Annex 1**.

- ***OCTAVE intensive field campaign workshop*****,** BIRA-IASB, Brussels, 4-5 October 2018 (20 participants)
  The aim of the workshop was to present the status of the instruments and the data processing among the different scientific groups who participated to the OCTAVE Intensive field campaign. Besides the OCTAVE project partners (BIRA-IASB, ULB and LACy) in the workshop participated all international teams who performed measurements at Reunion during the OCTAVE campaign. The teams are from Colorado (US), University of Hokkaido (Japan), Helsinki University (Finland), LaMP, LSCE, Université de Toulouse and Université de Grenoble-Alpes (France).

- ***2nd Annual OCTAVE progress meeting & intensive field campaign workshop*****,** BIRA-IASB, Brussels, 16-17 May 2019 (27 participants)
  The aim of the workshop was to present progress during the second year of the OCTAVE project with focus on the analysis of the measurements acquired during the intensive field campaign. The agenda of the meeting and a short summary are available in **Annex 2**.

- ***3rd Annual OCTAVE workshop*****,** 18 May 2020 (14 participants, online)
  The aim of the workshop was to present progress during the third year of the OCTAVE project and on the analysis of the measurements acquired during the OCTAVE field campaign. The agenda of the meeting and a short summary are available in **Annex 3**.

- ***Final OCTAVE workshop*****,** 30 September-1 October 2021 (37 participants, online)
  The aim of the workshop was to present progress during the fourth year of the OCTAVE project, to discuss about future research directions and possible collaborations. The agenda of the meeting is available in **Annex 4**.

5.5 Other

- **OCTAVE Intensive field campaign movie**
  A 3-minute movie on the spring 2018 OCTAVE campaign which was performed at Reunion Island was produced thanks to the efforts of the team from the University of Colorado, who participated to the OCTAVE intensive field campaign. The movie will be presented on special events (e.g. Open Door Days).

- **OCTAVE flyer:** http://octave.aeronomie.be/images/OCTAVE_Flyer.pdf

- **OCTAVE website :** http://octave.aeronomie.be

ANNEXES

Annex 1. 1st Annual OCTAVE meeting, 1 March 2018

OCTAVE
Oxygenated Compounds in the Tropical Atmosphere : Variability and Exchanges

http://octave.aeronomie.be

Royal Belgian Institute for Space Aeronomy, BIRA-IASB, Avenue Circulaire 3, B-1180, Brussels

Meeting Room: Nicolet 1

Participants :

Crist Amelynck, Maite Bauwens, Martine De Mazière, Jean-Francois Müller, Niels Schoon, Jenny Stavrakou, Corinne Vigouroux (BIRA-IASB) ; Lieven Clarisse, Pierre Coheur, Bruno Franco (ULB) ; Jérôme Brioude, Jean-Pierre Cammas, Pierre Tulet (Univ. Reunion, LACy) ; Aurelie Colomb (LaMP, Clermont-Ferrand) ; Bert Verreyken (BIRA-IASB & LACy) ;

Follow-up committee: Dylan Millet (Univ. Minnesota, US), Miguel Portillo-Estrada (Univ. Antwerp), K. Sindelarova (Charles Univ., Czech Republic)

BELSPO Scientific officer: Martine Vanderstraeten

Agenda

10:00-10:15	Welcome, Current project status	Jenny Stavrakou
10:15-10:40	First PTR-MS VOC measurements at Reunion Island, influences of biomass burning and back trajectory calculations	Crist Amelynck Bert Verreyken
10:40-10:50	FTIR column observations at Reunion Island Simulated air composition at Maido using the IMAGES CTM	Corinne Vigouroux Jenny Stavrakou
10:50-11:00		
11:00-11:20	Coupling FLEXPART to the AROME mesoscale operational model	Bert Verreyken
	11:20 Coffee break	
11:40-12:10	The OCTAVE intensive field campaign	Jerome Brioude
12:10-12:30	Applying VOC measurements to a wide spectrum of experiments in ecology	Miguel Portillo Estrada
	12:30 Lunch	

13:30-14:00	VOC retrievals from IASI using neural networks : quasi-global distributions of methanol, formic acid and PAN	Bruno Franco
14:00-14:20	Modelled estimates of global biogenic VOC emissions and their variation due to land cover changes	Katerina Sindelarova
	14:20 Coffee break	
14:40-15:10	Improved chemical mechanism and physical processes in the updated IMAGES CTM	Jean-François Müller
15:10-15:30	Research activities at the Atmospheric Composition and Chemistry Group of Univ. of Minnesota	Dylan Millet
15:30-15:50	Discussion and next steps	All

Short summary

The first PTR-MS measurements at Reunion are presented. The installation of the instrument at the Maïdo Observatory in October 2017, the operating principles, and the measured compounds are discussed. The presenters show the first data series of 14 VOCs, and the diurnal variation for the target species, namely methanol, acetaldehyde and acetone. The average concentrations over October-December 2017 are in fair agreement with those obtained at other marine sites of the Southern Hemisphere. FTIR measurements at 2 sites at Reunion Island are presented: at Saint-Denis (2004-2013) and at Maïdo (2013-present).

The coupling between FLEXPART and AROME models is presented. The turbulent motion is of great importance if one aims to interpret the observations at Reunion Island. However, there are difficulties with the parameterizations. Thomson method is implemented in FLEXPART-AROME. Validation efforts have been conducted, and the Thomson method was found to better conserve a well-mixed tracer. FLEXPART-AROME is a fast tool to model local air masses. The first back trajectory calculations were completed.

The OCTAVE intensive field campaign is discussed. It is an international effort conducted by Reunion, Belgium, France, US, Finland and Japan. The campaign will cast light on the drivers of VOC diurnal variability, the VOC speciation and the origin of VOCs.

The first quasi-global distributions of methanol, formic acid, and PAN from IASI are presented. The fast retrievals are based on supervised feedforward neural networks.

An improved chemical mechanism and physical processes in the updated IMAGES/MAGRITTE CTM is discussed. It includes updates for (i) isoprene and other BVOCs, photolysis of hydroperoxy carbonyls and a new source of HCOOH, (ii) the methanol formation in the $CH_3O_2 + OH$ reaction, (iii) Henry's Law constants, and (iv) dry deposition scheme. The new oxidation scheme is nearly finalized and ready for use in the CTMs.

Annex 2. 2rd Annual OCTAVE meeting and Intensive Field Campaign Workshop, 16-17 May 2019

OCTAVE
Oxygenated Compounds in the Tropical Atmosphere : Variability and Exchanges

http://octave.aeronomie.be

Royal Belgian Institute for Space Aeronomy, BIRA-IASB, Avenue Circulaire 3, B-1180, Brussels

Meeting Room: Nicolet 1 and 2

Participants:

Crist Amelynck, Maite Bauwens, Martine De Mazière, Dominique Fonteyn, Jean-Francois Müller, Niels Schoon, Jenny Stavrakou, Corinne Vigouroux (BIRA-IASB) ; Lieven Clarisse, Pierre Coheur, Bruno Franco (ULB) ; Jérôme Brioude, Jean-Pierre Cammas, Pierre Tulet (Univ. Reunion, LACy) ; Aurelie Colomb, Manon Rocco (LaMP, Clermont-Ferrand) ; Bert Verreyken (BIRA-IASB & LACy) ; Siiharth Iyer, Matti Rissanen (Helsinki Univ.) ; Yuzo Miyazaki (Hokkaido Univ.) ; Olivier Magand (Univ. Grenoble-Alpes) ; Henning Finkenzeller, Theodore Koenig, Christopher Francis Lee, Rainer Volkamer, Kyle Zarzana (Univ. Colorado)

Follow-up committee: Dylan Millet (Univ. Minnesota, US), Miguel Portillo-Estrada (Univ. Antwerp), K. Sindelarova (Charles Univ., Czech Republic)

Invited: Martin Bruggemann (Leipzig Institute for Tropospheric Research, TROPOS)

Agenda

Thursday 16 May

9:15-9:30	Welcome	
9:30-9:45	Overview and progress during OCTAVE 2nd year	Jenny Stavrakou
9:45-9:50	Research activities in the PLECO group	Miguel Portillo-Estrada
9:50-10:20	The OCTAVE 2018 intensive field campaign : Atmospheric transport during the campaign and impact on Maïdo measurements	Jérôme Brioude (to be presented by Jenny Stavrakou)
10:20-10:50	Formaldehyde sources from measurements in Maïdo Observatory	Manon Rocco
10:50-11:10 : *Coffee Break*		
11:10-11:20	*Reunion 2018 : the OCTAVE campaign*	
11:20-11:50	Contribution of marine sources to organic aerosols at Maïdo based on their stable isotopic and molecular characterization	Yuzo Miyazaki
11:50-12:20	Iodic acid and new particle formation observed at Maïdo	Matti Rissanen
12:20-12:50	18 months of PTR-MS measurements at Maïdo	Bert Verreyken
13:00-14:15 : *Lunch break*		

14:30-15:00	Nucleating agents in Maïdo	Siddharth Iyer
15:00-15:30	Field evidence for novel interfacial chemistry in the remote tropical free troposphere	Rainer Volkamer
15:30-16:00	A general framework for global OVOC retrievals from IASI	Bruno Franco
16:00-16:15 : *Coffee break*		
16:15-16:45	Primary vs. secondary sources of formic acid	Dylan Millet
16:45-17:15	Interfacial photochemistry at the ocean surface : a global source of organic vapor and aerosols	Martin Brüggemann
17:15-17:45	The global methanol budget revisited based on IASI constraints	Jenny Stavrakou
19:15 : *Dinner*		

Friday 17 May

9:30-10:00	Stratospheric ozone and NO_2, and halogen/SO_2 by MAX-DOAS during the IOP	Ted Koenig & Chris Lee
10:00-10:15	Progress on mercury measurements in Maïdo Observatory	Olivier Magand
10:15-10:45	Glyoxal in the free troposphere : in situ measurements and air mass assignment at Maïdo Observatory	Henning Finkenzeller
10:45-11:00	FTIR measurements at Reunion Island	Corinne Vigouroux
11:00-11:15 : *Coffee Break*		
11:15-11:45	Evaluation of WRF-Chem model against Reunion measurements	Jean-François Müller
11:45-12:15	Turbulent scheme in the FLEXPART-AROME Lagrangian particle dispersion model	Bert Verreyken
12:15-12:45	Formic and acetic acid : emission sources and seasonal cycles	Bruno Franco
13:00-14:15 : *Lunch break*		
14:30-14:40	Plans for the 3rd year of the OCTAVE project	Jenny Stavrakou
14:40-15:00	Paper plan for the OCTAVE field campaign	All
15:00 : *End of Workshop*		

Short summary

Numerous discussions took place during the workshop between the Belgian and the international teams and it would be impractical to report all this information here. The annual meetings combined with the workshops open new ways for strengthening the existent collaborations between the Belgian teams and create opportunities for building new collaborations. As an example, the collaboration with the University of Colorado on the interpretation of the TORERO and OCTAVE mission data is very relevant for the Belgian teams and will be very beneficial for the OCTAVE partners.

After discussion with the Belgian and international collaborators, we scheduled the ***3rd Annual OCTAVE Progress Meeting and Intensive Field Campaign Workshop*** on **18 May 2020** at BIRA-IASB. Due to the pandemic the meeting was held online.

Annex 3. 3rd Annual OCTAVE Workshop, 18 May 2020 (Online)

OCTAVE
Oxygenated Compounds in the Tropical Atmosphere : Variability and Exchanges

http://octave.aeronomie.be

Participants:

Crist Amelynck, Maite Bauwens, Martine De Mazière, Dominique Fonteyn, Jean-Francois Müller, Catalina Poraicu, Niels Schoon, Jenny Stavrakou, Corinne Vigouroux (BIRA-IASB); Lieven Clarisse, Pierre Coheur, Bruno Franco (ULB); Jérôme Brioude (Univ. Reunion, LACy); Bert Verreyken (BIRA-IASB & LACy); BELSPO Scientific Officers: Martine Vanderstraeten and Aline Van der Werf

Agenda

9:30-9:45	Welcome and short presentation	J. Stavrakou
9:45-10:10	Variability of local OVOC concentrations at Maïdo at different time scales	C. Amelynck, N. Schoon, B. Verreyken, J.-M. Metzger, C. Vigouroux
10:10-10:35	Characterization of African biomass burning plumes and impact on South-west Indian ocean air masses	B. Verreyken, J. Brioude, C. Amelynck, N. Schoon, J.-M. Metzger, A. Colomb, J. Stavrakou, J.-F. Müller
10:35-10:50	Update on FTIR observations at Maïdo	C. Vigouroux, M. De Mazière
10:50-11:15	IASI VOC retrievals: recent developments, a focus on recent wildfires and introducing ethylene from space	B. Franco, L. Clarisse, P.-F. Coheur, C. Clerbaux, D. Hurtmans
11:15-11:40	WRF-Chem model simulations for Reunion Island and comparisons with PTR-MS and FTIR measurements	J.-F. Müller, D. Fonteyn, J. Stavrakou, M. Bauwens
11:40-12:00	Atmospheric transport during BIOMAIDO 2019 as seen by FLEXPART-MESONH and FLEXPART-AROME	J. Brioude, B. Verreyken et al.
12:00-12:20	Discussion and plans for 2020-2021	All

Summary. The partners presented contributions on the (i) transport during the OCTAVE Intensive Field Campaign; (ii) detailed analysis of the 2-year long PTR-MS datasets of 15 (O)VOCs; (iii) current developments in satellite IASI retrievals and new global-scale IASI products; (iv) characterization of the African fire plumes and their impact on air masses at Reunion; (v) chemical-transport simulations using WRF-Chem to interpret PTR-MS and FTIR data. The partners presented their plans for the coming year. Among those, extensive validation of the IASI new satellite products using FTIR data at Reunion as well as additional column observations from ground-based networks will be undertaken. At least 3 publications are currently in preparation by the OCTAVE partners. Many interactions took place among the partners and it would be impractical to report all the discussions here. The ***Final OCTAVE Workshop*** is scheduled on **30 September and 1 October 2021**. The meeting will comprise presentations on the measurements

of the OCTAVE campaign and other campaigns conducted at La Reunion (e.g., BIOMAIDO 2019), PTR-MS and FTIR data, satellite OVOCs from IASI and TROPOMI, and data interpretation using models (WRF-Chem, MAGRITTE, FLEXPART-AROME).

Annex 4. Final OCTAVE Workshop, 30 September and 1 October 2021 (Online)

OCTAVE
Oxygenated Compounds in the Tropical Atmosphere : Variability and Exchanges

http://octave.aeronomie.be

Participants:

Crist Amelynck, Maite Bauwens, Martine De Mazière, Dominique Fonteyn, Jean-Francois Müller, Beata Opacka, Catalina Poraicu, Niels Schoon, Jenny Stavrakou, Corinne Vigouroux (BIRA-IASB) ; Lieven Clarisse, Pierre Coheur, Bruno Franco (ULB) ; Jérôme Brioude, Jean-Pierre Cammas, Pierre Tulet (Univ. Reunion, LACy) ; Aurelie Colomb, Manon Rocco, Clemence Rose, Karine Sellegri, Agnès Borbon (LaMP, Clermont-Ferrand) ; Bert Verreyken (BIRA-IASB & LACy) ; Siiharth Iyer, Matti Rissanen, Yee Jun Tham (Helsinki Univ.) ; Yuzo Miyazaki (Hokkaido Univ.) ; Alkuin Koenig, Olivier Magand, Aurélien Domergue (Univ. Grenoble-Alpes) ; Henning Finkenzeller, Theodore Koenig, Christopher Francis Lee, Rainer Volkamer, Kyle Zarzana (Univ. Colorado) ; Valérie Gros (LSCE, Paris) ; Maud Leriche (CNRS, Paris) ; Jeroen Sonke (Géosciences Environnement Toulouse)

Agenda: Thursday 30 September

15:00-15:05	Setup remote connection	
15:05-15:15	OCTAVE Overview	J. Stavrakou
15:15-15:30	Bio-physicochemistry of tropical clouds at Maïdo (La Reunion Island) : overview of results from the BIO-MAIDO campaign	Maud Leriche *et al*
15:30-15:45	Overview of the latest developments on the VOC retrievals from IASI	Bruno Franco *et al*
15:45-15:50	Short break	
15:50-16:05	Origin of water-soluble organic aerosols at the Maïdo observatory during the OCTAVE 2018 intensive field campaign	Sharmine Akter Simu *et al*
16:05-16:20	Top-down methanol budget: the view from IASI, FTIR and in situ measurements	Jean-François Müller *et al*
16:20-16:30	Discussion	

Friday 1 October

15:00-15:05	Setup remote connection	
15:05-15:20	Dynamics of atmospheric mercury at Maïdo observatory in the tropical Indian ocean	Alkuin Koenig *et al*
15:20-15:35	Long-term MAX-DOAS observations of NO_2, O_3 and IO at Maïdo observatory	Christopher Francis Lee *et al*
15:35-15:45	Short break	

15:45-16:00	Evaluating the formation of iodic acid using field measurements at Maïdo	Henning Finkenzeller *et al*
16:00-16:15	VOCs at Maïdo: variations in time and source attribution	Bert Verreyken *et al*
16:15-16:30	Discussion	

Annex 5. List of acronyms

ANNI	Artificial Neural Network
AROME	Applications of Research to Operations at Mesoscale Model
BB	Biomass Burning
BIRA-IASB	Royal Belgian Institute for Space Aeronomy
CAMS-NRT	Copernicus Atmospheric Monitoring Service Near-Real-Time atmospheric composition model
CKB	Chemical-Kinetics-Based
CNRS	Centre national de la Recherche Scientifique
ECMWF	European Center for Medium-range Weather Forecasts
EPA	United States Environmental Protection Agency
FLEXPART	FLEXible PARTicle dispersion model
FTIR	Fourier transform infrared (FTIR) solar absorption spectrometry
GFAS	Global Fire Assimilation System
HRI	Hyperspectral Range Index
hs-PTR-MS	(high resolution) Proton-transfer-reaction mass spectroscopy
IASI	Infrared Atmospheric Sounding Interferometer
IFS	Integrated Forecasting System (ECMWF model)
IMAGES	Intermediate Model of Annual and Global Evolution of Species
IRWG	NDACC Infra-Red Working Group
LACy	Laboratoire des Cyclones (Reunion Island)
LPDM	Lagrangian Particle Dispersion Model
MAGRITTE	Model of Atmospheric composition at Global and Regional scales using Inversion Techniques for Trace gas Emissions
Meso-NH	Non-Hydrostatic Mesoscale atmospheric model
MVK/MACR	Methyethylketone/methacrolein
NDACC	Network for the Detection of Atmospheric Composition Change
OCTAVE-IOP	OCTAVE Intensive Observation Period
(O)VOC(s)	(Oxygenated) volatile organic compound(s)
PAN	Peroxyacetyl nitrate
PBL	Planetary boundary layer
PMF	Positive Matrix Factorization
STILT	Stochastic Time-Inverted Lagrangian Transport
TKE	Turbulent kinetic energy
TROPOMI	TPOPOspheric ozone Monitoring Instrument
ULB	Université libre de Bruxelles
WRF-Chem	Weather Research and Forecasting - Chemistry

REFERENCES

Akagi, S. K., Burling, I. R., Mendoza, A., Johnson, T. J., Cameron, M., Griffith, D. W. T., Paton-Walsh, C., Weise, D. R., Reardon, J., and Yokelson, R. J.: Field measurements of trace gases emitted by prescribed fires in southeastern US pine forests using an open-path FTIR system. *Atmospheric Chemistry and Physics*, 14, 199-215, 2014.

Andreae, M. O.: Emission of trace gases and aerosols from biomass burning – An updated assessment. *Atmospheric Chemistry and Physics*, 19, 8523–8546, https://doi.org/10.5194/acp-19-8523-2019, 2019.

Andrews, D., Heazlewood, B. R., Maccarone, A. T., Conroy, T., Payne, R. J., Jordan, M. J. T. and Kable, S. H.: Photo-tautomerization of acetaldehyde to vinyl alcohol: A potential route to tropospheric acids. *Science*, 337, 1203-1208, 2012.

Angevine, W. M., Brioude, J., McKeen, S., and Holloway, J. S.: Uncertainty in Lagrangian pollutant transport simulations due to meteorological uncertainty from a mesoscale WRF ensemble, *Geoscientific Model Development*, 7, 2817–2829, 2014.

Assaf, E., Song, B., Tomas, A., Schoemaecker, C. and Fittschen, C.: The rate constant of the reaction between CH_3O_2 radicals and OH radicals revisited. *Journal of Physical Chemistry A*, 120, 8923–8932, 2016.

Assaf, E., Sheps, L., Whalley, L., Heard, D., Tomas, A., Schoemacker, C. and Fittschen, C.: The reaction between CH_3O_2 and OH radicals: Product yields and atmospheric implications. *Environmental Science and Technology*, 2017, 51, 2170–-2177, 2017.

Assaf, E., Schoemacker, C., Vereecken, L., and Fittschen, C.: Experimental and theoretical investigation of the reaction of RO_2 radicals with OH radicals: Dependence of the HO_2 yield on the size of the alkyl group. *International Journal of Chemical Kinetics*, 1–11, 2018.

Baasandorj, M., Millet, D. B., Hu, L., Mitroo, D., and Williams, B. J.: Measuring acetic and formic acid by proton-transfer-reaction mass spectrometry: sensitivity, humidity dependence, and quantifying interferences. *Atmospheric Measurement Techniques*, 8, 1303-1321, 2015.

Bauwens, M., Stavrakou, T., Müller, J.-F., Van Schaeybroeck, B., De Cruz, L., De Troch, R., Giot, O., Hamdi, R., Termonia, P., Laffineur, Q., Amelynck, C., Schoon, N., Heinesch, B., Holst, T., Arneth, A., Ceulemans, R., Sanchez-Lorenzo, A., and Guenther, A.: Recent past (1979–2014) and future (2070–2099) isoprene fluxes over Europe simulated with the MEGAN–MOHYCAN model, *Biogeosciences*, 15, 3673–3690, 2018.

Bougeault, P. and Lacarrère, P.: Parameterization of Orography-Induced Turbulence in a Mesobeta–Scale Model. Monthly Weather Reviews, 117, 1872–1890, 1989.

Brioude, J., Arnold, D., Stohl, A., Cassiani, M., Morton, D., Seibert, P., Angevine, W., Evan, S., Dingwell, A., Fast, J. D., Easter, R. C., Pisso, I., Burkhart, J., and Wotawa, G.: The Lagrangian

particle dispersion model FLEXPART-WRF version 3.1, *Geoscientific Model Development* 6, 1889–1904, https://doi.org/10.5194/gmd-6-1889-2013, 2013.

Cady-Pereira, K. E. et al. Methanol from TES global observations : retrieval algorithm and seasonal and spatial variability, *Atmospheric Chemistry and Physics*, 12, 8189, 2012.

Chaliyakunnel, S., D. B. Millet, K. C. Wells, K. E. Cady-Pereira, M. W. Shephard: A large underestimate of formic acid from tropical fires: constraints from space-borne measurements, *Environmental Science and Technology*, 50 (11), 5631-5640, 2016.

Clarisse, L., R'Honi, Y., Coheur, P.-F., Hurtmans, D., and Clerbaux, C.: Thermal infrared nadir observations of 24 atmospheric gases. *Geophysical Research Letters*, 38, L10802, 2011.

Clarisse, L., Clerbaux, C., Franco, B., Hadji-Lazaro, J., Whitburn, S., Kopp, A. K., Hurtmans, D., and Coheur, P.-F.: A decadal data set of global atmospheric dust retrieved from IASI satellite measurements. *Journal of Geophysical Research: Atmospheres*, 124, 1618– 1647. https://doi.org/10.1029/2018JD029701, 2019.

Coheur, P. F., Barret, B., Turquety, S., Hurtmans, D., Hadji-Lazaro, J., and Clerbaux, C.: Retrieval and characterization of ozone vertical profiles from a thermal infrared nadir sounder. *Journal of Geophysical Research*, 110, D24303, 2005.

Coheur, P.-F., Clarisse, L., Turquety, S., Hurtmans, D., and Clerbaux, C.: IASI measurements of reactive trace species in biomass burning plumes. *Atmospheric Chemistry and Physics*, 9(15), 5655-5667, 2009.

Cornwell, G. C., Xiao, H., Berg, L. K., and Burrows, S. M.: Simulated dust transport in the convective boundary layer. *Journal of Geophysical Research: Atmospheres*, 126, e2020JD033429, https://doi.org/10.1029/2020JD033429, 2021.

de Gouw, J. A., Warneke, C., Stohl, A., Wollny, A. G., Brock, C. A., Cooper, O. R., Holloway, J. S., Trainer, M., Fehsenfeld, F. C., Atlas, E. L., Donnelly, S. G., Stroud, V., and Lueb, A.: Volatile organic compounds composition of merged and aged forest fire plumes from Alaska and western Canada, *Journal of Geophysical Research*, 111, https://doi.org/10.1029/2005JD006175, 2006.

De Longueville, H., Clarisse, L., Whitburn, S., Franco, B., Bauduin, S., Clerbaux, C., Camy-Peyret, C., and Coheur, P.-F.: Identification of short and long-lived atmospheric trace gases from IASI space observations. *Geophysical Research Letters*, 48, e2020GL091742. https://doi.org/10.1029/2020GL091742, 2021.

Duflot, V., Wespes, C., Clarisse, L., Hurtmans, D., Ngadi, Y., Jones, N., Paton-Walsh, C., Hadji-Lazaro, J., Vigouroux, C., De Mazière, M., Metzger, J.-M., Mahieu, E., Servais, C., Hase, F., Schneider, M., Clerbaux, C., and Coheur, P.-F.: Acetylene (C_2H_2) and hydrogen cyanide (HCN) from IASI satellite observations: global distributions, validation, and comparison with model. *Atmospheric Chemistry and Physics*, 15, 10509-10527, 2015.

Duflot, V., Tulet, P., Flores, O., Barthe, C., Colomb, A., Deguillaume, L., Vaïtilingom, M., Perring, A., Huffman, A., Hernandez, M. T., Sellegri, K., Robinson, E., O'Connor, D. J., Gomez, O. M., Burnet, F., Bourrianne, T., Strasberg, D., Rocco, M., Bertram, A. K., Chazette, P., Totems, J., Fournel, J., Stamenoff, P., Metzger, J.-M., Chabasset, M., Rousseau, C., Bourrianne, E., Sancelme, M., Delort, A.-M., Wegener, R. E., Chou, C., and Elizondo, P.: Preliminary results from the FARCE 2015 campaign: multidisciplinary study of the forest–gas–aerosol–cloud system on the tropical island of La Réunion. *Atmospheric Chemistry and Physics*, 19, 10591–10618, https://doi.org/10.5194/acp-19-10591-2019, 2019.

Dufour, G., Szopa, S., Harrison, J. J., Boone, C. D., and Bernath, P. F.: Seasonal variations of acetone in the upper troposphere–lower stratosphere of the northern mid-latitudes as observed by ACE-FTS. *Journal of Molecular Spectroscopy*, 323, 67–77, 2016.

Fischer, E. V. et al. Atmospheric peroxyacetyl nitrate (PAN): a global budget and source attribution, *Atmospheric Chemistry and Physics*, 14, 2679, 2014.

Foucart, B., Sellegri, K., Tulet, P., Rose, C., Metzger, J.-M., and Picard, D.: High occurrence of new particle formation events at the Maïdo high-altitude observatory (2150 m), Réunion (Indian Ocean). *Atmospheric Chemistry and Physics*, 18, 9243-9261, https://doi.org/10.5194/acp-18-9243-2018, 2018.

Franco, B., Clarisse, L., Stavrakou, T., Müller, J. F., Van Damme, M., Whitburn, S., Hadji-Lazaro, J., Hurtmans,D., Taraborrelli, D., Clerbaux, C. and Coheur, P. F.: A general framework for global retrievals of trace gases from IASI: Application to methanol, formic acid, and PAN. *Journal of Geophysical Research*, 123, 13,963–13,984, 2018.

Franco, B., Clarisse, L., Stavrakou, T., Müller, J.-F., Pozzer, A., Hadji-Lazaro, J., Hurtmans,D., Clerbaux, C. and Coheur, P. F.: Acetone atmospheric distribution retrieved from space. *Geophysical Research Letters*, 46, 2884–2893, 2019.

Franco, B., Clarisse, L., Stavrakou, T., Müller, J.-F., Taraborrelli, D., Hadji-Lazaro, J., Hannigan, J. W., Hase, F., Hurtmans, D., Jones, N., Lutsch, E., Mahieu, E., Ortega, I., Schneider, M., Strong, K., Vigouroux, C., Clerbaux, C., and Coheur, P.-F.: Spaceborne measurements of formic and acetic acids: A global view of the regional sources. *Geophysical Research Letters*, 47, e2019GL086239, 2020.

Fried, A., Mckeen, S., Sewell, S., Harder, J., Henry, B., Goldan, P., Kuster, W., Williams, E., Baumann, K., Shetter, R. et al. Photochemistry of formaldehyde during the 1993 Tropospheric OH Photochemistry Experiment. *Journal of Geophysical Research,* 102, 6283–6296, 1997.

Goede, J.G., R. J. Yokelson, D. E. Ward, R. A. Susott, R. E. Babbitt, M. A. Davies, and W. M. Mao: Measurements of excess O_3, CO_2, CO, C_2H_4, C_2H_2, HCN, NO, NH_3, HCOOH, CH_3COOH, HCHO, and CH_3OH in 1997 Alaskan biomass burning plumes by airborne Fourier Transform infrared spectroscopy (AFTIR). *Journal of Geophysical Research*, 105, 22147, 2000.

Guerette, E.-A. Measurements of Volatile organic compound sources and ambient concentrations

in south-East Australia, Doctor of Philosophy thesis, University of Wollongong, http://ro.uow.edu.au/theses/4855, 2016.

Hersbach, H., Bell, B., Berrisford, P., Hirahara, S., Horányi, A., Muñoz-Sabater, J., Nicolas, J., Peubey, C., Radu, R., Schepers, D., Simmons, A., Soci, C., Abdalla, S., Abellan, X., Balsamo, G., Bechtold, P., Biavati, G., Bidlot, J., Bonavita, M., Chiara, G., Dahlgren, P., Dee, D., Diamantakis, M., Dragani, R., Flemming, J., Forbes, R., Fuentes, M., Geer, A., Haimberger, L., Healy, S., Hogan, R. J., Hólm, E., Janisková, M., Keeley, S., Laloyaux, P., Lopez, P., Lupu, C., Radnoti, G., Rosnay, P., Rozum, I., Vamborg, F., Villaume, S., and Thépaut, J.-N.: The ERA5 global reanalysis. *Quarterly Journal of the Royal Meteorological Society*, 146, 1999–2049, https://doi.org/10.1002/qj.3803, 2020.

Holzinger, R., Williams, J., Salisbury, G., Klüpfel, T., de Reus, M., Traub, M., Crutzen, P. J., and Lelieveld, J.: Oxygenated compounds in aged biomass burning plumes over the Eastern Mediterranean: evidence for strong secondary production of methanol and acetone. *Atmospheric Chemistry and Physics*, 5, 39-46, https://doi.org/10.5194/acp-5-39-2005, 2005.

Huang, G., Brook, R., Crippa, M., Janssens-Maenhout, G., Schieberle, C., Dore, C., Guizzardi, D., Muntean, M., Schaaf, E., and Friedrich, R.: Speciation of anthropogenic emissions of non-methane volatile organic compounds: a global gridded data set for 1970–2012. *Atmospheric Chemistry and Physics*, 17, 7683-7701, https://doi.org/10.5194/acp-17-7683-2017, 2017.

Janssens-Maenhout, G., Crippa, M., Guizzardi, D., Dentener, F., Muntean, M., Pouliot, G., Keating, T., Zhang, Q., Kurokawa, J., Wankmüller, R., Denier van der Gon, H., Kuenen, J. J. P., Klimont, Z., Frost, G., Darras, S., Koffi, B., and Li, M.: HTAP_v2.2: a mosaic of regional and global emission grid maps for 2008 and 2010 to study hemispheric transport of air pollution. *Atmospheric Chemistry and Physics*, 15, 11411-11432, 2015.

Jost, C., Trentmann, J., Sprung, D., Andreae, M. O., and Dewey, K.: Deposition of acetonitrile to the Atlantic Ocean off Namibia and Angola and its implications for the atmospheric budget of acetonitrile. *Geophysical Research Letters*, 30, 1837-1841, https://doi.org/10.1029/2003G *Atmospheric Chemistry and Physics* L017347, 2003.

Lac, C., Chaboureau, J.-P., Masson, V., Pinty, J.-P., Tulet, P., Escobar, J., Leriche, M., Barthe, C. et al.: Overview of the Meso-NH model version 5.4 and its applications. *Geoscientific Model Development*, 11, 1929–1969, https://doi.org/10.5194/gmd-11-1929-2018, 2018.

Lefer, B. L., Talbot, R. W., Harriss, R. H., Bradshaw, J. D., Sandholm, S. T., Olson, J. O., Sachse, G. W., Collins, J., Shipham, M. A., Blake, D. R., Klemm, K. I., Klemm, O., Gorzelska, K., and Barrick, J.: Enhancement of acidic gases in biomass burning impacted air masses over Canada. *Journal of Geophysical Research*, 99, 1721-1737, 1994.

Lesouëf, D., Gheusi, F., Delmas, R., and Escobar, J.: Numerical simulations of local circulations and pollution transport over Reunion Island. *Annals of Geophysics*, 29, 53–69, https://doi.org/10.5194/angeo-29-53-2011, 2011.

Lin, J. C., Gerbig, C., Wofsy, S. C., Andrews, A. E., Daube, B. C., Davis, K. J., and Grainger, C. A.: A near-field tool for simulating the upstream influence of atmospheric observations: The Stochastic Time-Inverted Lagrangian Transport (STILT) model. *Journal of Geophysical Research,* 108, https://doi.org/10.1029/2002JD003161, 4492, 2003.

Liu, Z., V. S. Nguyen, J. Harvey, J.-F. Müller, and J. Peeters: Theoretically derived mechanisms of HPALD photolysis in isoprene oxidation. *Physical Chemistry Chemical Physics*, 19, 9096-9106, doi:10.1039/c7cp00288b, 2017.

Liu, Z., Nguyen, V. S., Harvey, J., Müller, J.-F., and Peeters, J.: The photolysis of alpha-hydroperoxycarbonyls. *Physical Chemistry Chemical Physics*, 20, 6970-6979, DOI: 10.1039/C7CP08421H, 2018.

Mahieu, E., Fischer, E. V., Franco, B., Palm, M., Wizenberg, T., Smale, D., Clarisse, L., Clerbaux, C., Coheur, P.-F., Hannigan, J. W., Lutsch, E., Notholt, J., Pardo Cantos, I., Prignon, M., Servais, C., and Strong, K.: First retrievals of peroxyacetyl nitrate (PAN) from ground-based FTIR solar spectra recorded at remote sites, comparison with model and satellite data. *Elementa: Science of the Anthropocene*, 9 (1), 00027, https://doi.org/10.1525/elementa.2021.00027, 2021.

Mascaut, F., O. Pujol, B. Verreyken, R. Peroni, J.-M. Metzger, L. Blarel, T. Podvin, P. Goloub, K. Sellegri, T. Thornberry, V. Duflot, P. Tulet, J. Brioude: Aerosol characterization in an oceanic context around Reunion Island (AEROMARINE field campaign). *Atmospheric Environment*, 268, 2022, 118770, ISSN 1352-2310, https://doi.org/10.1016/j.atmosenv.2021.118770, 2022.

Millet, D. B., Guenther, A., Siegel, D. A., Nelson, N. B., Singh, H. B., de Gouw, J. A., Warneke, C., Williams, J., Eerdekens, G., Sinha, V., Karl, T., Flocke, F., Apel, E., Riemer, D. D., Palmer, P. I., and Barkley, M.: Global atmospheric budget of acetaldehyde: 3-D model analysis and constraints from in-situ and satellite observations. *Atmospheric Chemistry and Physics*, 10, 3405-3425, https://doi.org/10.5194/acp-10-3405-2010, 2010.

Müller, J.-F., Z. Liu, V. S. Nguyen, T. Stavrakou, J. Harvey, and J. Peeters, The reaction of methyl peroxy and hydroxyl radicals as a major source of atmospheric methanol. *Nature Communications*, 7, 13213, doi:10.1038/ncomms13213, 2016.

Müller, J.-F., Stavrakou, T., and Peeters, J.: Chemistry and deposition in the Model of Atmospheric composition at Global and Regional scales using Inversion Techniques for Trace gas Emissions (MAGRITTEv1.0). Part A. Chemical mechanism. *Geoscientific Model Development*, 12, 2307-2356, https://doi.org/10.5194/gmd-12-2307-2019, 2019.

Müller, J.-F., Liu, Z., Nguyen, V. S., Stavrakou, T., Harvey, J. N. and Peeters, J.: The reaction of methyl peroxy and hydroxyl radicals as a major source of atmospheric methanol. *Nature Communications*, 7, 13213, 2016.

Neefs, E., De Mazière, M., Scolas, F., Hermans, C., and Hawat, T. : BARCOS, an automation and

remote control system for atmospheric observations with a Bruker interferometer. *Review of Scientific Instruments*, 78, 035109, 2007.

Nguyen, T., Tyndall, G., Crounse, J. D., Teng, A., Bates, K., Schwantes, R., Coggon, M., Zhang, L., Feiner, P., Miller, D., Skog, K., Rivera-Rios, J., Dorris, M., Olson, K. Koss, A., Wild, R., Brown, S., Goldstein, A., de Gouw, J., Wennberg, P.: Atmospheric Fates of Criegee Intermediates in the Ozonolysis of Isoprene. *Physical Chemistry Chemical Physics*, 18, 10.1039/C6CP00053C, 2016.

Norris, G., Duvall, R., Brown, S., and Bai, S.: EPA Positive Matrix Factorization (PMF) 5.0 Fundamentals and User Guide, United States, Environmental Protection Agency (EPA), https://www.epa.gov/air-research/epa-positive-matrix-factorization-50-fundamentals-and-user-guide (last access: 26 August 2021), 2014.

Parrish, D.D., Stohl, A., Forster, C., Atlas, E.L., Blake, D.R., Goldan, P.D., Kuster, W.C., De Gouw, J.A., Parrish, C. Effects of mixing on evolution of hydrocarbon ratios in the troposphere. *Journal of Geophysical Research*, 112, 10–34, 2007.

Peeters, J., J.-F. Müller, T. Stavrakou, and S. V. Nguyen, Hydroxyl radical recycling in isoprene oxidation driven by hydrogen bonding and hydrogen tunneling: the upgraded LIM1 mechanism. *Journal of Physical Chemistry A*, 118, 8625-8643, DOI: 10.1021/jp5033146, 2014.

Peeters, J., V. S. Nguyen, and J.-F. Müller, Atmospheric vinyl alcohol to acetaldehyde tautomerization revisited. *Journal of Physical Chemistry Letters*, 6, 4005-4011, 2015.

Pernov, J. B., Bossi, R., Lebourgeois, T., Nøjgaard, J. K., Holzinger, R., Hjorth, J. L., and Skov, H.: Atmospheric VOC measurements at a High Arctic site: characteristics and source apportionment. *Atmospheric Chemistry and Physics*, 21, 2895–2916, https://doi.org/10.5194/acp-21-2895-2021, 2021.

Pisso, I., Sollum, E., Grythe, H., Kristiansen, N. I., Cassiani, M., Eckhardt, S., Arnold, D., Morton, D., Thompson, R. L., Groot Zwaaftink, C. D., Evangeliou, N., Sodemann, H., Haimberger, L., Henne, S., Brunner, D., Burkhart, J. F., Fouilloux, A., Brioude, J., Philipp, A., Seibert, P., and Stohl, A.: The Lagrangian particle dispersion model FLEXPART version 10.4. *Geoscientific Model Development,* 12, 4955–4997, https://doi.org/10.5194/gmd-12-4955-2019, 2019.

Pommier, M., Clerbaux, C., Coheur, P.-F., Mahieu, E., Müller, J.-F., Paton-Walsh, C., Stavrakou, T., and Vigouroux, C.: HCOOH distributions from IASI for 2008–2014: comparison with ground-based FTIR measurements and a global chemistry-transport model. *Atmospheric Chemistry and Physics*, 16, 8963-8981, 2016.

Razavi, A., Karagulian, F., Clarisse, L., Hurtmans, D., Coheur, P. F., Clerbaux, C., Müller, J. F., and Stavrakou, T.: Global distributions of methanol and formic acid retrieved for the first time from the IASI/MetOp thermal infrared sounder. *Atmospheric Chemistry and Physics*, 11, 857-872, 2011.

Read, K. A. et al. Multiannual Observations of Acetone, Methanol, and Acetaldehyde in Remote Tropical Atlantic Air: Implications for Atmospheric OVOC Budgets and Oxidative Capacity, Environmental Science and Technology, 46, 11028 – 11039, 2012.

Rocco, M., A. Colomb, J.-L. Baray, C. Amelynck, B. Verreyken, A. Borbon, J.-M. Pichon, L. Bouvier, N. Schoon, V. Gros, R. Sarda-Esteve, P. Tulet, J.-M. Metzger, V. Duflot, C. Guadagno, G. Peris, and J. Brioude: Analysis of Volatile Organic Compounds during the OCTAVE campaign: sources and distributions of Formaldehyde on Reunion Island. *Atmosphere*, 140, https://doi.org/10.3390/atmos11020140, 2020.

Rosanka, S., Franco, B., Clarisse, L., Coheur, P.-F., Pozzer, A., Wahner, A., and Taraborrelli, D.: The impact of organic pollutants from Indonesian peatland fires on the tropospheric and lower stratospheric composition. *Atmospheric Chemistry and Physics*, 21, 11257–11288, https://doi.org/10.5194/acp-21-11257-2021, 2021.

Rose, C., Rissanen, M. P., Iyer, S., Duplissy, J., Yan, C., Nowak, J. B., Colomb, A., Dupuy, R., He, X.-C., Lampilahti, J., Tham, Y. J., Wimmer, D., Metzger, J.-M., Tulet, P., Brioude, J., Planche, C., Kulmala, M., and Sellegri, K.: Investigation of several proxies to estimate sulfuric acid concentration under volcanic plume conditions. *Atmospheric Chemistry and Physics*, 21, 4541–4560, https://doi.org/10.5194/acp-21-4541-2021, 2021.

Schwantes, R. H.; Teng, A. P.; Nguyen, T. B.; Coggon, M. M.; Crounse, J. D.; St. Clair, J.; Zhang, X.; Schilling, K. A.; Seinfeld, J. H. and Wennberg, P. O.: Isoprene NO_3 oxidation products from the $RO_2 + HO_2$ pathway. *Journal of Physical Chemistry A*, 119, 10158-10171, 2015.

Sheps, L., Rotavera, B., Eskola, A. J., Osborn, D. L., Taatjes, C. A., Au, K., Shallcross, D. E., Khan, M. A. H. and Percival, C. J.: The reaction of Criegee intermediate CH_2OO with water dimer: primary products and atmospheric impact. *Physical Chemistry Chemical Physics*, 19, 21970-21979, 2017.

Stavrakou, T., Guenther, A., Razavi, A., Clarisse, L., Clerbaux, C., Coheur, P.-F., Hurtmans, D., Karagulian, F., De Mazière, M., Vigouroux, C., Amelynck, C., Schoon, N., Laffineur, Q., Heinesch, B., Aubinet, M., Rinsland, C., and Müller, J.-F.: First space-based derivation of the global atmospheric methanol emission fluxes. *Atmospheric Chemistry and Physics*, 11, 4873–4898, 2011.

Stavrakou, T., Müller, J.-F., Peeters, J., Razavi, A., Clarisse, L., Clerbaux, C., Coheur, P.-F., Hurtmans, D., Mazière, M. D., Vigouroux, C., Deutscher, N. M., Griffith, D. W. T., Jones, N., and Paton-Walsh, C.: Satellite evidence for a large source of formic acid from boreal and tropical forests. *Nature Geoscience*, 5, 26–30, 2012.

Stavrakou, T., Müller, J.-F., Bauwens, M., I. De Smedt, M. Van Roozendael, A. Guenther: Impact of short-term climate variability on volatile organic compounds emissions assessed using OMI satellite formaldehyde observations. *Geophysical Research Letters*, 45, 1621-1629, http://doi.org/10.1029/2018GL078676, 2018.

Stohl, A., M. Hittenberger, and G. Wotawa: Validation of the Lagrangian particle dispersion model FLEXPART against large scale tracer experiments. *Atmospheric Environment* 32, 4245-4264, 1998.

Teng, A. P., Crounse, J. D., and Wennberg, P. O.: Isoprene peroxy radical dynamics. *Journal of the American Chemical Society*, 139, 15, 5367-5377, 2017.

Tereszchuk, K. A., Moore, D. P., Harrison, J. J., Boone, C. D., Park, M., Remedios, J. J., Randel, W. J., and Bernath, P. F.: Observations of peroxyacetyl nitrate (PAN) in the upper troposphere by the Atmospheric Chemistry Experiment-Fourier Transform Spectrometer (ACE-FTS). *Atmospheric Chemistry and Physics*, 13, 5601-5613, 2013.

Thomson, D. J.: Criteria for the selection of stochastic models of particle trajectories in turbulent flows. *Journal of Fluid Mechanics,* 180, 529–556, https://doi.org/10.1017/S0022112087001940, 1987.

Thomson, D. J., Physick, W. L. and Maryon, R. H.: Treatment of interfaces in random walk dispersion models. *Journal of Applied Meteorology*, 36, 1284-1295, 1997.

Tulet, P., Di Muro, A., Colomb, A., Denjean, C., Duflot, V., Arellano, S., Foucart, B., Brioude, J., Sellegri, K., Peltier, A., Aiuppa, A., Barthe, C., Bhugwant, C., Bielli, S., Boissier, P., Boudoire, G., Bourrianne, T., Brunet, C., Burnet, F., Cammas, J.-P., Gabarrot, F., Galle, B., Giudice, G., Guadagno, C., Jeamblu, F., Kowalski, P., Leclair de Bellevue, J., Marquestaut, N., Mékies, D., Metzger, J.-M., Pianezze, J., Portafaix, T., Sciare, J., Tournigand, A., and Villeneuve, N.: First results of the Piton de la Fournaise STRAP 2015 experiment: multidisciplinary tracking of a volcanic gas and aerosol plume. *Atmospheric Chemistry and Physics*, 17, 5355–5378, https://doi.org/10.5194/acp-17-5355-2017, 2017.

Van Damme, M., Whitburn, S., Clarisse, L., Clerbaux, C., Hurtmans, D., and Coheur, P.-F.: Version 2 of the IASI NH3 neural network retrieval algorithm: near-real-time and reanalysed datasets. *Atmospheric Measurement Techniques*, 10, 4905-4914, 2017.

Verreyken, B., Brioude, J., and Evan, S.: Development of turbulent scheme in the FLEXPART-AROME v1.2.1 Lagrangian particle dispersion model, *Geoscientific Model Development*, 12, 4245-4259, https://doi.org/10.5194/gmd-12-4245-2019, 2019.

Verreyken, B., Amelynck, C., Brioude, J., Müller, J.-F., Schoon, N., Kumps, N., Colomb, A., Metzger, J.-M., Lee, C. F., Koenig, T. K., Volkamer, R., and Stavrakou, T.: Characterisation of African biomass burning plumes and impacts on the atmospheric composition over the South-West Indian Ocean. *Atmospheric Chemistry and Physics*, 20, 14821–14845, https://acp.copernicus.org/articles/20/14821/2020, 2020.

Verreyken, B., C. Amelynck, N. Schoon, J.-F. Müller, J. Brioude, N. Kumps, C. Hermans, J.-M. Metzger, and T. Stavrakou: Measurement report: Source apportionment of volatile organic compounds at the remote high-altitude Maïdo observatory. *Atmospheric Chemistry and Physics*, 21, 12965–12988, https://doi.org/10.5194/acp-21-12965-2021, 2021.

Vigouroux, C., Hendrick, F., Stavrakou, T., Dils, B., De Smedt, I., Hermans, C., Merlaud, A., Scolas, F., Senten, C., Vanhaelewyn, G., Fally, S., Carleer, M., Metzger, J.-M., Müller, J.-F., Van Roozendael, M., and De Mazière, M.: Ground-based FTIR and MAX-DOAS observations of formaldehyde at Réunion Island and comparisons with satellite and model data. *Atmospheric Chemistry and Physics*, 9, 9523–9544, https://doi.org/10.5194/acp-9-9523-2009, 2009.

Vigouroux, C., Stavrakou, T., Whaley, C., Dils, B., Duflot, V., Hermans, C., Kumps, N., Metzger, J.-M., Scolas, F., Vanhaelewyn, G., Müller, J.-F., Jones, D. B. A., Li, Q., and De Mazière, M.: FTIR time-series of biomass burning products (HCN, C_2H_6, C_2H_2, CH_3OH, and HCOOH) at Reunion Island (21° S, 55° E) and comparisons with model data. *Atmospheric Chemistry and Physics*, 12, 10367-10385, https://doi.org/10.5194/acp-12-10367-2012, 2012.

Vigouroux, C., Bauer Aquino, C. A., Bauwens, M., Becker, C., Blumenstock, T., De Mazière, M., García, O., Grutter, M., Guarin, C., Hannigan, J., Hase, F., Jones, N., Kivi, R., Koshelev, D., Langerock, B., Lutsch, E., Makarova, M., Metzger, J.-M., Müller, J.-F., Notholt, J., Ortega, I., Palm, M., Paton-Walsh, C., Poberovskii, A., Rettinger, M., Robinson, J., Smale, D., Stavrakou, T., Stremme, W., Strong, K., Sussmann, R., Té, Y., and Toon, G.: NDACC harmonized formaldehyde time series from 21 FTIR stations covering a wide range of column abundances. *Atmospheric Measurement Techniques*, 11, 5049-5073, 2018.

Vigouroux, C., Langerock, B., Bauer Aquino, C. A., Blumenstock, T., De Mazière, M., De Smedt, I., Grutter, M., Hannigan, J., Jones, N., Kivi, R., Lutsch, E., Mahieu, E., Makarova, M., Metzger, J.-M., Morino, I., Murata, I., Nagahama, T., Notholt, J., Ortega, I., Palm, M., Pinardi, G., Röhling, A., Smale, D., Stremme, W., Strong, K., Sussmann, R., Té, Y., van Roozendael, M., Wang, P. and Winkler, H.: TROPOMI/S5P formaldehyde validation using an extensive network of ground-based FTIR stations. *Atmospheric Measurement Techniques*, 13, Issue 7, 3715-3767, doi:10.5194/amt-13-3751-2020, 2020.

Walker, J. C., Dudhia, A., and Carboni, E.: An effective method for the detection of trace species demonstrated using the MetOp Infrared Atmospheric Sounding Interferometer. *Atmospheric Measurement Techniques*, 4, 1567–1580, https://doi.org/10.5194/amt-4-1567-2011, 2011.

Wells, K. C. et al. Quantifying global terrestrial methanol emissions using observations from the TES satellite sensor, *Atmospheric Chemistry and Physics*, 14, 2555, 2014.

Whitburn, S., Van Damme, M., Clarisse, L., Bauduin, S., Heald, C. L., Hadji-Lazaro, J., Hurtmans, D., Zondlo, M. A., Clerbaux, C., and Coheur, P.-F.: A flexible and robust neural network IASI-NH_3 retrieval algorithm. *Journal of Geophysical Research*, 121, 6581–6599, 2016.

Yokelson, R. J., Bertschi, I. T., Christian, T. J., Hobbs, P. V., Ward, D. E., and Hao, W. M.: Trace gas measurements in nascent, aged, and cloud-processed smoke from African savanna fires by airborne Fourier transform infrared spectroscopy (AFTIR). *Journal of Geophysical Research*, 108, https://doi.org/10.1029/2002JD002322, 2003.

Yuan, B., Shao, M., De Gouw, J., Parrish, D.D., Lu, S., Wang, M., Zeng, L., Zhang, Q., Song, Y., Zhang, J. et al. Volatile organic compounds (VOCs) in urban air: How chemistry affects the interpretation of positive matrix factorization (PMF) analysis. *Journal of Geophysical Research*, 117 (D24), https://doi.org/10.1029/2012JD018236, 2012.

Zhou, M., Langerock, B., Vigouroux, C., Sha, M. K., Ramonet, M., Delmotte, M., Mahieu, E., Bader, W., Hermans, C., Kumps, N., Metzger, J.-M., Duflot, V., Wang, Z., Palm, M., and De Mazière, M.: Atmospheric CO and CH4 time series and seasonal variations on Reunion Island from ground-based in situ and FTIR (NDACC and TCCON) measurements. *Atmospheric Chemistry and Physics*, 18, 13881-13901, 2018.